# International Ultraviolet Explorer (IUE)

NASA NEWSLETTER

New Spectral Image Processing System Information Manual: Low Dispersion Data - Version 1.0
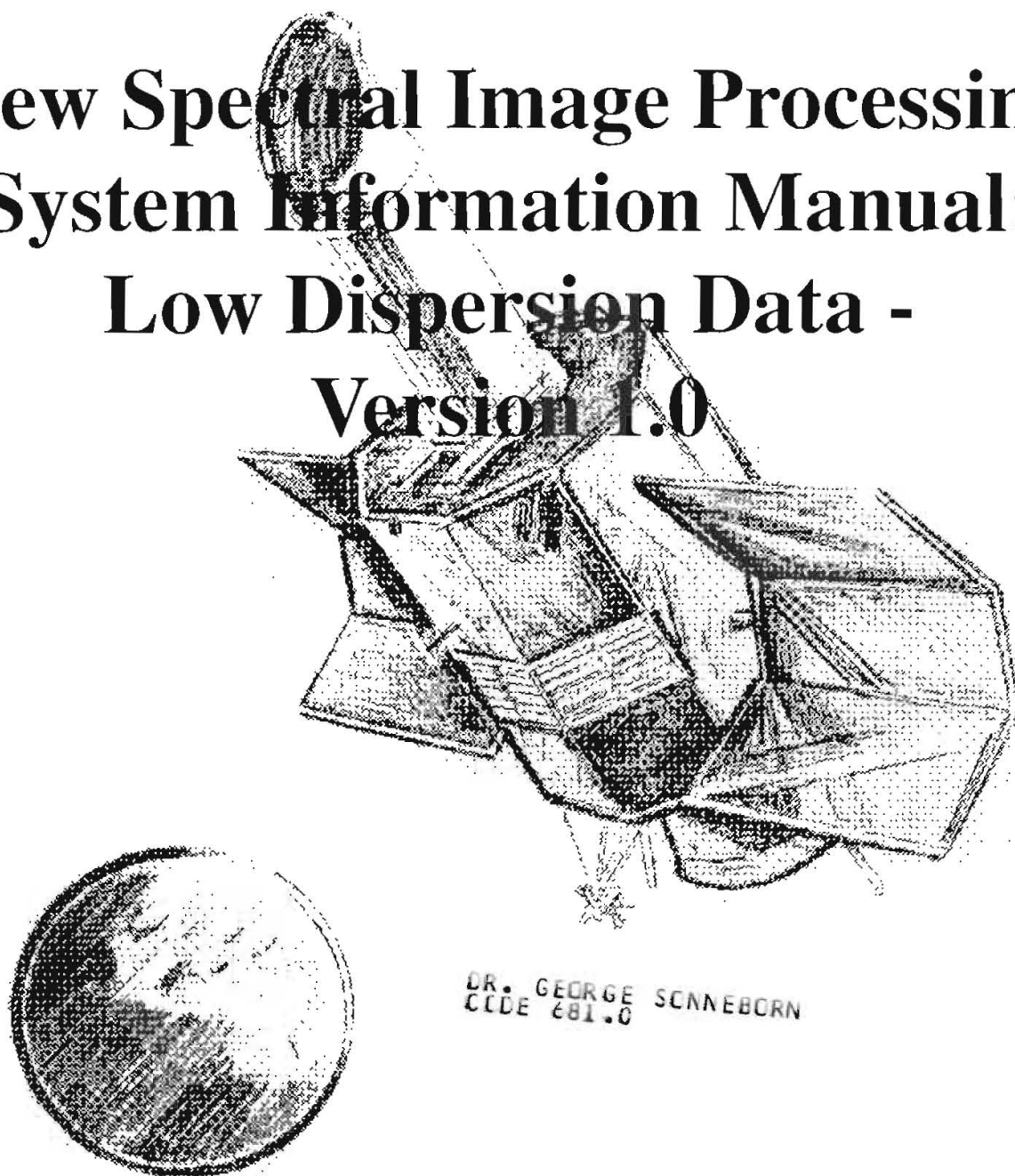
DR. GEORGE SONNEBORN
CODE 681.0

June 20, 1994

Dear Colleague:

It is a pleasure to transmit to you **IUE NEWSLETTER #53**. The entire issue is devoted to an article "New Spectral Image Processing System Information Manual: Low Dispersion Data, Version 1.0". The efforts of the authors and able assistance of Mona Drexler are greatly appreciated.

Sincerely,

Walter A. Feibelman
Code 684.1
Laboratory for Astronomy and
Solar Physics

International Ultraviolet Explorer
New Spectral Image Processing System
Information Manual: Low-Dispersion Data
Version 1.0

Prepared By

J.S. Nichols, M.P. Garhart, M.D. De La Peña, and K.L. Levay

Computer Sciences Corporation

Abstract

This document is intended for use by researchers who wish to analyze data acquired by the *International Ultraviolet Explorer* (*IUE*) and processed for the *IUE* Final Archive with the New Spectral Image Processing System (NEWSIPS) at both Goddard Space Flight Center (GSFC) and VILSPA. The information contained in this document explains the instrument characteristics and the processing methodology and calibration techniques used in the NEWSIPS system to produce the output products available to researchers. This initial version of the NEWSIPS Information Manual describes the processing techniques for low-dispersion *IUE* data and includes the wavelength and absolute flux definitions for low-dispersion SWP and LWP data. Output products for the high-dispersion NEWSIPS processing are also described briefly in this document. The description of the high-dispersion processing algorithms and the definition of the LWR wavelength and absolute flux calibrations will be addressed in subsequent versions of this document.

This document is a reprint of CSC/SD-93/6062, issued in December 1993 under the same title.

Acknowledgments

Table of Contents

List of Tables

List of Figures

Chapter 1

Introduction

1.1 Purpose of Document

This document provides the researcher who plans to analyze images acquired with the *International Ultraviolet Explorer* (*IUE*) with the information necessary to understand the raw data characteristics and image processing operations, and to interpret the processed output products for data processed with the New Spectral Image Processing System (NEWSIPS). The document also provides detailed descriptions of each procedure and algorithm in the image processing system, the techniques used to calibrate the data in wavelength and absolute flux, and a complete specification of output file formats for SWP and LWP low-dispersion data.

Data acquired with the *IUE* satellite were originally processed with the *IUE* Spectral Image Processing System (IUESIPS) from the time of satellite launch. Over the years, IUESIPS underwent a number of enhancements and modifications, which were documented in the IUE Image Processing Information Manual Versions 1.0 (Turnrose and Harvel 1980), 1.1 (Turnrose *et al.* 1981), and 2.0 (Turnrose and Thompson 1984). These manuals are still the standard reference to be used with Guest Observer (GO) format data processed with IUESIPS. The NEWSIPS system described in this document is fundamentally different in algorithm and technique from the previous IUESIPS. For FITS format data processed with NEWSIPS, this document supersedes and replaces all previous versions of the IUE Image Processing Information Manual.

1.2 Philosophy of the IUE Final Archive Image Processing

The philosophy that governed the development of the NEWSIPS system was intended to address four fundamental requirements:

1. *Create a uniformly processed and calibrated archive as the final product of the IUE mission*

1

IUE data have been processed using the IUESIPS system since launch in 1978. However, the IUESIPS system has undergone a number of modifications and enhancements since that time, rendering the IUESIPS archived data inhomogeneous and not fully intercomparable. The original IUESIPS system was documented in the IUE Image Processing Information Manual Versions 1.0 and 1.1. A major change to the IUESIPS system occurred in 1981 and this newer version of the software is documented in the IUE Image Processing Information Manual Version 2.0. A modification to the resampling algorithm used to create the spatially resolved (ELBL) file for low dispersion was implemented in 1985. A new photometric calibration was implemented for the LWP camera data in 1988. Later changes have customarily been documented in *IUE* Newsletters.

2. *Exploit new image processing techniques to improve the photometric accuracy and signal-to-noise ratio of the data*

   A number of new image processing techniques had been identified since the design of IUESIPS that were demonstrated to produce a more accurate photometric correction and increased signal-to-noise ratio of the extracted *IUE* data. Implementation of these techniques significantly improves the quality of the Final Archive.

3. *Verify and correct fundamental information for each image*

   In addition to providing a uniformly processed archive with improved photometric and signal-to-noise properties, the *IUE* Project has expended considerable effort in verifying the information available for each image in the *IUE* Final Catalog of observations.

4. *Base the contents of the Final Archive on requirements from the research community*

   In defining the specifications for the *IUE* Final Archive, and in developing the new processing algorithms and calibrations, the *IUE* Project has been guided for the last five years by the recommendations of the Final Archive Definition Committee, chaired by J. Linsky. This very active committee represents a unique grassroots effort by the astronomical community to assist in defining the scientific content of a NASA space mission, optimizing its utility for future researchers.

It is important to note that the data processed with NEWSIPS differ in fundamental ways from the data processed with IUESIPS. Images processed with these two systems are not directly intercomparable.

1.2.1   Uniform Archive

One of the primary assets of the *IUE* archive is the long timeline of observations taken with a remarkably stable photometric instrument. To exploit this asset, observations must be fully intercomparable over the entire lifetime of *IUE*. In order to satisfy the first requirement, that of uniformity, it was essential to develop a fully automated system that allowed no human intervention and was sufficiently robust to process all images acquired by *IUE*. Thus the

algorithms developed were designed to yield the best overall result for all types of images. These algorithms may not yield the best result for a particular image or particular class of images because of this design requirement. This represents a change in philosophy from IUESIPS. For example, the data were processed with IUESIPS according to Guest Observer (GO) specifications concerning the width of the extraction slit and the registration of the spectrum with respect to the pseudo extraction slit. In the NEWSIPS system, the width of the extraction slit is automatically determined and registration is always automatic.

1.2.2   New Processing Algorithms and Calibrations

The new processing algorithms that have been developed by the NASA *IUE* Project allow several significant improvements in the processed data. The new approach exploits the presence of fixed pattern noise (pixel-to-pixel sensitivity variations in the cameras) as a reliable fiducial to register the raw science image with the raw Intensity Transfer Function (ITF) image. Proper registration of *IUE* images is crucial to accurate photometric correction because the variability of the geometrical distortions introduced by the SEC-Vidicon cameras ensures that raw science images are never perfectly aligned with the ITF. While reseau marks etched on the faceplates of the cameras were intended to be used to rectify geometrically the science images, they cannot be detected at the low exposure levels usually found in the background of *IUE* images. Therefore, the IUESIPS method of processing *IUE* images uses predicted reseau positions to align the science images with the ITF images. Unfortunately, these mean positions are poorly known and the application of a mis-registered ITF (by more than about 0.2 pixel) manifests itself as systematic noise in the photometrically corrected image, and ultimately in the spectrum.

To achieve proper alignment of the ITF images with each science image for the Final Archive reprocessing, the fixed pattern inherent in *IUE* images is used as a fiducial. Small patches of the science image are cross-correlated against corresponding areas on the appropriate ITF image to determine the spatial displacement between these two images. The displacement of each pixel in the science image from its corresponding pixel in the ITF can thus be determined to sub-pixel accuracy. Such an approach has several advantages: (1) a large number of fiducials can be found anywhere on the image, (2) fixed pattern can be detected even at the lowest exposure levels, and (3) fiducials are available near the edge of the image, where distortion is greatest. In the IUESIPS processing of *IUE* data, the ITF images have been resampled to geometrically correct space, significantly smoothing these calibration data. In the new processing system, the ITF images are retained in raw space, increasing the accuracy of the pixel-to-pixel photometric correction.

Only one resampling of the data is performed in the new processing system, minimizing the smoothing inherent in such an operation. The linearized pixel values are resampled into a geometrically rectified and rotated image, such that the spectral orders are horizontal in the image and the dispersion function of the spectral data within an order is linearized. The resampling algorithm used is a modified Shepard method which preserves not only the flux to 1–3%, depending on the noise level in the image, but also the spectral line shapes.

3

The low-dispersion spectral data are extracted by a weighted slit extraction method developed by Kinney *et al.* (1991). The advantages of this method over the IUESIPS boxcar extraction are: (1) the signal-to-noise ratio (S/N) of the spectrum is usually improved while flux is conserved, (2) most of the cosmic rays are automatically removed, and (3) the output includes an error estimate for each point in the flux spectrum.

An entirely new data product for the *IUE* Final Archive is a geometrically rectified and rotated high-dispersion image, with horizontal spectral orders. This new data product will allow future investigators to perform customized extractions on the high-dispersion data. One of the most significant problems with the analysis of high-dispersion *IUE* data has been the proper determination of the background in the region where the echelle orders are most closely spaced and begin to overlap. The new processing system includes a background removal algorithm that determines the background level of each high-dispersion image by fitting, in succession, one-dimensional Chebyshev polynomials, first in the spatial and then the wavelength direction. The extracted high-dispersion spectral data are available order-by-order and as a single concatenated spectrum uniformly sampled in wavelength.

In addition to the new algorithms for processing the *IUE* data for the Final Archive, all absolute flux calibrations have been rederived. The new calibrations use white dwarf models to determine the relative shapes of the instrumental sensitivity functions, while previous UV satellite and rocket observations of η UMa and other standard stars are used to set the overall flux scale. The *IUE* Final Archive extracted spectral data are also corrected for sensitivity degradation of the detectors over time and temperature, a calibration not previously available with IUESIPS processing.

These new processing algorithms for the creation of the Final Archive allow a significant improvement in the signal-to-noise ratio of the processed data, resulting largely from a more accurate photometric correction of the fluxes and weighted slit extraction, and greater spectral resolution due to a more accurate resampling of the data. Improvement in the signal-to-noise ratio of the extracted low-dispersion spectral data has been shown to range from 10–50% for most images, with factors of 2–4 improvement in cases of high-background and underexposed data (Nichols-Bohlin 1990).

1.2.3 Core Data Item Verifications

The value of the *IUE* Final Archive to future investigators will depend to a large degree on the accuracy and ease of use of the Final Catalog. Both *IUE* Observatories have verified the accuracy of the Final Catalog and the information in the image headers. A set of "core" data items (CDIs) has been identified which were verified from observatory records available at each station. These core items are generally the information necessary to process correctly the image and/or are crucial for scientific analysis. While many of the verification procedures are automated, it is necessary in some cases to consult the hand-written scripts or logs to obtain the correct information. The verification of the CDIs is performed before each image is reprocessed for the Final Archive.

1.2.4 Community Involvement

The *IUE* Final Archive Definition Committee (FADC), chaired by Jeffrey Linsky, was formed in November 1987 to provide recommendations and advice to the NASA *IUE* Project on the content of the Final Archive and on the algorithms and methods used to process the data for the Archive. The FADC also provided estimates of resources needed to accomplish the recommended goals. The committee is composed of 24 people, selected for having demonstrated interest in improving the S/N of *IUE* data for their own research. The committee met every 3–6 months for 5 years, producing at each meeting a written report of recommendations and near-term goals. These reports are published in the *IUE* Newsletters Nos. 34, 36, 38, and 48. The FADC provided user representation by the astronomical community to define the content of the *IUE* Final Archive, optimizing its utility for future investigators.

Chapter 2

Description of IUE Data

2.1   Raw Image Data and Label Parameters

Each raw *IUE* image consists of a 768 × 768 array of 8-bit picture elements or "pixels". Partial-read images, which are not full 768 × 768 images, are discussed in Chapter 3.3. Each vidicon scan line consists of 768 pixels or "samples" obtained in minor frame units of 96 pixels; 768 such scan lines compose the entire image. Line 1, sample 1 is at the upper left corner of the image; line 768, sample 768 is at the lower right corner of the image. Each raw pixel value lies in the range 0 to 255 (integers only). The units of raw pixel values are data numbers (DN), which are proportional (up to the telemetry system limit of 255) to the integrated charge read out from the SEC Vidicon target in the camera scanning process. Since the telemetry system saturates at 255, the DN/charge proportionality breaks down at that level.

Associated with each raw image is a set of 20 header, or label, records. Each record is 360 8-bit bytes long (a concatenation of five 72-byte logical records). This set of 20 label records is generated by the *IUE* Operations Control Center (OCC) software during image acquisition and contains various identifying parameters and scientific/engineering data pertinent to the image.

Raw *IUE* images must be corrected for the instrumental effects of the SEC Vidicon camera system before quantitatively meaningful data can be extracted from them. The methods of compensation for the radiometeric (photometeric) non-linearities and non-uniformities and the geometric distortion introduced by the vidicon system are described in Chapters 5, 6, and 7. The layout of the spectral format in either dispersion mode is mathematically described by the methods discussed in Chapter 8. Figures 2.1 through 2.15 illustrate schematically the spectral formats in both dispersion modes, for both apertures, for all three operational cameras. These diagrams refer to raw image space. The square border defines the 768 × 768 array comprising the whole image, whereas the inscribed arcs roughly define the target ring, which is the area within which the photometeric correction is applied (Chapter 6) and from which spectral information is extracted. For high dispersion, the extracted odd and even echelle orders are shown in separate figures. Numbers and tick marks mark the wavelengths

in angstroms.

2.2 Spectrograph Geometry

Both the long and short wavelength *IUE* spectrographs have two entrance apertures: a small aperture (nominal 3 arcsec diameter circle) and a large aperture (nominal 10 arcsec by 20 arcsec slot). Although the various methods available for determining the fundamental dimensions do not always yield results which agree to within the limits set by the internal consistency of each (see Panek 1982), the *IUE* Three Agency Coordination Meeting adopted recommended values for certain dimensions, which are presented in Table 2.1. These values do not reflect the true physical size of the apertures but rather the size as projected on the camera faceplate. As a result, each spectrograph has its own distinct measurement of the aperture sizes.

Table 2.1: Officially Adopted Dimensions for the Apertures in Each Spectrograph, Measured on LWP and SWP Images

Dimension	LWP	SWP
Major Axis Trail Length (*arcsec*)	21.84±0.39	21.48±0.39
Large-Aperture Length (*arcsec*)	22.51±0.40	21.65±0.39
Minor Axis Trail Length (*arcsec*)	10.21±0.18	9.24±0.11
Large-Aperture Width (*arcsec*)	9.91±0.17	9.07±0.11
Large-Aperture Area (*arcsec*^{2})	203.26±9.28	209.74±6.23
Small-Aperture Area (*arcsec*^{2})	6.32±0.86	6.58±0.86

An accurate measurement of the trail length is needed, as such information is used to calculate the trailed exposure time. In addition, knowledge of the effective aperture area is needed to calibrate properly spectra of extended objects.

For the purposes of image processing, we continue to utilize the previously quoted plate scale of 1.525±0.01 arcsec/pixel (Bohlin *et al.* 1980). Coupled with the known separation of the large and small apertures (approximately 40 arcsec in the short wavelength spectrograph and 41 arcsec in the long wavelength spectrograph) and the known geometrical orientation of the apertures (see the discussion of Figures 2.16 through 2.18 below), the aperture separations in the directions along and perpendicular to the dispersion are given in Table 2.2.

These values are defined in the geometrically corrected frame of reference where the spectrum has been aligned horizontally in the image. The total offset is defined as the square root of the sum of the squares of the individual terms. The offsets along the dispersion have been incorporated into the geometric correction step such that the wavelength scales for the small and large apertures are aligned.

The geometry of the two entrance apertures in relation to the image scan lines and the high and low resolution dispersion directions are shown in Figures 2.16 through 2.18 for

7
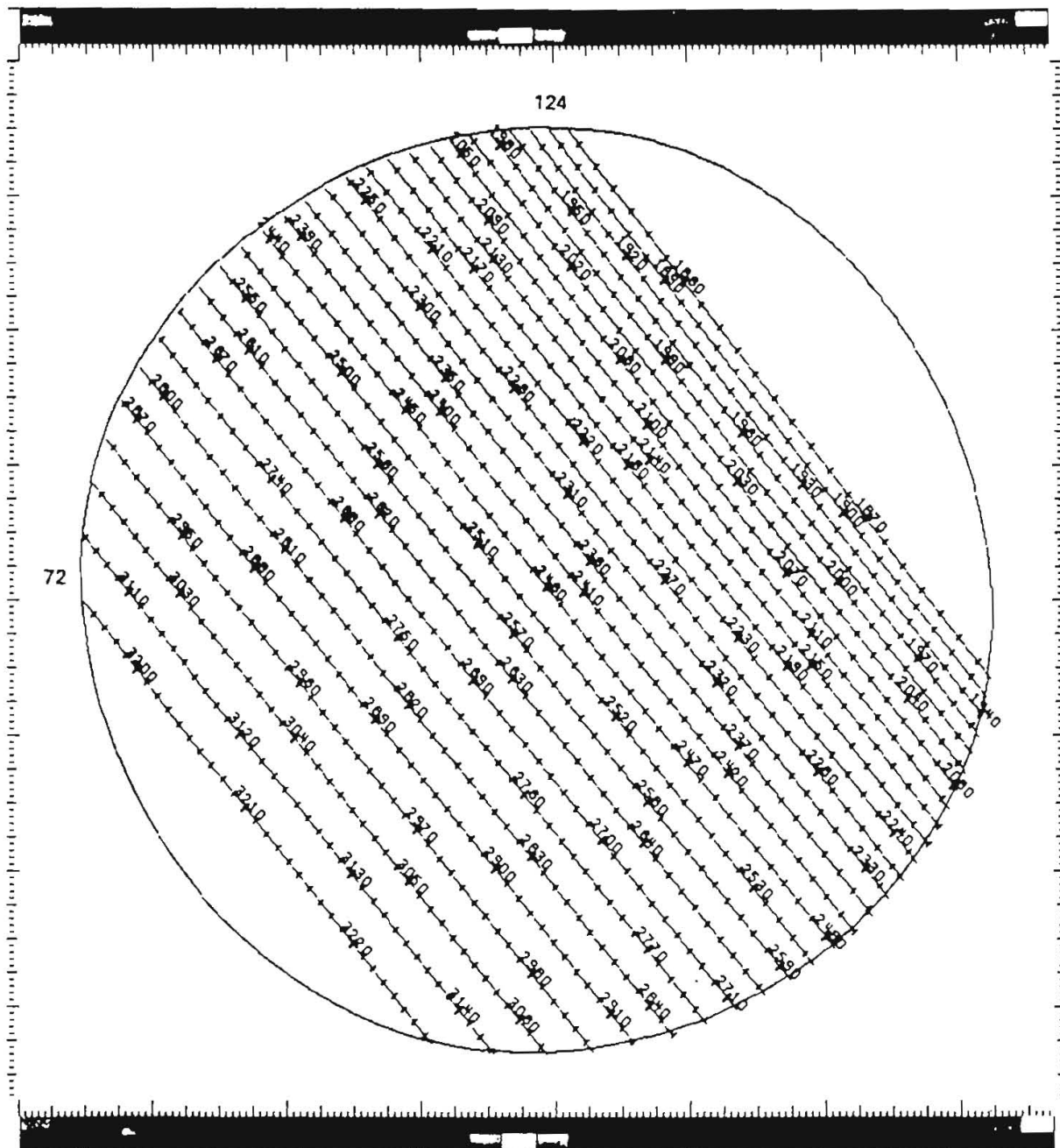
Figure 2.1: LWP small-aperture high-dispersion (even orders) format.
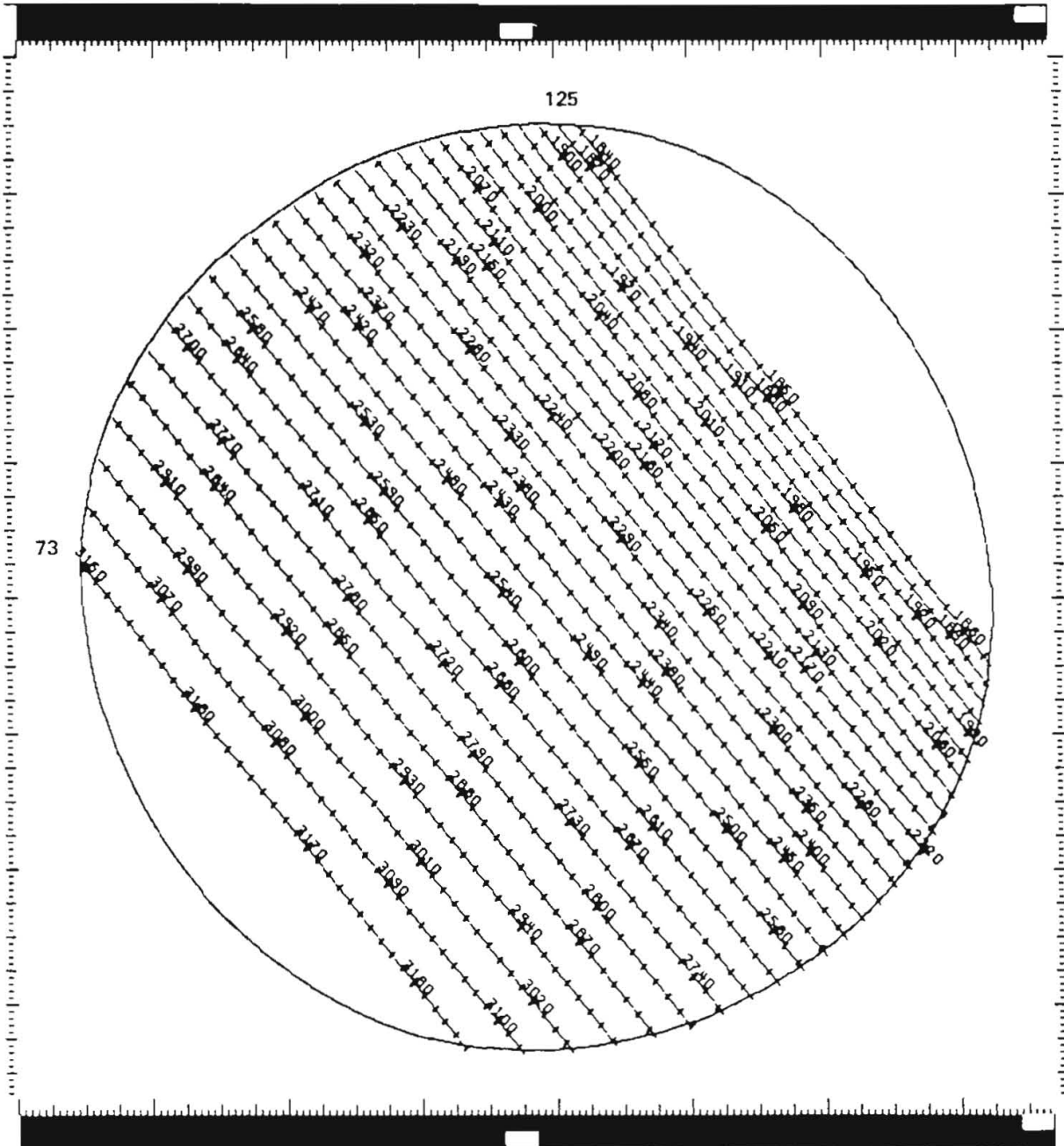
Figure 2.2: LWP small-aperture high-dispersion (odd orders) format.
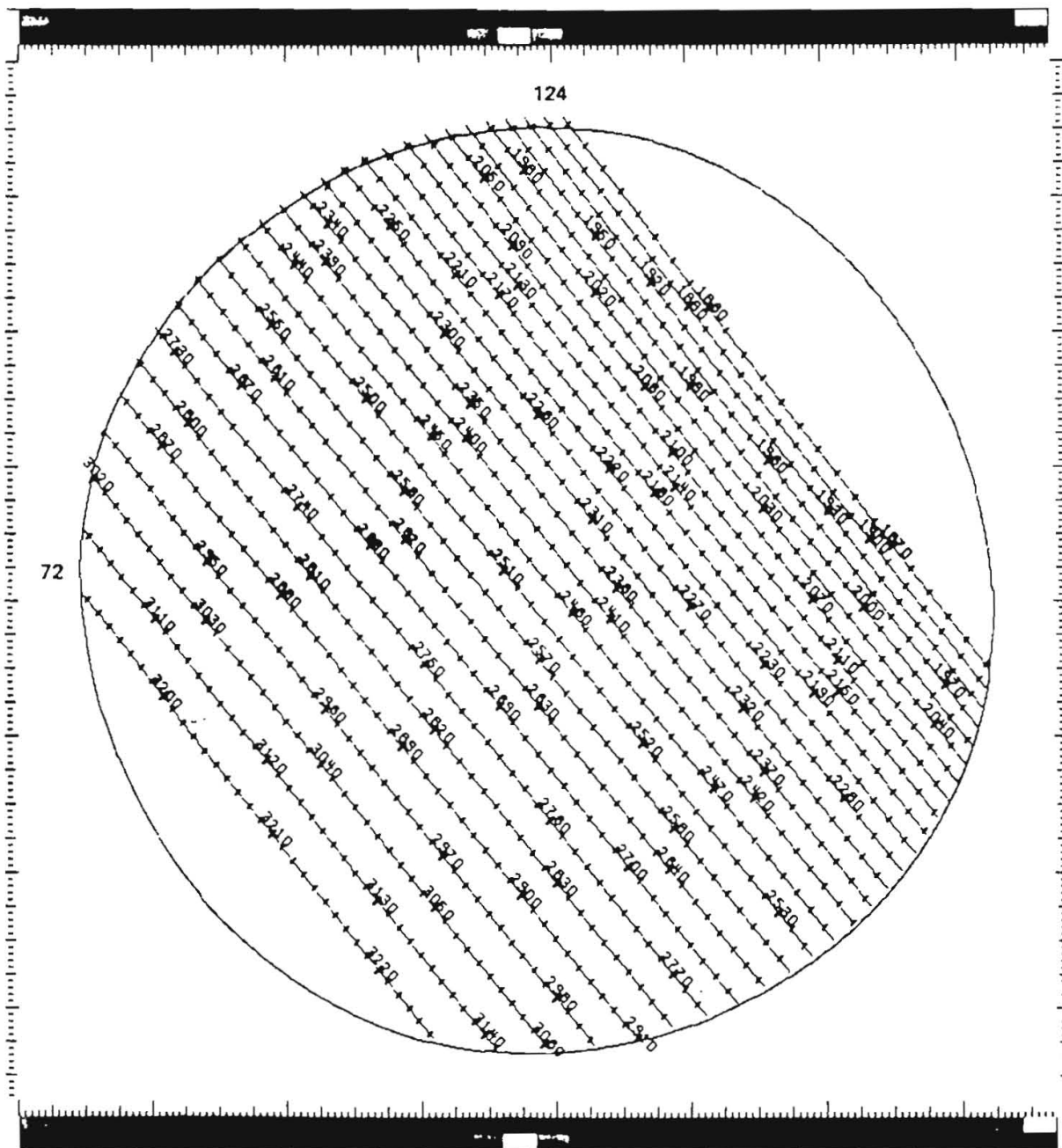
Figure 2.3: LWP large-aperture high-dispersion (even orders) format.
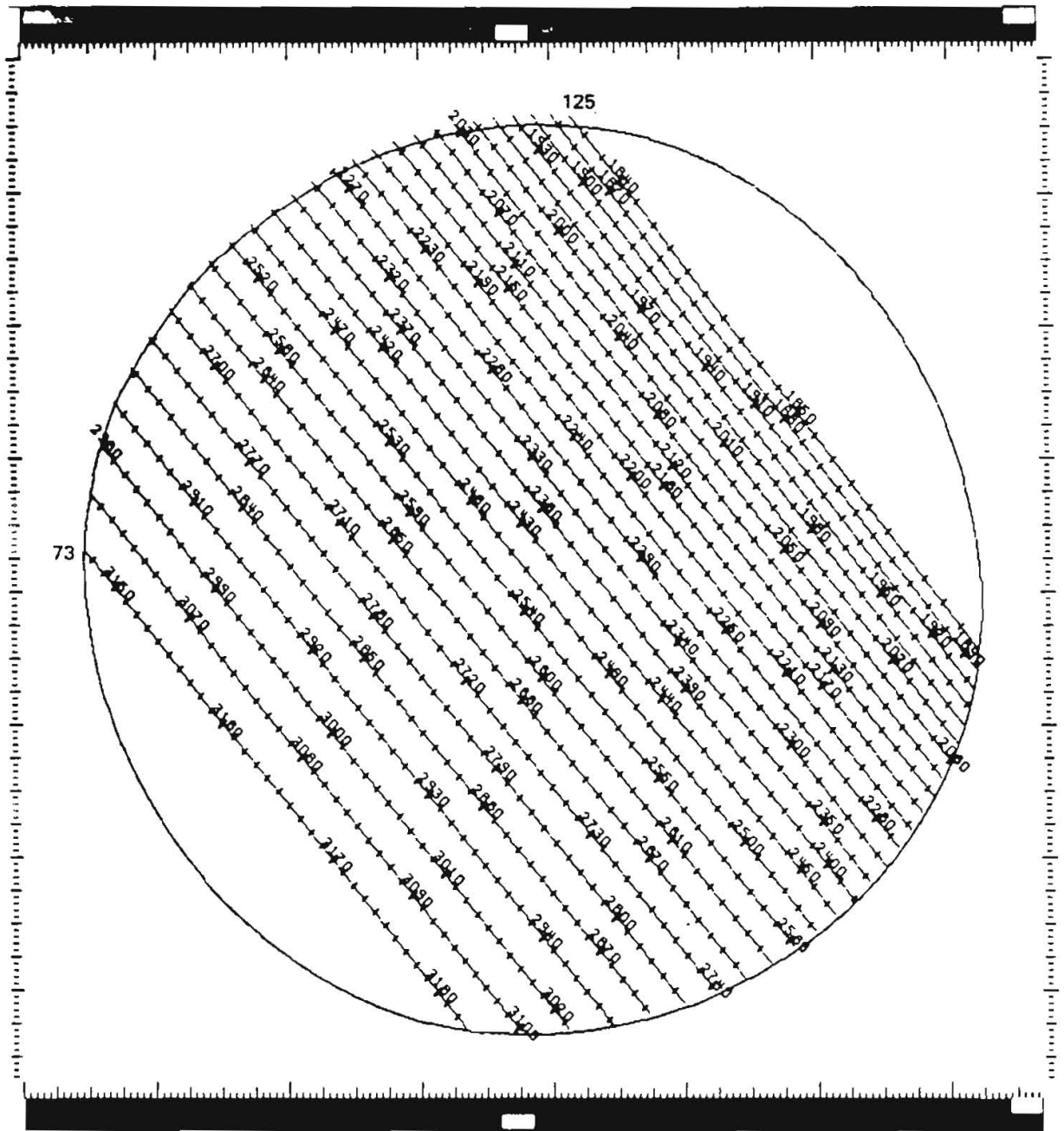
Figure 2.4: LWP large-aperture high-dispersion (odd orders) format.

11
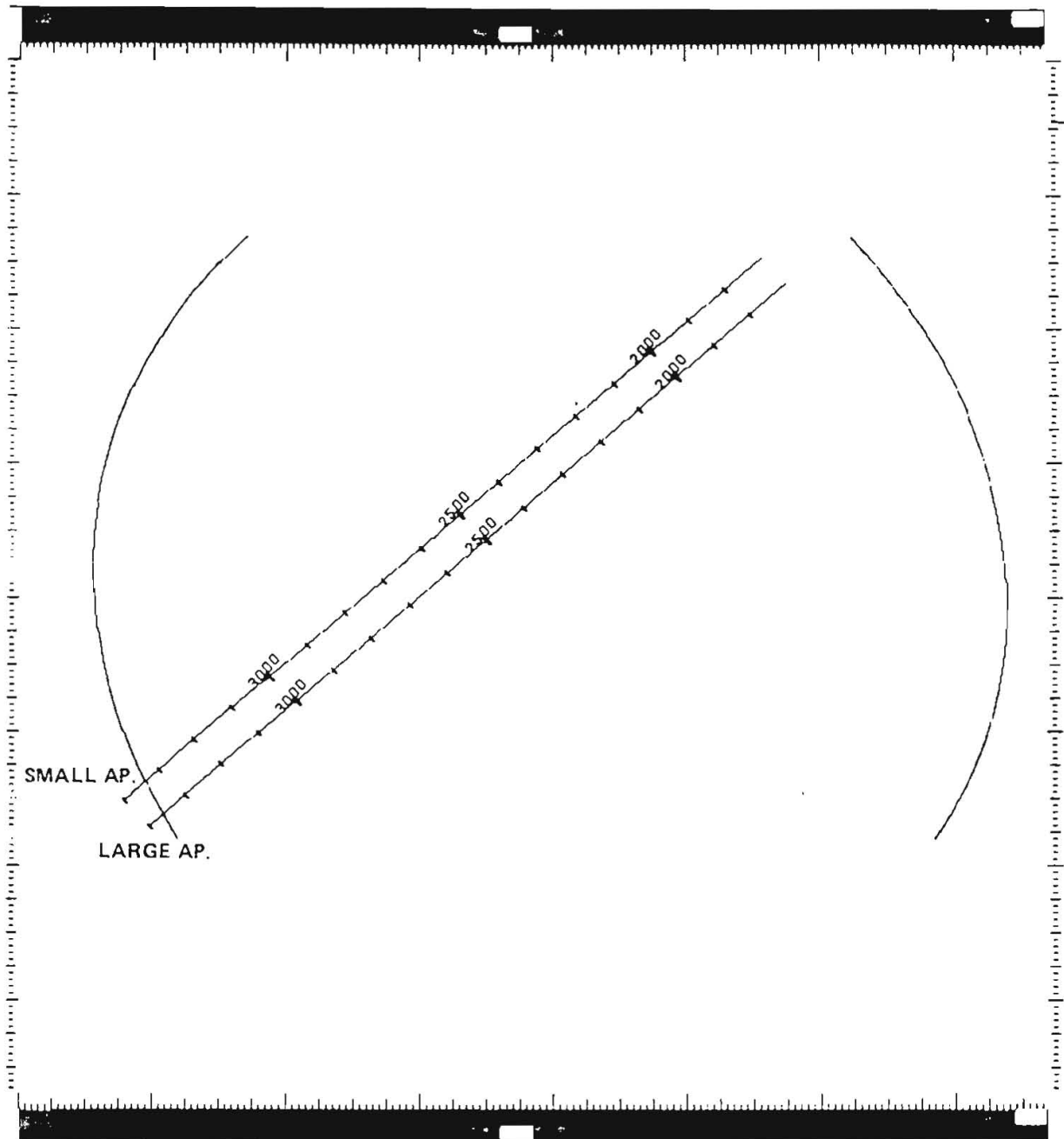
Figure 2.5: LWP large- and small-aperture low-dispersion format.
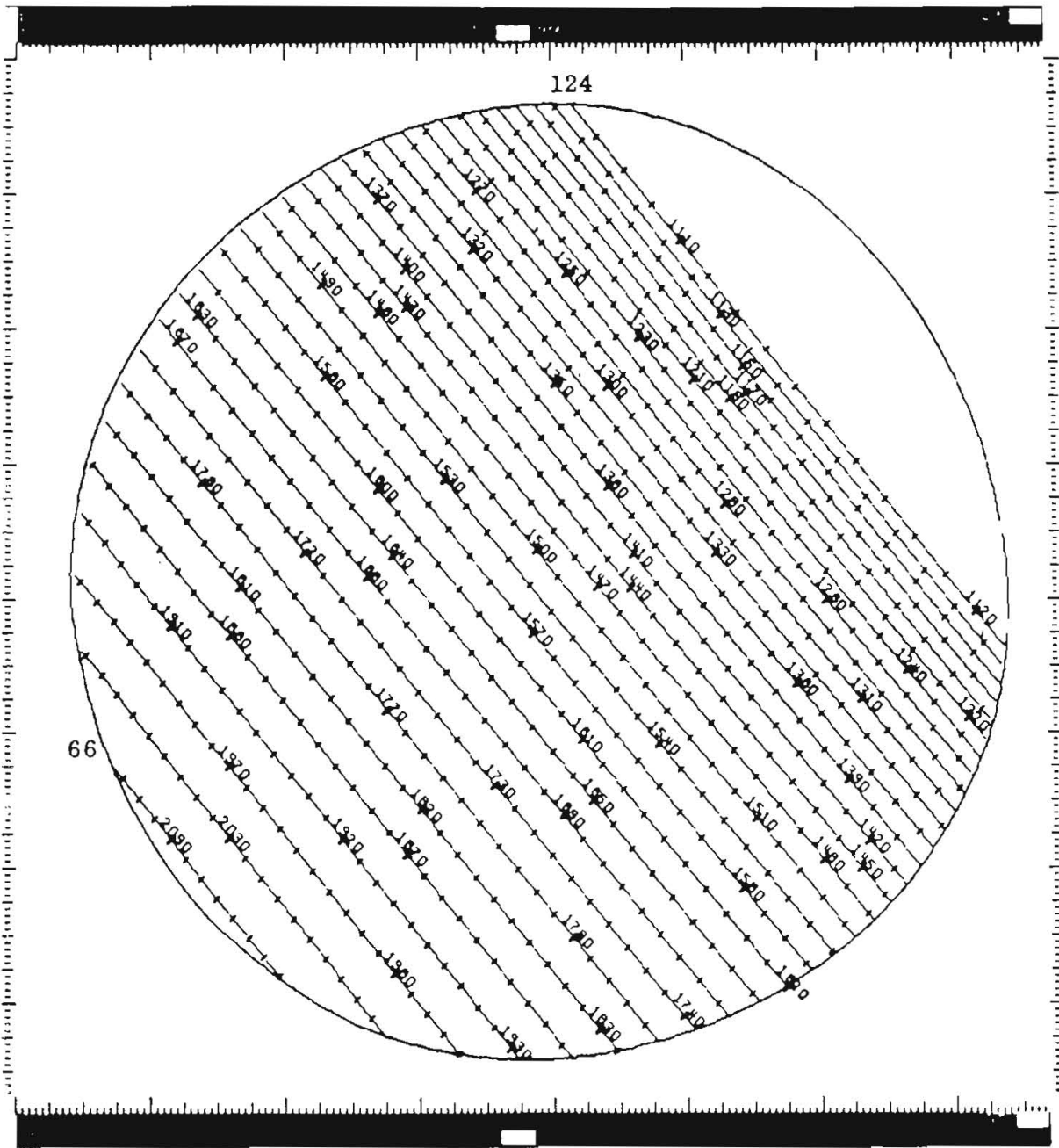
Figure 2.6: SWP small-aperture high-dispersion (even orders) format.

Figure 2.7: SWP small-aperture high-dispersion (odd orders) format.
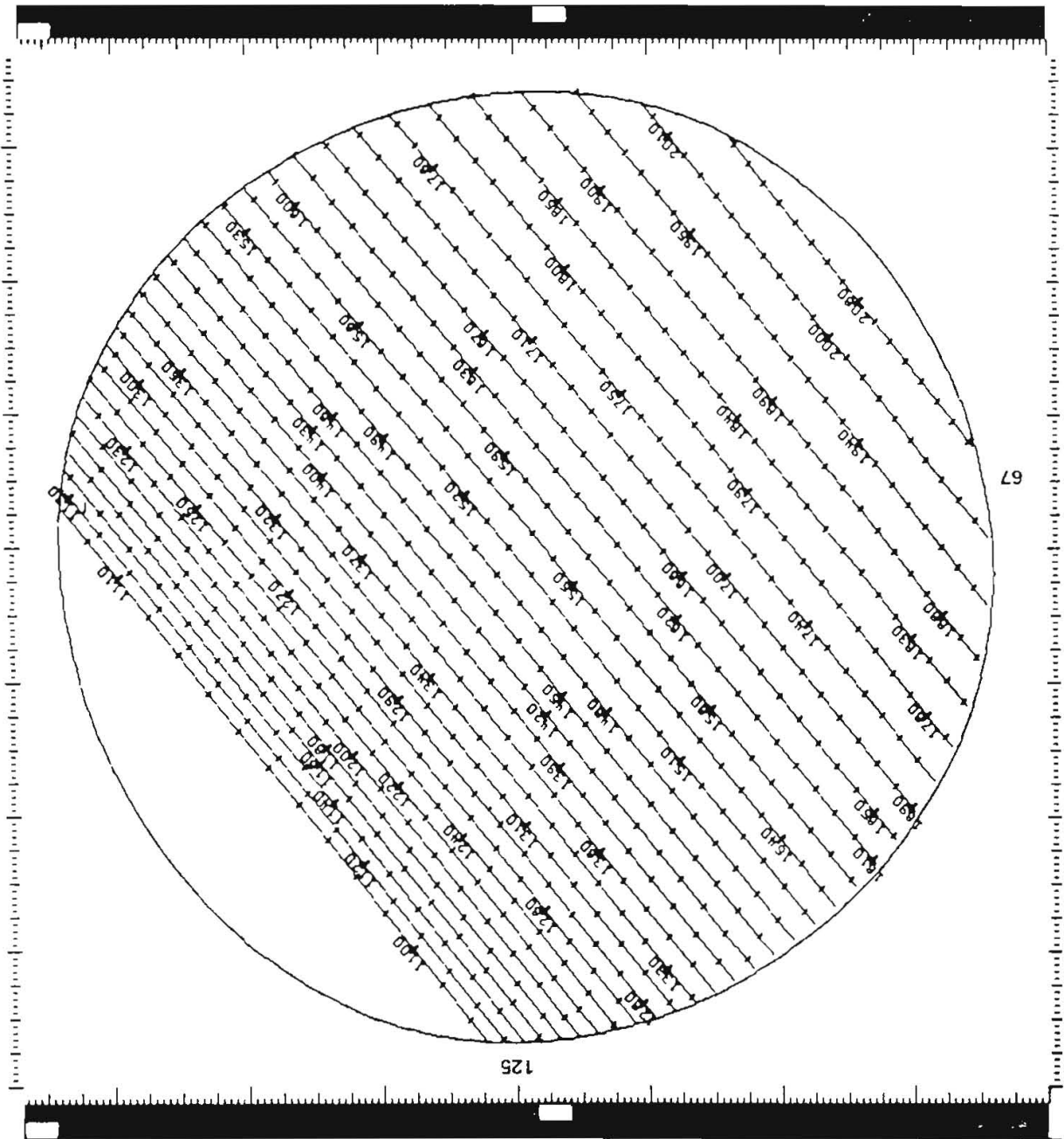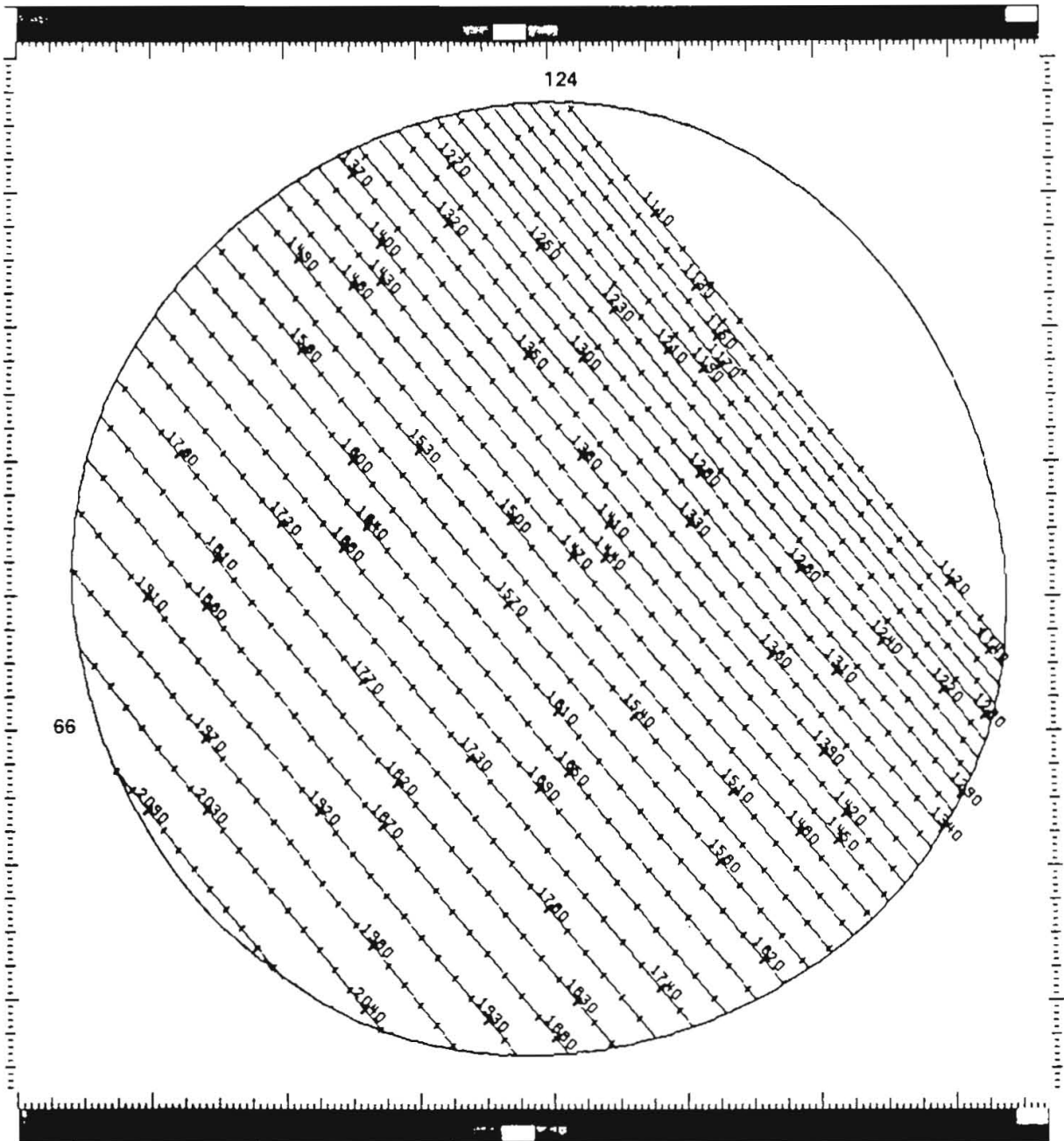
Figure 2.8: SWP large-aperture high-dispersion (even orders) format.
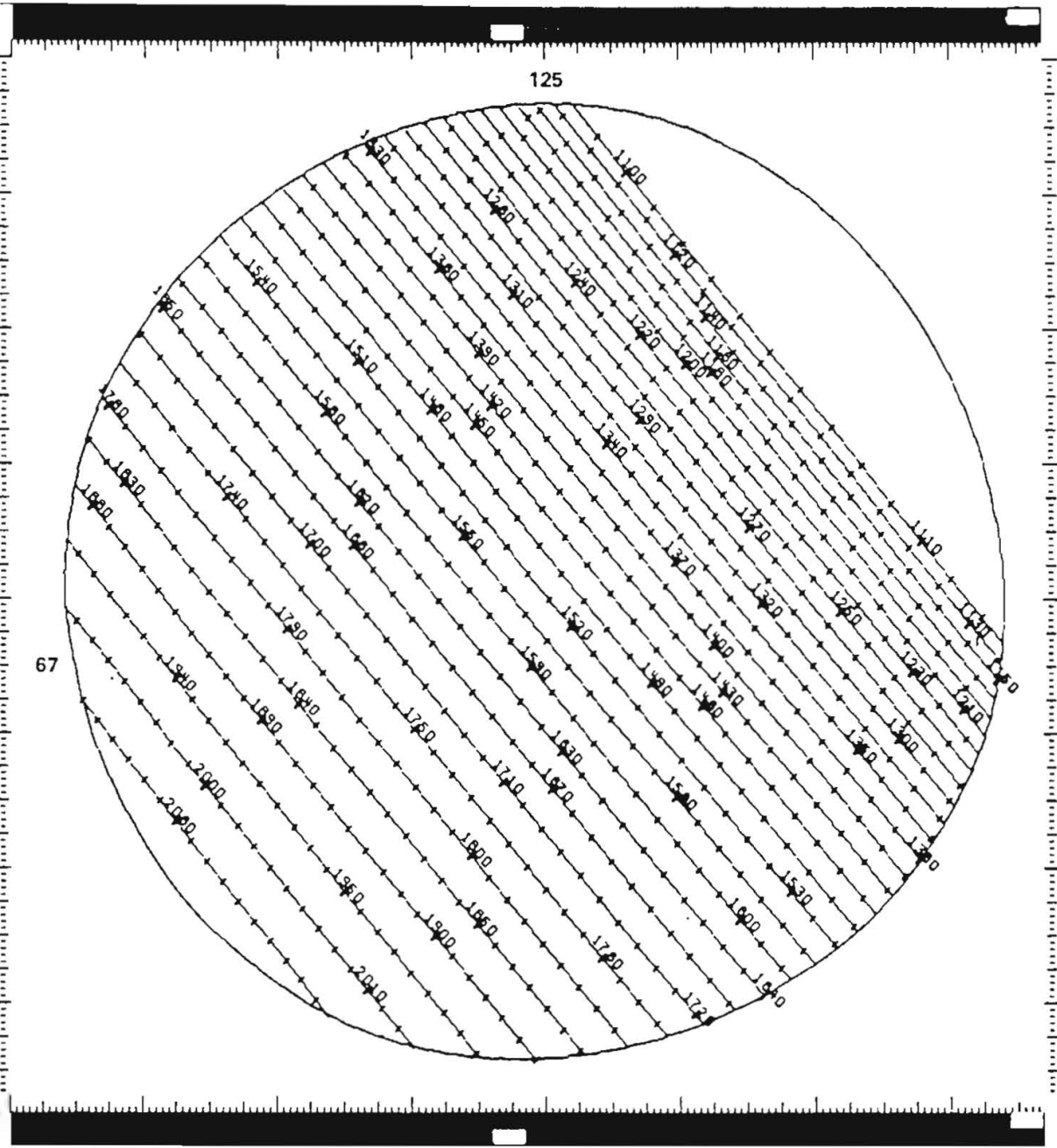
Figure 2.9: SWP large-aperture high-dispersion (odd orders) format.
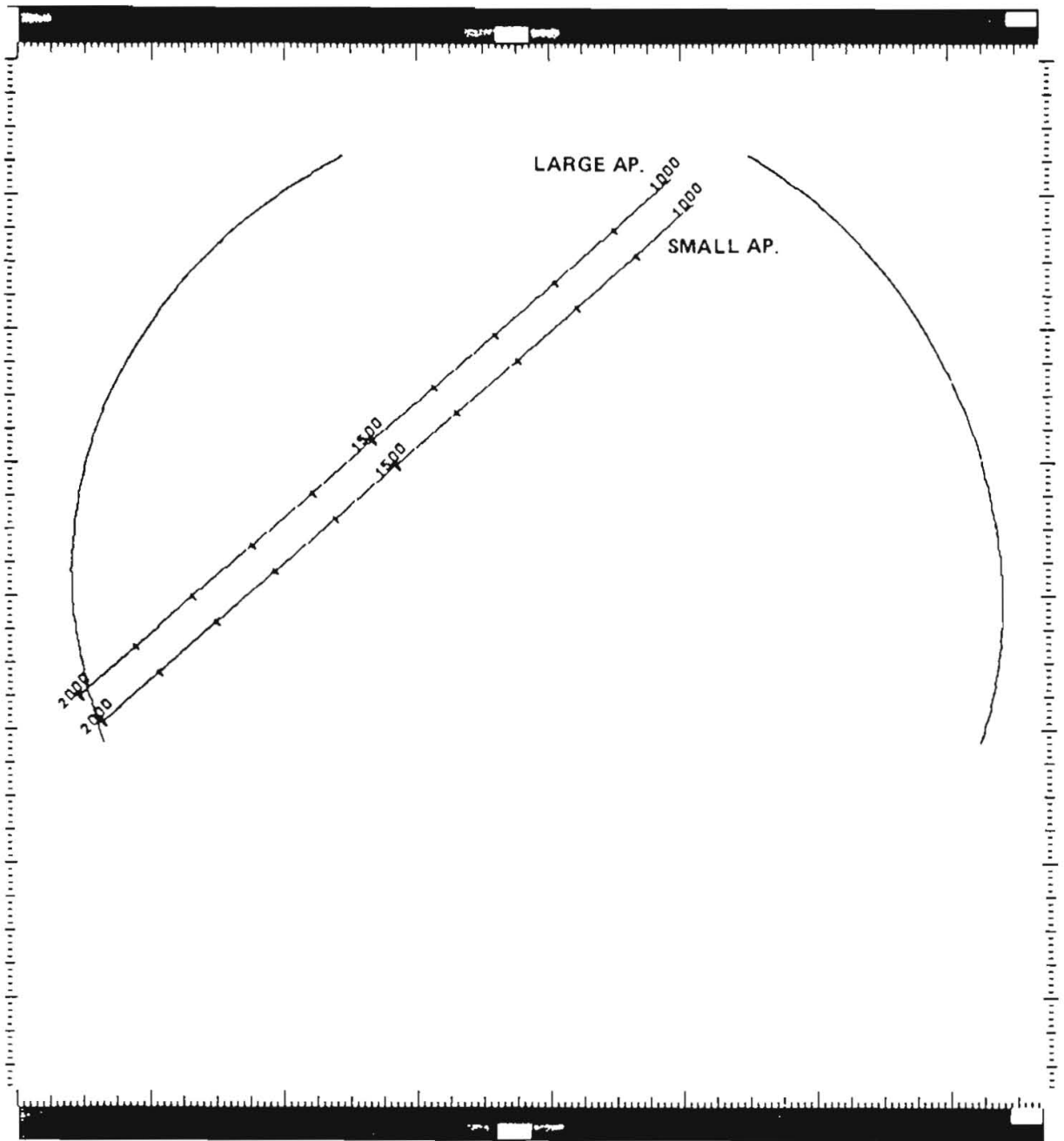
Figure 2.10: SWP large- and small-aperture low-dispersion format.
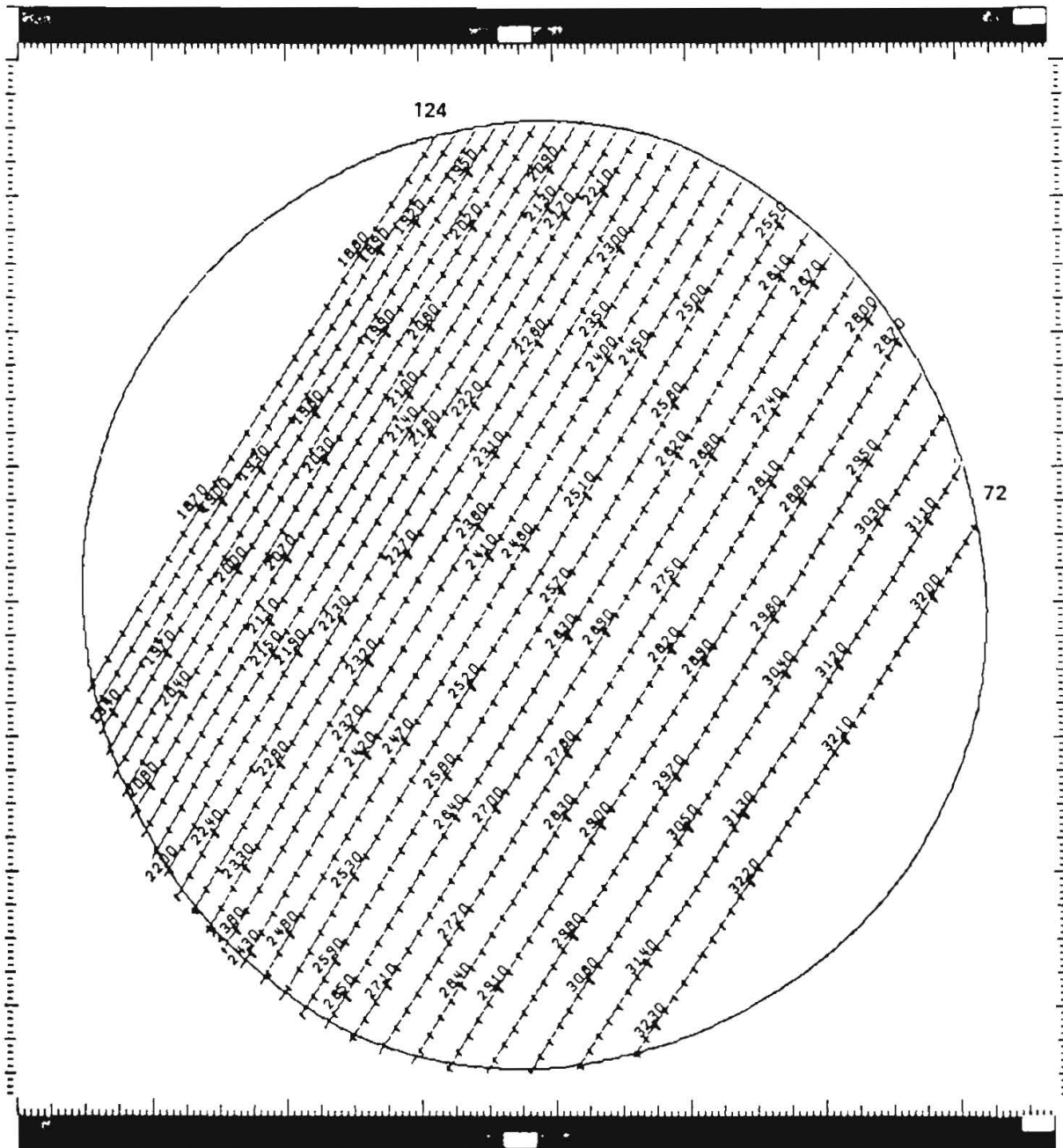
Figure 2.11: LWR small-aperture high-dispersion (even orders) format.
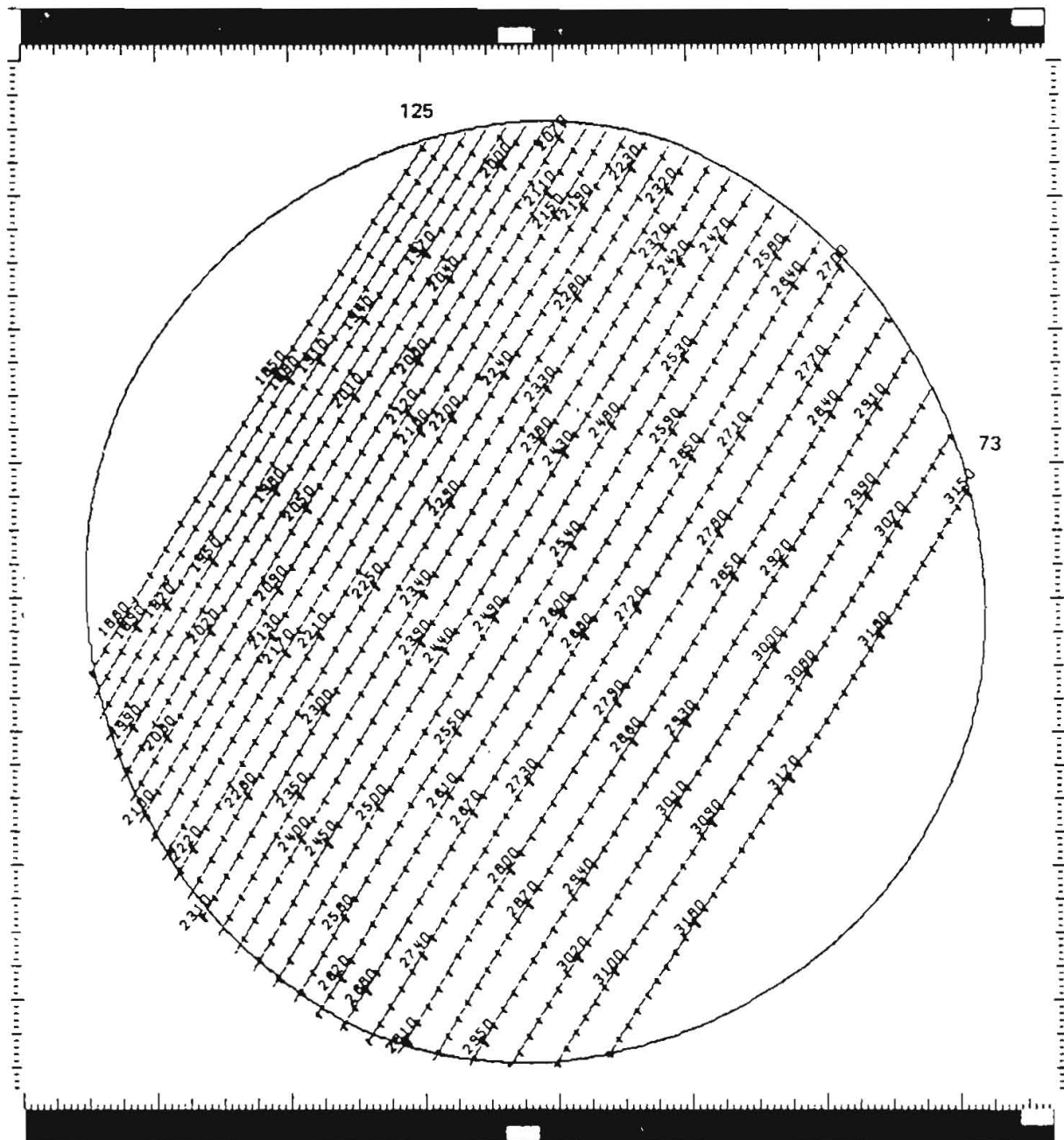
Figure 2.12: LWR small-aperture high-dispersion (odd orders) format.
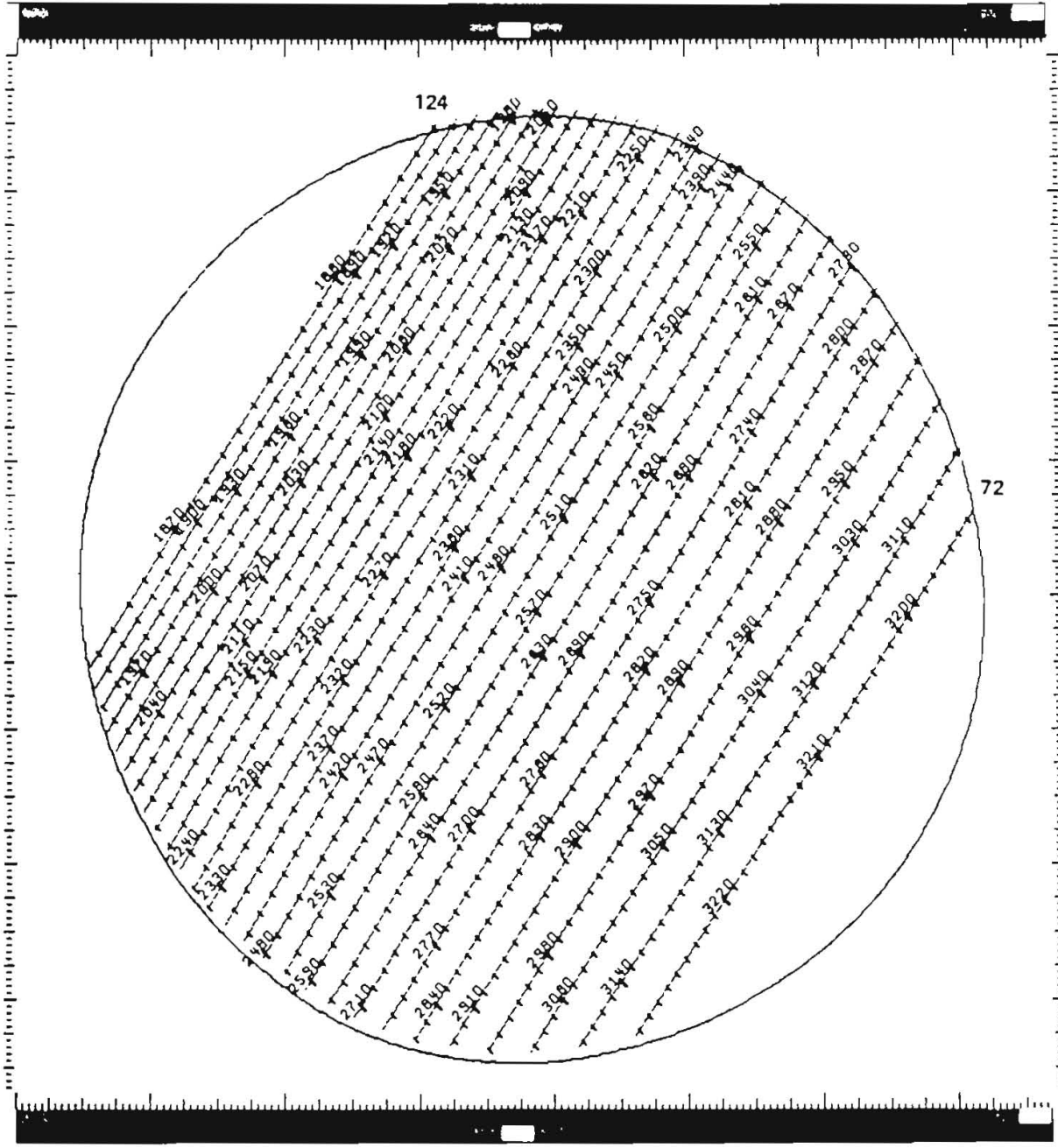
Figure 2.13: LWR large-aperture high-dispersion (even orders) format.
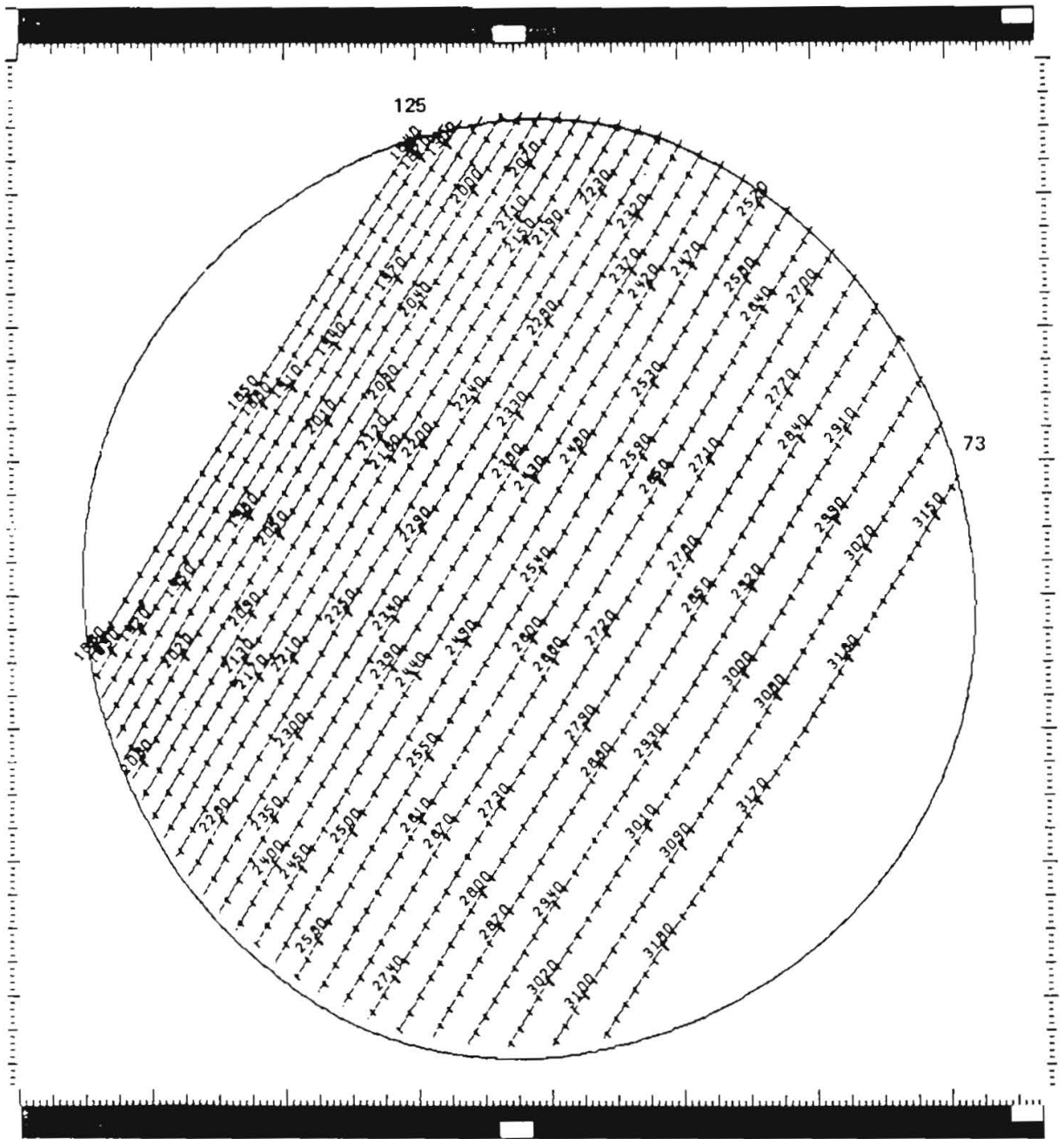
Figure 2.14: LWR large-aperture high-dispersion (odd orders) format.
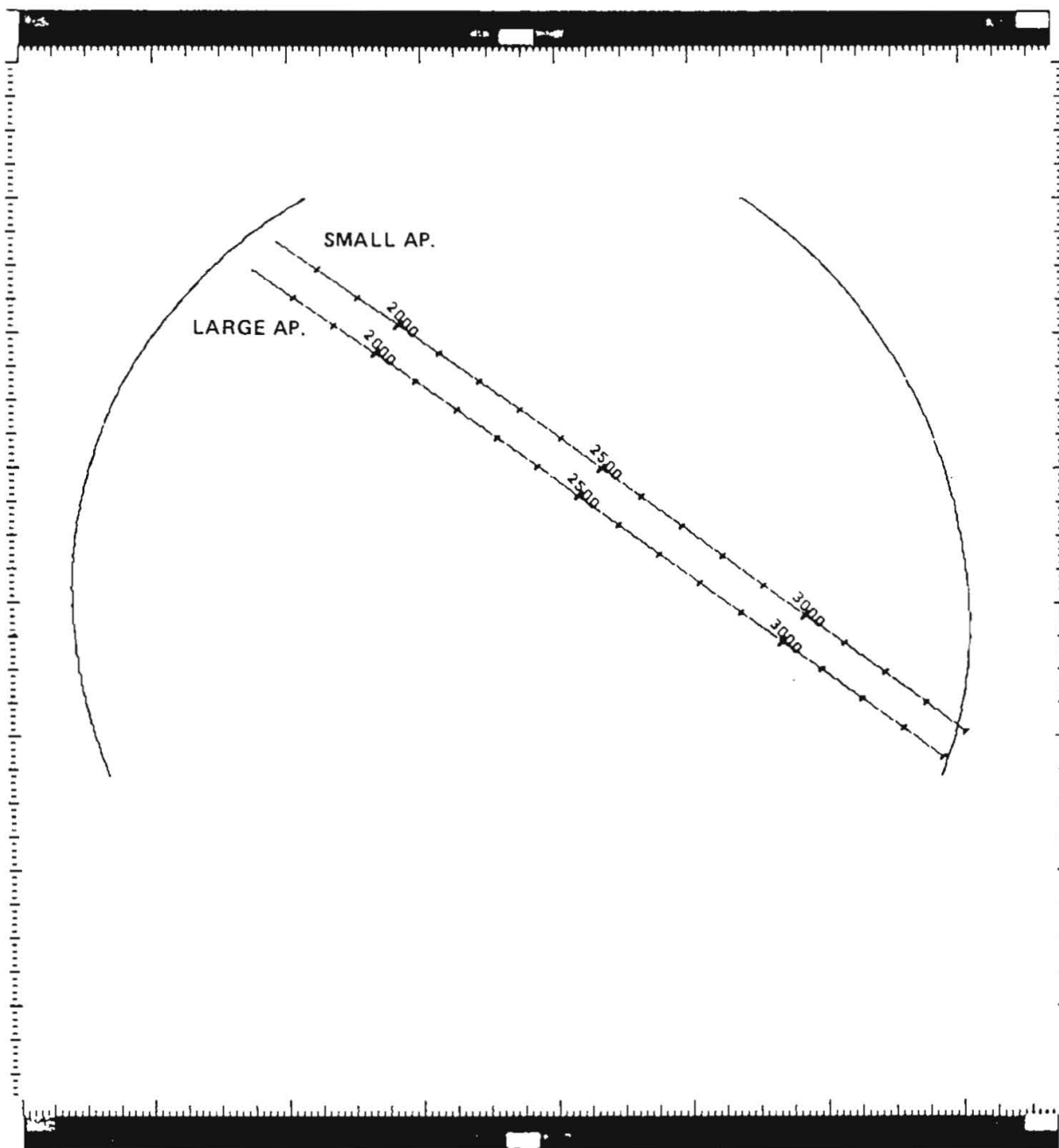
Figure 2.15: LWR large- and small-aperture low-dispersion format.

Table 2.2: Standard Offsets from the Small to the Large Spectrograph Aperture as used by NEWSIPS (in pixels)

Camera	Along Dispersion	$\perp$ to Dispersion	Total Offset
LWP	-2.3	26.2	26.3
LWR	-2.3	26.4	26.5
SWP	0.8	26.1	26.1

the SWP, LWP, and LWR cameras. These figures are drawn in the geometrically corrected frame of reference with the origin at the upper left. Note particularly the fact that the displacement between the short wavelength large aperture (SWLA) and the short wavelength small aperture (SWSA) is very nearly along the echelle dispersion direction. Therefore, short wavelength high-dispersion images in which both apertures are exposed will result in nearly complete superposition of the large- and small-aperture spectra (with a wavelength offset). The displacement of the long wavelength large aperture (LWLA) and the long wavelength small aperture (LWSA) is less coincident with the echelle dispersion direction in those spectrographs, so that superposition of large- and small-aperture high-dispersion spectra is not as serious in the long wavelength spectrograph.

For the purposes of judging the extent and separation of the apertures in the spectral domain, the scales given in Table 2.3 may be used in conjunction with the quantities in Tables 2.1 and 2.2. Note that in high dispersion a given shift along the dispersion corresponds closely to a constant Doppler velocity shift, whereas in low dispersion a given shift corresponds to a constant wavelength shift.

Table 2.3: Approximate Spectral Scales in Each Dispersion Mode

Camera	Low Dispersion ($\mathring{A}$/px)	High Dispersion (km/s/px)
LWP	2.66	7.21
LWR	2.66	7.27
SWP	1.68	7.72

2.3 Instrumental Resolution

The instrumental resolution (both spectral and spatial) is determined by the camera resolution, the dispersion mode, the aperture used, the focussing conditions in the telescope, and the pointing stability of the spacecraft. While the dominant effect is the camera resolution, telescope focus and stability of spacecraft pointing also play a major role in defining the

LOW DISPERSION ORDER

SWLA

IMAGE SCAN LINE

38'.9

48°6

51°9

60°1

λ

SWSA

AXIS OF SWLA

HIGH DISPERSION (ECHELLE ORDER 100)

λ

10 PIXELS
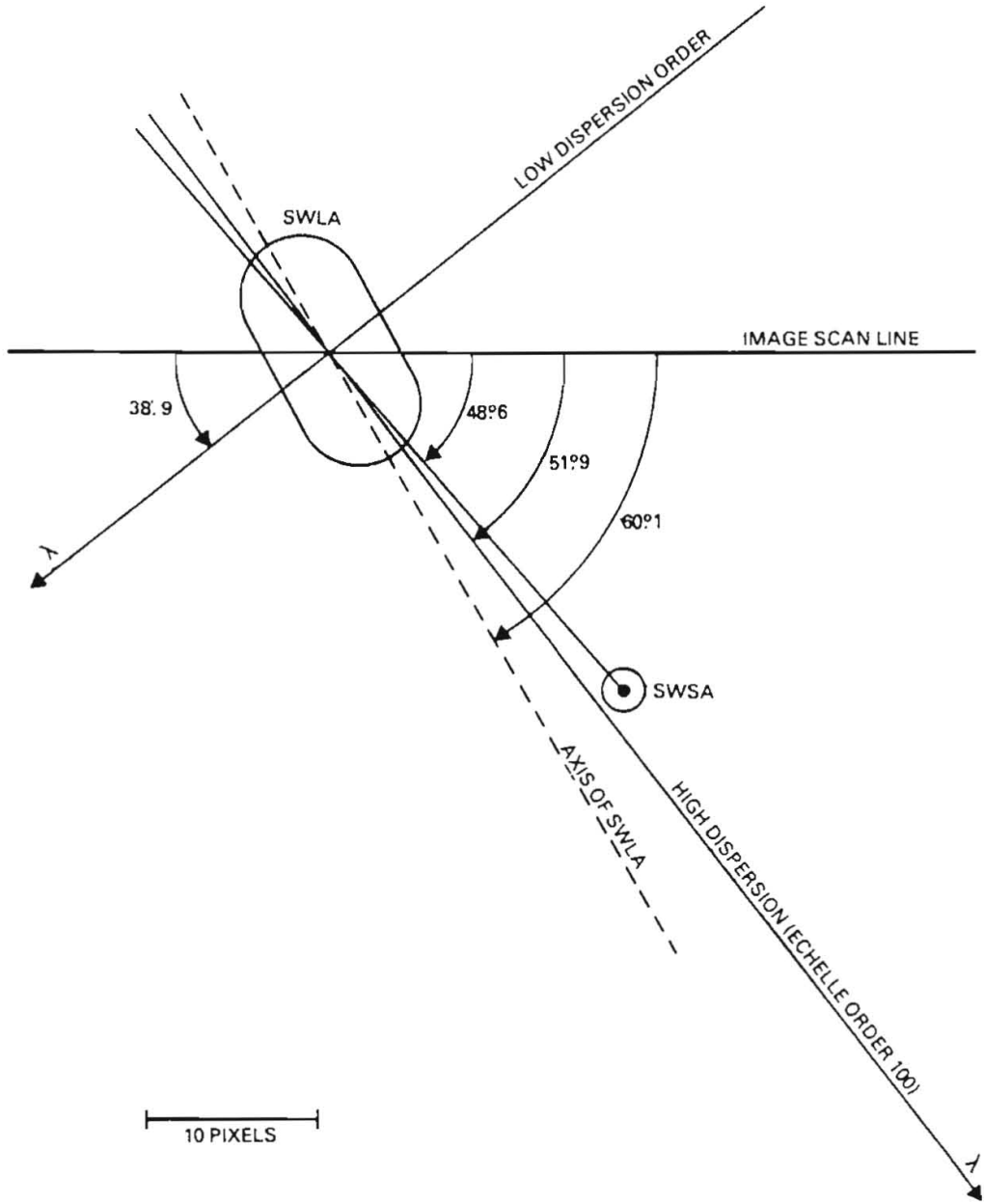
Figure 2.16: SWP Geometry

24
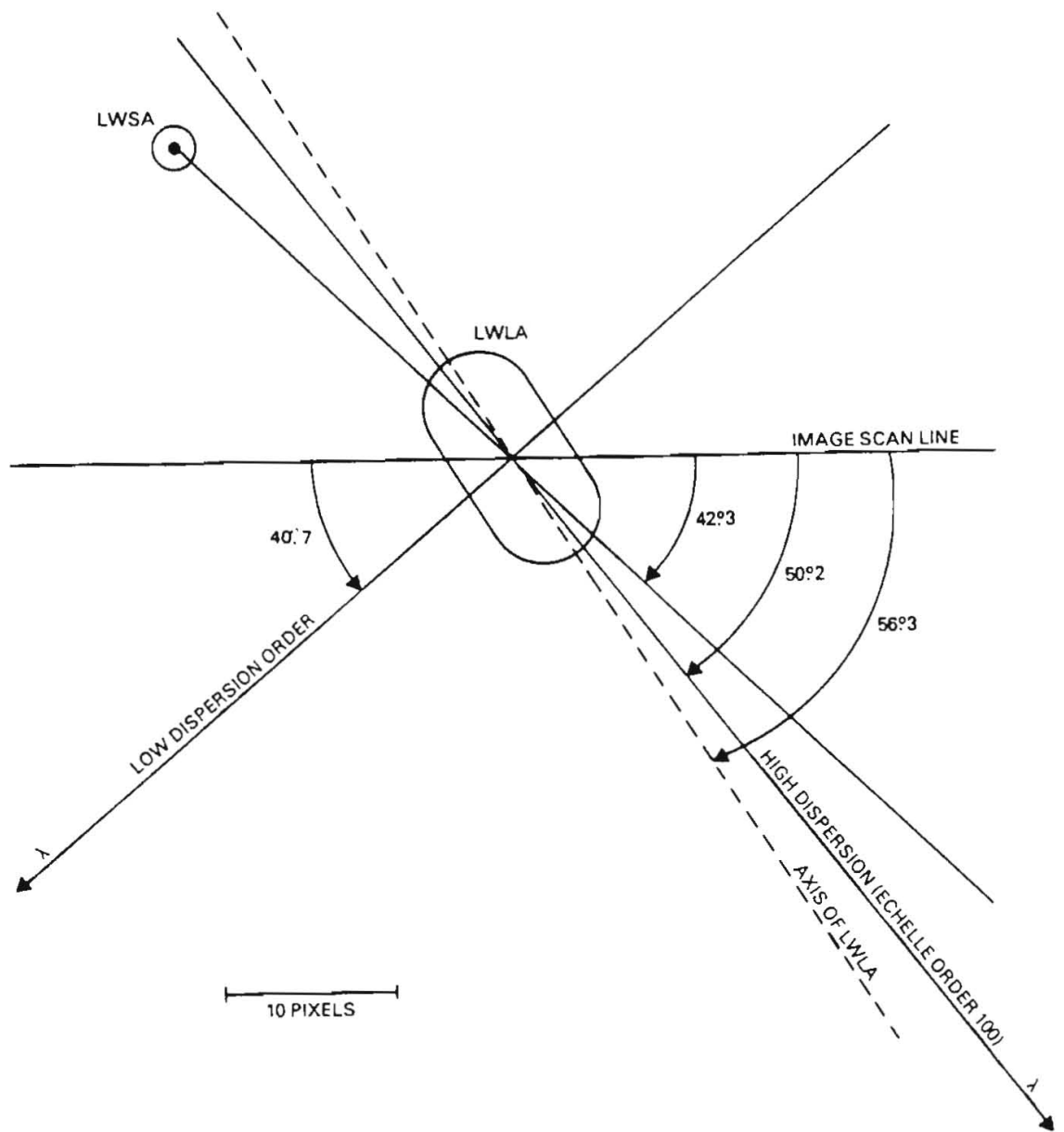
Figure 2.17: LWP Geometry

25

Figure 2.18: LWR Geometry

10 PIXELS

HIGH DISPERSION (ECHELLE ORDER 100)

AXIS OF LWLA

Y

LOW DISPERSION ORDER

Y

36°7

46°3

54°1

60°3

IMAGE SCAN LINE

LWLA

LWSA
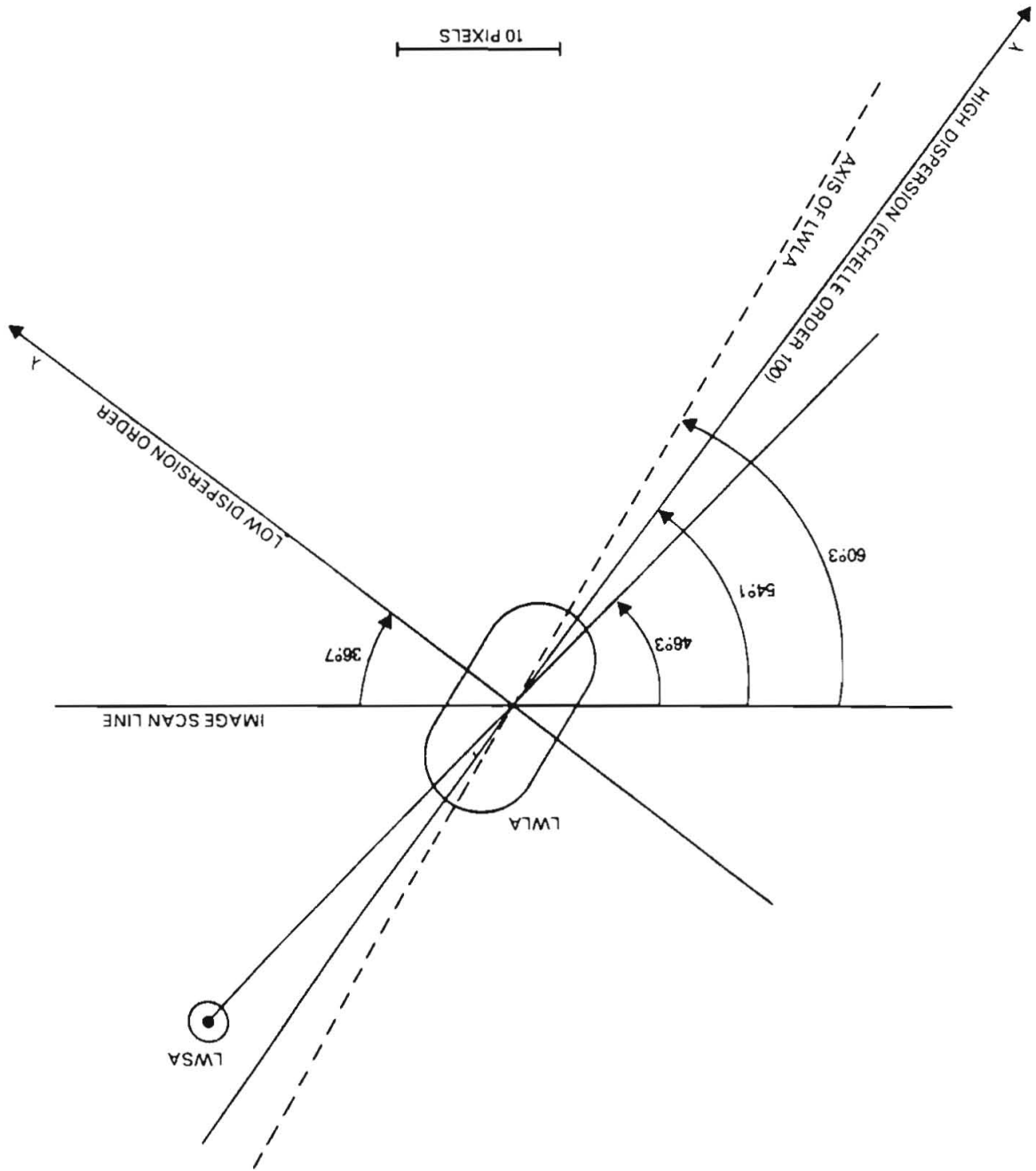
resolution. In addition, it is well known that the camera resolution is highly wavelength-dependent. According to the *IUE* Camera Users Guide (Coleman *et al.* 1977), the camera point spread function (PSF) consists of a narrow, gaussian-like core with long shallow wings. The actual resolution in either the spatial or spectral direction can be defined as a function of the full width at half maximum (FWHM). Two spectra (spatial direction) or two spectral features (spectral direction) can be resolved provided their separation is as follows:

$$d \geq 0.849 \times FWHM$$

where d is the distance separating the two features (or spectra). Spatial resolution is specified in pixels, while spectral resolution is denoted in angstroms.

2.3.1 Low-Dispersion Mode

2.3.1.1 Resolution Along the Dispersion

A study of the NEWSIPS spectral resolution was performed by measuring the FWHM of several features for the emission line sources V1016 Cyg, RR Tel, AG Dra, CI Cyg, and Z And. The analysis indicates a slight improvement in the NEWSIPS resolution (approximately 10% for the SWP and 7% for the LWR) over the IUESIPS results reported by Cassatella, Barbero, and Benvenuti (1985). Plots of the spectral resolution data are shown in Figure 2.19. The small-aperture data are slightly offset in wavelength from the large-aperture data for clarity.

LWP - Large-aperture spectral resolution is best between 2700 and 2900Å with an average FWHM of 5.2Å and decreases to approximately 8.0Å on either side of this range. Small-aperture resolution is optimal between 2400 and 3000Å with an average FWHM of 5.5Å and decreases to 8.1Å at the extreme wavelengths.

LWR - Maximum resolution in the large aperture occurs longward of 2300Å, with an average FWHM of 5.3Å, while shortward of this point the FWHM decreases to 7.7Å. Small-aperture resolution is best from 2700–3200Å, with an average FWHM of 5.4Å, and decreases to 7.7Å at 3350Å and 7.5Å shortward of 2400Å.

SWP - The best resolution occurs around 1200Å, with a FWHM of 4.6Å in the large aperture and 3.0Å in the small aperture, and gradually worsens towards longer wavelengths: 6.7Å at 1900Å in the large aperture and 6.3Å in the small. On average, the small-aperture resolution is approximately 10% better than the large-aperture resolution.

2.3.1.2 Resolution Perpendicular to the Dispersion

The NEWSIPS spatial resolution has been determined by analyzing the spectra of several low-dispersion standard stars (*viz.*, HD 60753, HD 93521, BD+33° 2642, and BD+75° 325). The FWHM of large- and small-aperture spectra were measured at several wavelengths and plotted (see Figure 2.20). As is the case with the spectral resolution studies, the NEWSIPS
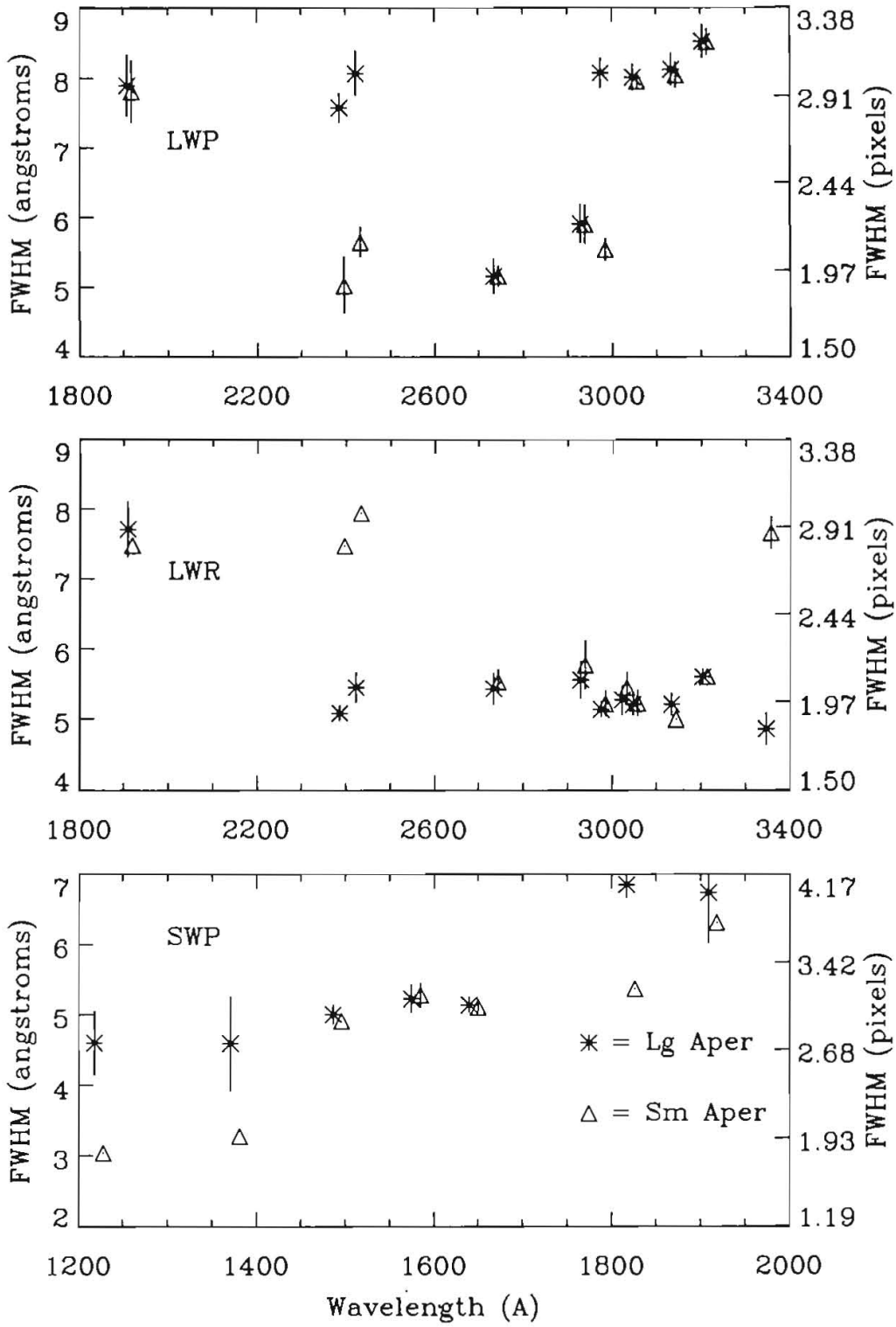
Figure 2.19: Low-dispersion spectral resolution.

values show, in general, an improvement over IUESIPS. As is the case with the spectral resolution plots, the small-aperture data are slightly offset from the large-aperture data.

LWP - The spatial resolution for the LWP is best near 3000Å where the FWHM for the large aperture is 2.4 pixels (3.6 arcsec), and decreases to values of around 3.0 pixels at the short and long wavelength ends of the spectrum. There is no significant difference between the large- and small-aperture spatial resolutions.

LWR - The behavior of the LWR camera as a function of wavelength is similar to the LWP, with the smallest FWHM values for the large aperture of 2.6 pixels (3.9 arcsec) occurring near 3000Å, and increasing to 3.6 and 3.0 pixels at the wavelength extremes. The small aperture, unlike the other two cameras, shows a dramatic decrease in resolution of approximately 10%.

SWP - The SWP camera shows the best spatial resolution near 1400Å with mean FWHM values for the large aperture of 2.7 pixels (4.1 arcsec), increasing slightly to 2.8 pixels at 1250Å, and 3.7 pixels at 1950Å. The SWP small-aperture resolution response is approximately the same as the large-aperture resolution.
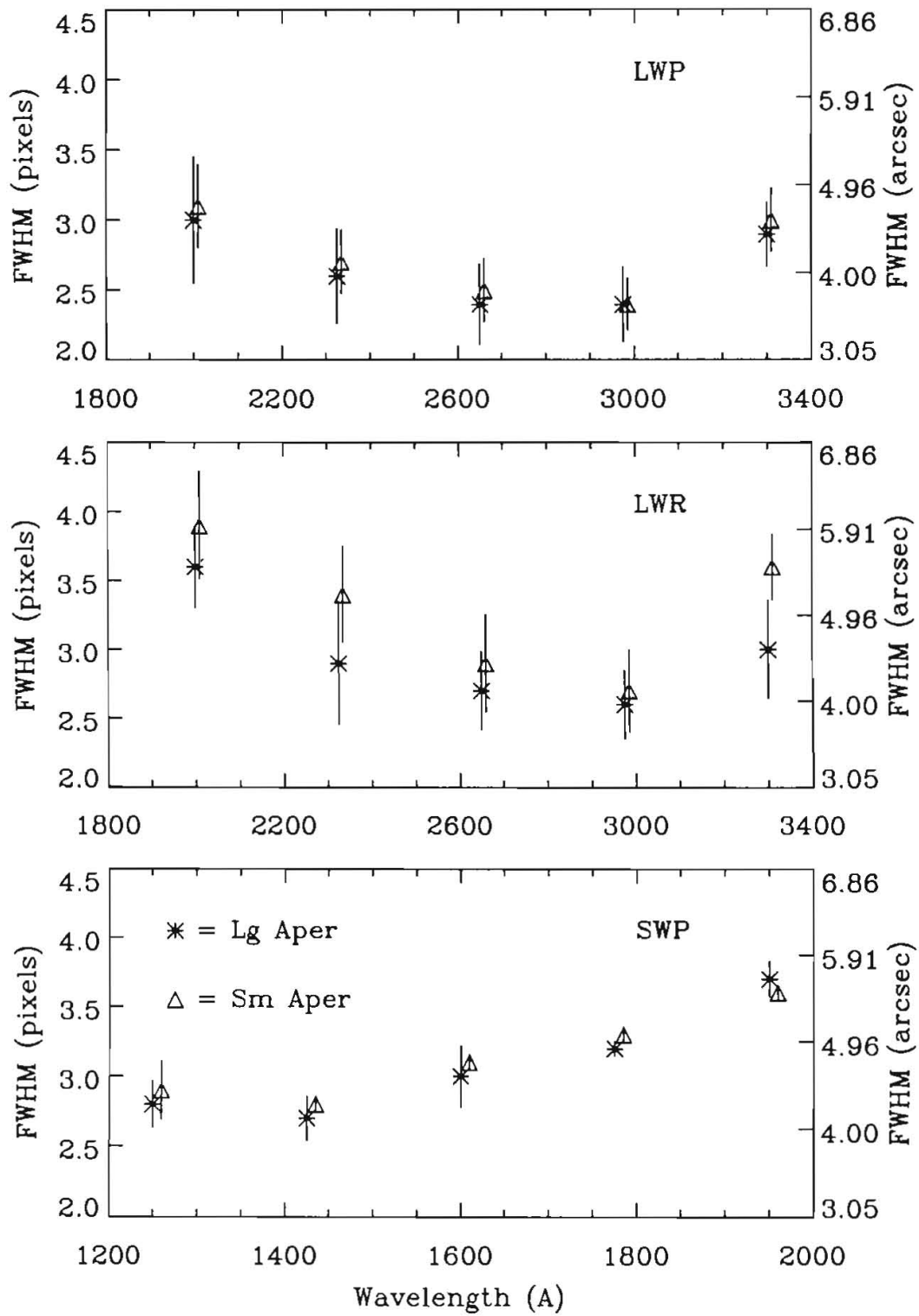
Figure 2.20: Low-dispersion spatial resolution.

Chapter 3

Raw Image Screening

Certain operations performed by NEWSIPS may be categorized as screening or preprocessing operations which prepare the data for subsequent processing. The procedures of this nature which are performed on *IUE* data are described in this chapter.

3.1   Bright-Spot Detection

Long *IUE* exposures characteristically contain "bright spots", *i.e.*, pixels with unusually high DN (data number) values which are comprised of discrete impulse noise often reaching the saturation level. Such bright spots are thought to be caused either by permanent blemishes in the target surface, by extraordinarily sensitive ("hot") pixels which result in recurrent bright spots at fixed locations, or by radiation-induced events within the UV converter which result in randomly placed, nonrecurrent bright spots (Ponz, 1980a,b).

Ponz (1980a,b) has described an algorithm for detecting in raw images bright spots of either kind on the basis of their limited spatial extent and unusual brightness values, primarily through a median filtering technique. The NEWSIPS bright spot detection algorithm is based on the procedure used in standard IUESIPS processing, which incorporates this method to flag bright spots as described below.

Let DN (i,j) be the DN value of the pixel at line i, sample j. Further, let AVE and MED represent operators which return the weighted average and median values of their argument, respectively. Then the pixel at (i,j) is detected as a bright spot if:

$$DN(i,j) > AVE\{DN(k,l)\} + \Delta \tag{3.1}$$

and

$$DN(i,j) > MED\{DN(k,l)\} + \Delta \tag{3.2}$$

where Δ is a DN threshold value, and (k,l) are positional elements of a 7-pixel spatial window centered on the pixel at (i,j) and oriented on the diagonal (*i.e.*, nearly along the dispersion direction). The condition in equation 3.1 is included to reduce the number of times the median operation in equation 3.2 is performed, thereby saving computer time.

In practice, the spatial windows are weighted according to the weights $(0, 0, 1, 0, 1, 0, 0)$, and a threshold value of $\Delta = 90$ DN is employed. The area of the image searched for bright spots corresponds to the entire camera faceplate regardless of dispersion. This differs from the IUESIPS approach, which only examined the regions containing spectral information. Pixel locations detected as bright spots are written to an output flag file (Chapter 5) subsequently read by the spectral extraction routines (Chapter 9) so that extracted fluxes derived from bright spot pixels may be flagged appropriately.

Several reports have been written that list the permanent or recurrent bright spots for the three cameras. Ponz (1980a,b) has published partial listings of recurrent bright spots in the SWP and LWR cameras which are listed in Tables 3.1 and 3.2. The table entries include the line and sample positions in the raw frame of reference and the approximate corresponding wavelengths for the various dispersion modes and apertures. The "B" notation means the background spectrum is affected. This work has been supplemented by Imhoff (1984a), who provided positions of additional permanent blemishes in the LWP and LWR cameras, given in Table 3.3. A more recent publication by Crenshaw *et al.* (1990) also details the recurrent bright spots, which are labeled as "camera artifacts", in low-dispersion spectra. These features appear at fixed locations in spectra with long exposure times yet are not detectable in spectra with exposure times shorter than an hour. They also determined that the artifacts appear to scale in intensity with the total background exposure level. Artifact positions of the more prominent features are listed in Table 3.4 as a function of wavelength.

3.2 Microphonic Noise Detection

IUE images are preprocessed in order to detect the presence of periodic noise interference ("microphonic noise"). In the SWP camera, interference often covers all of the image and its amplitude is generally low (often only 1–3 DN) compared to random background noise (Northover, 1980), making detection difficult. In the LWR, however, the microphonic noise has different characteristics, being localized chiefly in a small number of image lines, well-modeled by an exponentially dampened sinusoid, and with a peak amplitude typically in excess of 20 DN (Northover, 1980; Panek and Schiffer, 1981). The LWR microphonic noise is descriptively referred to as a "ping" because of its sudden onset and rapid decay. Unless an extended heater warm-up prior to image read is used as a ping avoidance technique, a given LWR image has about an 85% probability of suffering a ping, generally in the lower one-third of the image (Holm and Panek, 1982). If the heater warmup procedure is used, the ping is typically displaced to the top of the image where it does not impact the useful data. .

Utilizing techniques developed by K. Northover (1980), the microphonics screening done by NEWSIPS for all LWR images is based on the characteristics of the image data in the last 32 samples of each image line. This area is outside of the target region, and pixel values are zero except for noise. Lines affected by the microphonics are initially identified by thresholding the variance of the last 32 samples; the interference amplitude is then estimated

Table 3.1: Hot Pixels in the LWR Camera

| Raw Image | | Low Dispersion (Å) | |
Line	Sample	Large Aper.	Small Aper
126	291		
170	200	1780	1775 B
175	369		
178	610		
208	391		
215	326		2130
257	323	2190	
333	317		
412	385		
434	479		
518	545		
532	307		
680	332		

Table 3.2: Hot Pixels in the SWP Camera

| Raw Image | | Low Dispersion (Å) | |
Line	Sample	Large Aper.	Small Aper
292	413		
352	501		
392	127	1795 B	
398	521		
410	535		
482	342		
568	127		
611	387		

Table 3.3: Permanent Blemishes in the LWP and LWR Cameras

Camera	Raw Image		Comments
	Line	Sample	
LWP	101	525	
	205	319	
	396	384	Fuzzy Patch at $\lambda \sim 2482$Å in order 93
	409	208	Hole at $\lambda \sim 2880$Å in order 80
	426	435	
	455	35	
LWR	169	499	
	364	60	

Table 3.4: Low-Dispersion Camera Artifacts (Å)

Camera	Source Type	
	Point	Extended
LWP	None	None
LWR	2256	2256
	3087	3087
SWP	1279	1279
	1288	1288
		1491
		1535
	1663	
		1750

on the basis of the power spectrum of the sampled data, with successive image lines processed in pairs. Pixels in image lines with estimated noise amplitudes in excess of the chosen threshold (corresponding to a peak-to-peak noise amplitude of approximately 10 DN) are flagged in the quality flag image with a ν flag value of -16. This condition, which is documented by a notation in the image processing history portion of the label (Chapter 12) and noted in the core data item ABNMICRO, is subsequently used by the spectral extraction routine (Chapter 9) to flag extracted fluxes derived from lines affected by the microphonic interference.

3.3 Partial-Read Image Processing

"Partial-read" images are those for which only a portion of the target has been read. By not having a full 768×768 array readout, a substantial fraction of the operations overhead time associated with the camera readout and subsequent preparation for the next exposure is reduced. Partial-read images are used only in the low-dispersion mode and are always read out in a standard way so that a camera-dependent rectangular partial image, sufficient to encompass the entire region normally extracted in low-dispersion processing (Chapter 9), is generated. The partial-read images are preprocessed to imbed the partial-read area into a full 768×768 array for which DN values outside of the partial-read area are zero. This is done to enable the normal NEWSIPS processing, which works on 768×768 images, to occur without further special consideration of the partial-read nature of the images.

In order to prepare an image file in which to place the partial data, a zero filled blank image of 768 lines by 768 samples is generated. The partial-read data are inserted into the blank image using the positions tabulated by Imhoff (1991).

3.4 Missing Minor Frame Detection

Missing minor frames (MMFs) or "data dropouts" are flagged and recorded in the quality flag image, as well as noted in the output core data item keyword ABNMINFR. A minor frame consists of 96 consecutive pixel values read down in batch from the satellite. Minor frames are used to reconstruct the image, beginning at line 1, sample 1 by assigning values for incremental samples. Occasionally, one or more minor frames are corrupted or missing from the telemetry stream resulting in consecutive values of zero in the image. Such missing minor frames are detected automatically in the NEWSIPS system by screening the data for 96 consecutive values of zero. Only the target region is screened for missing minor frames; therefore, any MMFs outside the target area will not be detected or flagged. These 96 pixels are then flagged with a ν flag value of -8192. No attempt is made to interpolate across or correct for such data loss. A more detailed description of the *IUE* telemetry system can be found in *IUE Technical Note No. 30*.

3.5 Source Type Determination

This portion of preprocessing determines if the spectral data will be extracted as a point or extended source, as such information is needed in order to define the extraction slit width. This procedure was set up to require no human interaction, since processing of the data must be as automated as possible, and works with data of any dispersion. A quick rotation of the image to align the spectrum with the line direction is performed using a nearest neighbor resampling algorithm and a portion of the spectral region and background perpendicular to the dispersion direction is extracted. Starting and ending at a point 22 pixels (low dispersion) above and below the center of the spectrum, the DN values for every pixel along each line are averaged together. The resultant 1-D array of numbers represents an average cross-cut of the spectrum and by counting the number of pixels that are above the average background (Table 3.5), NEWSIPS determines whether the spectrum is a point or extended source. If the number of pixels is more than the listed value, then the spectrum is considered to be extended, otherwise it is a point source. The determination of point or extended source for

Table 3.5: Source Type Determination Values (number of pixels)

Camera	Dispersion	
	Low	High
LWP	15	9
LWR	15	10
SWP	15	10

large-aperture data is used to activate the de-tilting algorithm in the geometric correction step for certain object classes and to set the width of the spectral extraction swath. If no flux is detected in the large aperture, the source type is set by default using an object class look-up table. Object classes 1–3 and 6–8 default to extended-source extraction. All other object classes default to point source extraction, with one notable exception. If a large-aperture spectrum is designated a multiple or a trailed exposure, it will always be extracted as extended, regardless of the results of the automated spectral width determination. Trailed images acquired along the x- or y-axis are not detilted; multiple exposures acquired along the aperture axis are detilted. For small-aperture data, the procedure only sets a flux/no flux flag, as all exposures in this aperture are considered to be point source for purposes of extraction.

3.6 Serendipitous Spectrum Recognition

Using the algorithm described above, the NEWSIPS software always searches for detectable flux in both apertures for low-dispersion data, regardless of the documentation on the original observing script of which and how many apertures were exposed. If flux is detected in an

aperture that was not originally documented as exposed, the FITS keyword "SERENDAP" will appear in the output files for that image indicating a serendipitous exposure is present and in which aperture.

If a serendipitous spectrum is detected with the NEWSIPS software, the aperture-dependent Core Data Items (CDIs) for the primary spectrum will be copied to the CDIs for the serendipitous spectrum. The coordinates for the serendipitous exposure will be calculated from the primary coordinates using the following algorithm:

$$RA(s) = RA(t) + \Delta RA$$

$$DEC(s) = DEC(t) + \Delta DEC$$

where $RA(s)$ and $DEC(s)$ are the coordinates of the serendipitous pointing, and $RA(t)$ and $DEC(t)$ are the coordinates of the target. ΔRA and ΔDEC are computed in units of arcseconds as follows:

$$\Delta RA = -0.2680 \times (FESX(s) - FESX(t)) \cos \Psi + 0.2617 \times (FESY(s) - FESY(t)) \sin \Psi$$

$$\Delta DEC = -0.2680 \times (FESX(s) - FESX(t)) \sin \Psi - 0.2617 \times (FESY(s) - FESY(t)) \cos \Psi$$

where Ψ = spacecraft roll angle + 28.31 deg, $FESX(s)$ and $FESY(s)$ are the FES x and y coordinates of the serendipitous aperture, and $FESX(t)$ and $FESY(t)$ are the FES x and y coordinates of the target aperture.

Table 3.6: FES Coordinates of Apertures

Aperture	FES x, y
SWSA	243, -89
SWLA	94, -90
LWSA	47, 65
LWLA	-106, 52

The target name for the serendipitous exposure will be NEAR XXX. The HISTORY portion of the label will reflect that the main object is in the other aperture and the APERTURE keyword will be changed to BOTH. In the case that the serendipitous exposure is in the small aperture and the large-aperture spectrum is trailed, the serendipitous exposure is considered a trailed overshoot. The large-aperture coordinates and object name are copied exactly to the appropriate entries for the small aperture, as well as the aperture-dependent CDIs. In this instance, the coordinates are not recalculated and the object name is not preceded by "NEAR".

The NEWSIPS system also searches for unexpected spectral data in images classified as sky background. These images are usually acquired simultaneously with a pointed spectral exposure in another camera. If an image has an object class of 07 (sky background) and

37

spectral data are detected with the algorithm described above, processing is terminated and the *IUE* staff attempts to identify the pointed observation obtained in another camera contemporaneously with the image. Assuming the associated image can be identified, the coordinates will be derived from those of the main object and the object class changed to that of the main object. The target name is "NEAR XXX". If the associated image cannot be identified, then the object class is changed to "unknown". A COMMENT line in the FITS header will say, "SERENDIPITY WITH CAMXXXXX". If no spectral flux is detected in the image, processing continues as for a large-aperture extended source.

3.7   Background and Continuum Intensity Estimation

This section of code determines the maximum continuum and average background DN levels for spectral data in the raw image, as such information is stored in the FITS header and history portion of the label as keywords. Several portions of the spectral and background regions along the dispersion direction are extracted from the rotated image used in Section 3.5, carefully avoiding any emission lines. The brightest pixels along the dispersion are averaged together to derive the peak continuum level for each region. The approximate low-dispersion wavelengths for each region are listed in Table 3.7. To determine the background

Table 3.7: Wavelength Regions for Continuum Estimation (Å)

LWP	LWR	SWP
2120–2285	2405–2480	1255–1300
2595–2685	2565–2710	1310–1365
2850–2910	2850–2925	1830–1880
3070–3120	2985–3035	1925–1975

level, the DN values of a line of pixels parallel to the dispersion, midway between the large- and small-aperture spectrum, are averaged. The values for each area are compared and the maximum continuum and mean background values are recorded.

Chapter 4

Raw Image Registration

The NEWSIPS system relies upon an explicit determination of the registration between the raw science image and the raw space Intensity Transfer Function (ITF) to apply an accurate photometric correction (discussion of the ITF is deferred until Chapter 6). The image registration is derived using a linear cross-correlation algorithm with the fixed pattern found in all *IUE* raw images as the registration fiducial. In this context the fixed pattern is a manifestation of systematic variations in sensitivity from pixel-to-pixel over the entire image.

4.1 Registration Fiducial

Although the reseaux have traditionally been used for image registration purposes, using the fixed pattern as the registration fiducial has several advantages over the reseaux – one being that fiducials can be found anywhere on the exposed part of the image, so that many more such fiducials are available than reseaux. Also, the fixed pattern can be detected at even the lowest exposure levels, which eliminates the need for predicted information. Finally, the presence of the exposed spectrum can be excluded from the cross-correlation region, and therefore, does not inhibit the use of the fixed pattern in the surrounding background (De La Peña *et al.* 1989, 1990).

A consistent fixed pattern has been shown to be present in the literally thousands of raw *IUE* images tested. However, using the ITFs as the fixed pattern reference, it is known that the character of the fixed pattern is modulated to some degree by observation date and camera temperature (Bushouse 1991b).

4.2 General Method

The registration algorithm employs a pattern matching technique which depends heavily upon the linear cross-correlation function to identify similar patterns between a raw science image and the raw space ITF. A rectangular grid of fiducial positions (centered 28 pixels

apart) has been defined for each camera and dispersion. At each defined position, a cross correlation is performed to determine the displacement between the raw image and the ITF at that locale. Specifically, at each locale an array (*template*) of 23×23 pixels of the raw science image is used for comparison to a corresponding array (*window*) of 29×29 pixels of the raw space ITF image. The window is larger than the template in both dimensions such that the template can be moved about the window to "search" for the best correlation location. It is known from a number of analyses that the maximum extent to the motion of the fixed pattern in most raw images is only a few pixels. Therefore, the window size is ordinarily set in the NEWSIPS pipeline processing to accommodate motion of only a few pixels, but the size can be varied, if necessary.

Once a pattern match location is found to whole pixel accuracy at a defined fiducial locale, the match location is evaluated via a series of statistical tests to validate the result. Upon validation, further computations refine this determination to the sub-pixel accuracy required for an accurate photometric correction.

After all the valid pattern match locations for a camera and dispersion have been derived to sub-pixel accuracy for the raw science image, the determinations are viewed as spatial deviations and examined as an ensemble for consistency. Displacements which do not conform in a general sense to a smoothly varying function are adjusted to conform. Finally, after all the fine tuning has been completed, a full three-dimensional displacement image ($768 \times 768 \times 2$) is created for ΔSample and ΔLine using a bi-cubic spline interpolation scheme.

4.3   Pattern Matching Algorithm – Step by Step

The following elaborates the procedures incorporated into the image registration algorithm. Fiducial locations which have been pre-defined for each camera and dispersion are accessed; these are hereafter referred to as the sampling locations. For each sampling location, the following steps are performed.

1. The raw science image template is classified by its computed median Data Number (DN), and the ITF level possessing a comparable DN value at that location is chosen for correlation purposes.

2. Any reseaux, hot spots, cosmic ray hits, and spectral information are ignored in the template during the correlation analysis. These artifacts contaminate the science template with features not present in the ITF window and are temporarily masked during the correlation procedure.

3. The template is sequentially positioned throughout the window, and at each position a linear cross correlation is performed. For each position a correlation coefficient is computed and the corresponding coordinates (pixel accuracy only) are saved. By virtue of the sizes of the template and search windows, a total of forty-nine correlation coefficients are computed to determine the best pattern match location to pixel accuracy for

each sampling location. These forty-nine coefficients are actually in the form of a 7×7 matrix which corresponds to the overlap positions of the template upon the window. The maximum coefficient in this sample is assumed to be the best representation for a true match.

The cross-correlation coefficient is defined as

$$r(m,n) = \frac{\sum_x \sum_y (w(x,y) - \overline{w(x,y)})(t(x-m,y-n) - \bar{t})}{(\sum_x \sum_y (w(x,y) - \overline{w(x,y)})^2 \sum_x \sum_y (t(x-m,y-n) - \bar{t})^2)^{1/2}} \qquad (4.1)$$

where $-1.0 \leq r \leq +1.0$. In this equation, $\bar{t}$ is the average value of the template, $\overline{w(x,y)}$ is the average value of the portion of the window which is currently coincident with the template $t(x,y)$, the line coordinate $m = 0, 1, 2, ..., (L-1)$, and the sample coordinate $n = 0, 1, 2, ..., (S-1)$. For the purposes of this implementation, $L = 29$ and $S = 29$ which are the nominal dimensions of the correlation window; the template dimensions are 23×23 pixels. Summations are performed over the coordinates common to both w and t.

4. The maximum correlation coefficient must pass several statistical tests to be considered a valid correlation:

   - There must be a minimum of 139 (13×13) non-rejected pixels in the template for the correlation to be performed at all (see Item 2);

   - The maximum correlation coefficient cannot reside on the edge of the correlation matrix;

   - The probability distribution criterion of less than 1% must be satisfied;

   - There can be no other "local" maxima in the correlation matrix within 0.25 sigma of the absolute maximum coefficient. Sigma is the standard deviation of the correlation coefficient matrix.

   - The maximum correlation coefficient must be at least two sigma greater than the rest of the coefficients in the matrix.

5. If the coefficient is deemed valid, the position of the pattern match is then determined to sub-pixel accuracy. The original ITF window data is resampled into successively finer and finer sub-pixel increments and the cross correlation with the template is repeated until 0.125 sub-pixel accuracy is achieved.

   If the coefficient is not validated by the tests described in Item 4, the sampling position is considered a bad location, and the algorithm passes onto the next sampling position.

4.3.1 Intermediate Registration Output

The intermediate results from the image registration algorithm can be used to monitor the geometric/photometric state of the raw science image. In the VD FITS output image, these

intermediate results are stored in a binary 3-D table extension containing the following output for each sampling position:

1. science image x-position (sample),

2. science image y-position (line),

3. ITF x-position of best match (sub-pixel accuracy),

4. ITF y-position of best match (sub-pixel accuracy),

5. maximum cross-correlation coefficient (computed for pixel location accuracy),

6. number of pixels used to calculate the correlation, and

7. the ITF level used for registration.

Items 1 and 2 are the pre-defined fiducial locations about which the image registration routine performs its search. Items 3 and 4 are the best match positions between the raw science image and the ITF image. Note that these final positions are in quantized units of 1/8 pixel; this is a consequence of the design of the image registration algorithm. Item 5 is the maximum correlation coefficient which can range between 0.0 and 1.0. In practice the correlations range between -1.0 and $+1.0$, but negative correlations have been deemed invalid. Item 6 is the number of points used to compute the correlation; this will range from 139–529 pixels for a 23×23 pixel template. If a larger template is used, the maximum number of points possible will change to be the size of the new template – $i.e.$, a 35×35 template $= 1225$ maximum number of points; the template is always a square. The minimum number of points is fixed at 139 pixels. Item 7 is the ITF level used for the correction and will range in value from 1 to 12.

The total number of entries in this binary 3-D table extension is both camera and dispersion dependent. Table 4.1 contains the number of fiducial locations defined at this time.

Table 4.1: Number of Fiducial Locations

Camera	Number of Locations Low Dispersion	Number of Locations High Dispersion
LWP	150	490
LWR	151	511
SWP	139	510

The data contained in the binary 3-D table extension can be used to produce diagnostic plots for the image registration. Figure 4.1a shows the displacements computed between an SWP low-dispersion image and the SWP ITF. The small boxes denote the fiducial locations where a successful correlation was determined. The associated vector represents

42

the computed displacement between the raw science image and the ITF; the displacement vectors have been magnified for visual clarity. Single points mark the locations of fiducials with unsuccessful correlations. The dashed lines represent the region of the image that is photometrically corrected. Figure 4.1b shows the magnitude of the correlation coefficients corresponding to the results in Figure 4.1a. Larger plus signs denote stronger correlations. Recall that all of these correlations have passed the 1% probability distribution test which means that there is less than a 1% probability any of these correlations could have arisen by random chance.

Figure 4.2 illustrates the same information as the previous figure, for the case of high-dispersion data.

4.4 Evaluation of the Raw Correlations

After all of the pre-defined fiducial locations have been investigated as individual entities, the computed results are examined as an ensemble of information. The goal is to create an idealized or smoothed version of the actual displacements and then compare the smoothed values to the actual values, making adjustments to the actual displacements if necessary.

The creation of the smoothed displacement image is done in two major stages. First, an averaging procedure is invoked for each successful correlation sample. The closest fiducial locations to the sample in question which also have successful correlations are weighted according to their "distance" from the sample in question and if there is deemed to be enough data, the displacements from all of these successful locations are averaged to yield a mean displacement for the smoothed image at the sample location in question. If enough data are not acquired in the pre-defined search region, the data point must be an isolated or semi-isolated correlation. Isolated or semi-isolated correlations which cannot adequately be compared to the immediate surroundings for spatial trends are considered invalid correlations "after-the-fact" and are permanently removed from consideration.

Once the averaged image is created, the displacements for the "missing" fiducial locations are filled in by an interpolation/extrapolation scheme. The search for missing data is performed in a radial sense, starting at the center of the low- or high-dispersion photometric correction region. An extrapolation of the mean displacements is performed well outside the photometric correction limits to ensure that the bi-cubic spline fit done during the last stage of the image registration module is well-behaved for all pertinent data regimes.

The actual displacements are then compared to the smoothed interpretation and any displacements that differ by 0.25 pixel from the smoothed array are modified to conform to the smoothed displacements. These final displacement vectors are then expanded into a full three-dimensional (768 × 768 × 2) floating point displacement image (ΔSample and ΔLine) using a bi-cubic spline interpolation algorithm. The ΔSample values are located in the first level of the final image; the ΔLine values are located in the second level of the image.
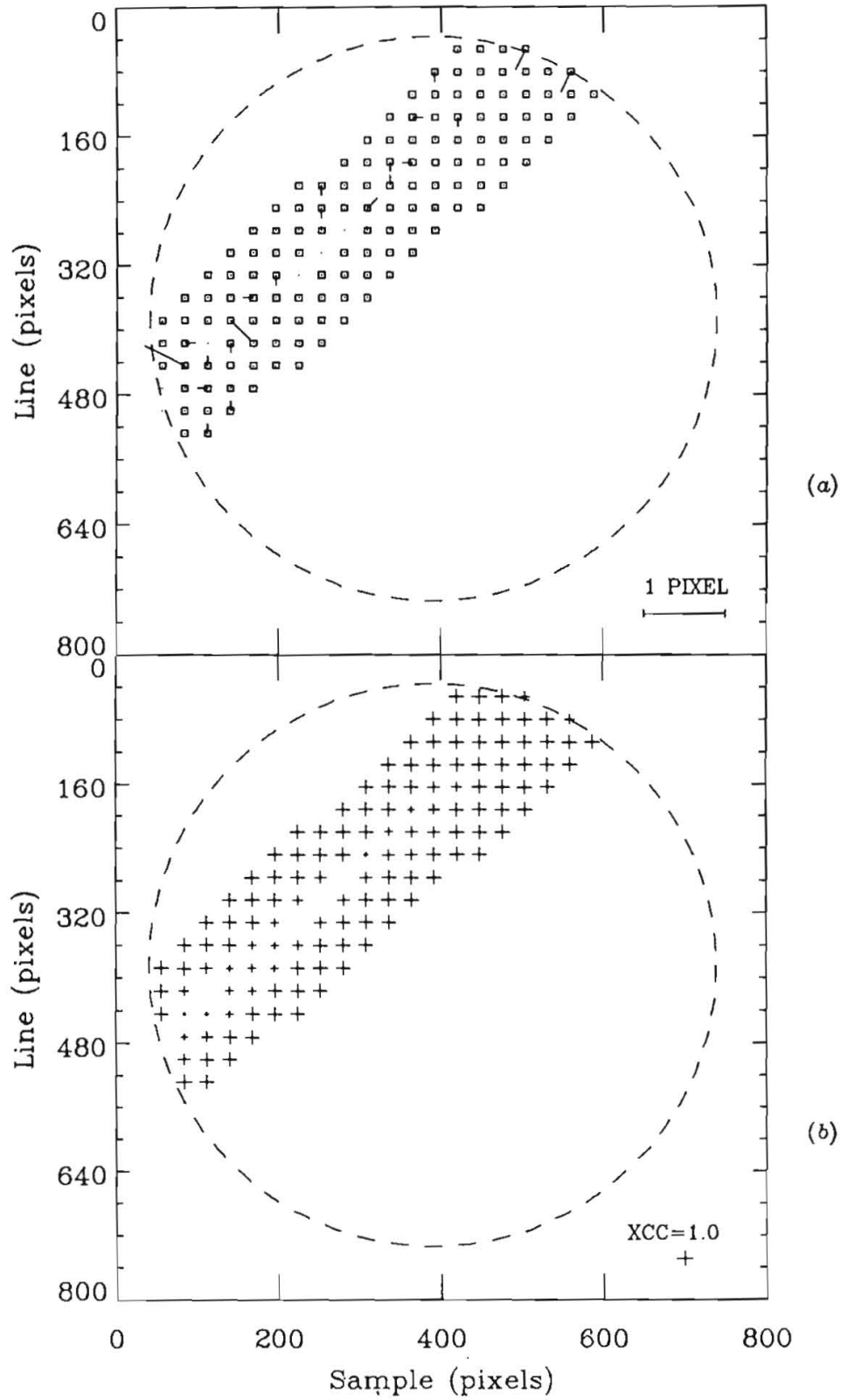
Figure 4.1: (a) Displacements computed between an SWP low-dispersion image and the SWP ITF. (b) Magnitude of the correlation coefficients corresponding to the results in Panel a.

44
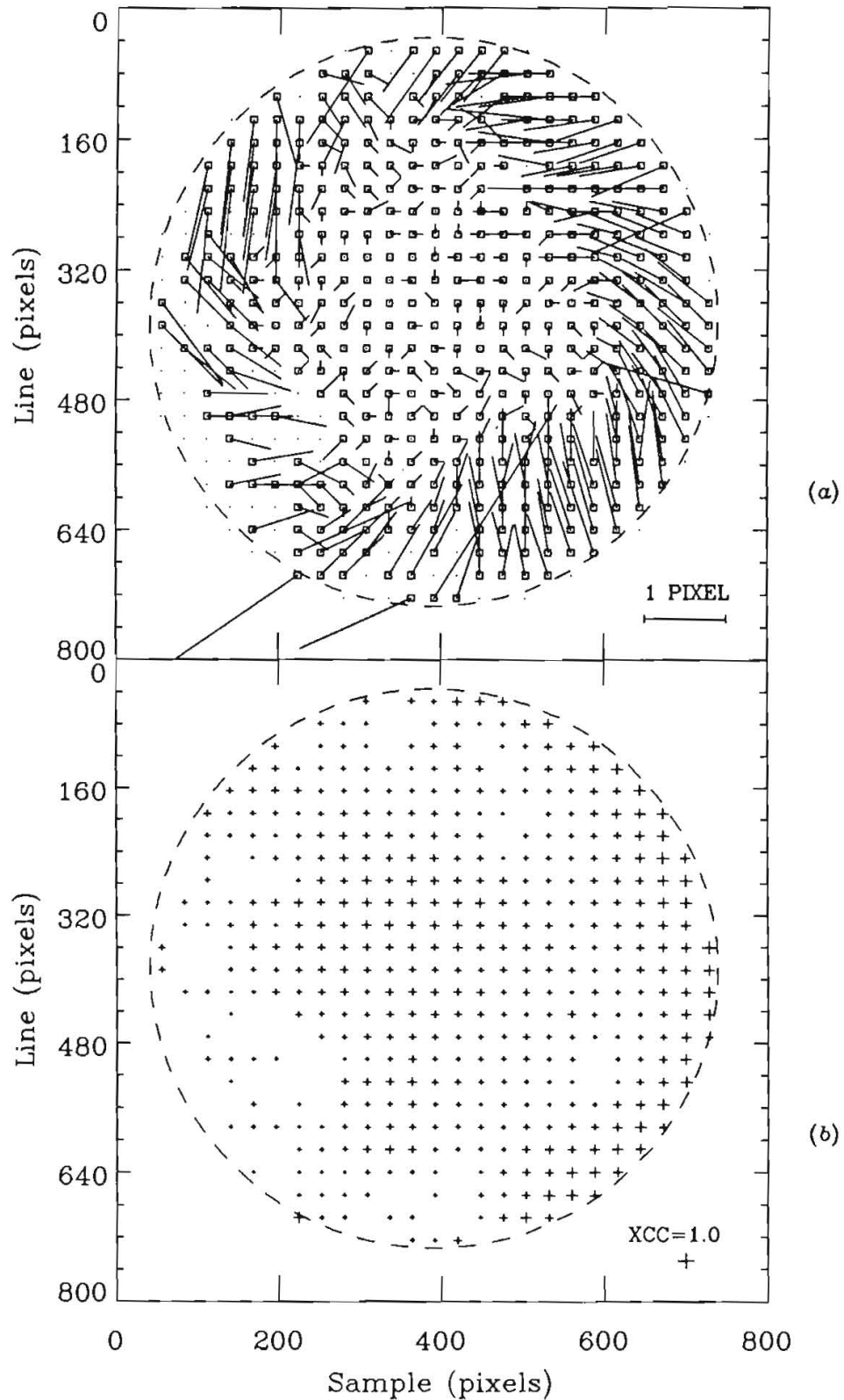
Figure 4.2: (a) Displacements computed between an SWP high-dispersion image and the SWP ITF. (b) Magnitude of the correlation coefficients corresponding to the results in Panel a.

4.5 Image Registration Output

The three-dimensional displacement image is the main output product for production processing from the image registration module. This image is used as input to the photometric correction scheme to align properly the raw science image to the raw space ITF image (Chapter 6). This image is also used by the geometric correction scheme as one of the vector components to the geometric resampling (Chapter 7). However, this specific image is not retained as an *IUE* Final Archive output product. As discussed in Chapter 7, the VD FITS image produced during the geometric correction procedure is the summation of all the geometric corrections implemented to perform the single image resampling. The raw cross-correlation information is retained as a binary 3-D table extension to the VD FITS image as discussed in a previous section of this chapter.

The image registration module writes information to the HISTORY portion of the image label for each raw science image processed:

- Window size,

- Template size,

- ITF identification,

- Number of successful correlations out of the total possible for that camera and dispersion,

- Median cross-correlation coefficient,

- Standard deviation of the cross-correlation coefficients,

- Average displacement computed,

- Maximum displacement computed, and

- Number of isolated or semi-isolated displacements filtered.

The image registration algorithm does not generate any ν flag values.

Chapter 5

Data Quality Flag Description

For the creation of the *IUE* Final Archive, data quality flags (ν flags) are provided on a pixel-by-pixel basis for the two-dimensional LI (photometrically corrected) and SILO/SIHI (resampled) output images, and as a function of wavelength in the one-dimensional extracted spectral data (MXLO). These quality flags denote exceptional conditions in the data which can range from fairly minor situations of telemetry dropouts in the background regions to quite serious conditions of telemetry dropouts in extracted spectral regions. The ν flag values have been assigned such that the more serious conditions have the more negative values in order to provide an immediate indication as to the severity of the problem condition. However, in contrast to the method of "epsilon" flagging as implemented in IUESIPS, where only one problem condition is noted (*i.e.* the most severe), the ν flags are encoded to indicate all problem conditions associated with each pixel or wavelength bin.

The flexibility of the ν flags is derived from the bit-encoding of the individual problem conditions. Using a total of 16 bits, the flags are stored as negative values (bit 16 contains the sign), and the remaining 15 bits are utilized to represent each defined problem condition. Table 5.1 describes the problem conditions and defines the assigned ν flag values. Once all problem conditions are identified for each pixel or wavelength bin, the individual flag values are added together to produce a total value which is a unique combination of its components.

Since additional data quality flags are available for the Final Archive dataset, and some problem conditions may have an altered definition when compared to the IUESIPS ϵ flags, a more detailed definition of the ν flags is in order. Some of the flags, or more properly, the pixel locations of the flags, have been pre-defined based upon the location of the condition in the ITF images. The region to be photometrically corrected is based upon the shape of the illuminated target region of the ITF; this region is nearly a circle for the SWP camera, but resembles more of a flattened circle for the long wavelength cameras. Consequently, the low-dispersion swath is a band contained within this pseudo-circular region, optimally positioned about the low-dispersion spectrum. The warning track is an approximately five pixel deep buffer zone on the data side of the edge of the non-photometrically corrected region. In most instances, the photometric correction of an individual pixel depends somewhat upon its neighbors. As the edge of the photometrically corrected region is approached, there can

Table 5.1: ν Flag Values

Condition	ν Flag Value	BIT
Pixels not photometrically corrected	−16384	15
Telemetry dropout (Missing Minor Frame)	−8192	14
Reseau (in the ITF)	−4096	13
Permanent ITF artifact	−2048	12
Saturated pixel (w.r.t. ITF pixel DN)	−1024	11
Warning track (near edge of PHOTOM region)	−512	10
Extrapolated ITF curve – above level 12	−256	9
Extrapolated ITF curve – far below level 1	−128	8
Cosmic ray hit/bright spot	−64	7
SWET "Cosmic Ray"	−32	6
Microphonics (LWR only)	−16	5
Interpolated background (high-disp. only)	−8	4
Telemetry dropout in extracted background	−4	3
Uncalibrated data point (extracted data only)	−2	2
No known problem condition	0	0

be wild fluctuations in the DN (and hence the resulting FN) values, so that the photometric correction may be less reliable in these regions, and hence, a warning is issued concerning these less reliable flux values. The positions for all permanent artifacts, reseaux, and blemishes are defined according to their locations in the ITF images, and are flagged after the science image and the ITF are properly registered. The saturation level for each pixel within the photometrically corrected region has been derived by examining the ITF curve of each pixel and determining the DN associated with any substantial leveling off of the ITF curve (DN vs. exposure time) with increased intensity. According to the analysis of the ITF images, there are a number of pixels which "saturate" at values considerably less than 255 DN. *Consequently, many more pixels may be considered saturated by the NEWSIPS system than IUESIPS*, since in IUESIPS only pixels with a DN of more than 250 are considered saturated.

During the raw image screening stage of the image processing, software modules examine the raw science image for cosmic ray hits/bright spots, microphonics (the LWR "ping"), and missing minor frames (MMFs). While the detection of cosmic rays/bright spots and microphonics are implemented as in IUESIPS, the detection and flagging of MMFs is a new implementation. Clearly, it is important to know of the existence of a MMF in the vicinity of the spectral information in order to evaluate the extent to which the MMF will affect the data.

The bright spot detection algorithm implemented in the two-dimensional pre-viewing stage of the raw science image is an application of a median filtering technique and identification of the spots is based upon their limited spatial extent and unusual brightness. This flag is differentiated from the SWET extraction cosmic ray flag, which is implemented during the extraction phase of the processing, and is essentially a sigma rejection criterion. SWET extraction examines the profile values in the cross-dispersion direction in each wavelength bin and compares the actual data to the profile, rejecting those values more than the estimated sigma from the fit, as determined by the SWET noise model. See Chapter 9.1.6 for the discussion of the creation of the 1-D ν flag vector which accompanies the extracted spectrum.

During the photometric correction stage of processing, extrapolations required for the conversion from DN to FN values are appropriately flagged as positive (DN above Level 12) or negative (DN far below Level 1). Positive extrapolations are not actually performed, but rather pixels whose DN values exceed the corresponding ITF Level 12 pixel DN are simply set to the FN associated with Level 12 of the ITF. Due to DN shifts in the null pedestal, the background regions of many raw science images have an average DN below that of the ITF. In order to make the negative extrapolation flag useful, only excessive negative extrapolations are flagged (*i.e.*, images with DN values below the negative extrapolation reference image). The negative extrapolation reference has been derived by smoothing an image with 50% of the intensity in the null. It should be understood that the FN for any pixel with a DN below the DN of the corresponding pixel in the null level of the ITF is determined with a two point extrapolation; only the excessive two point extrapolations are flagged.

The interpolated background flag is used to denote regions in the high-dispersion image

where the background has been modelled using an empirically determined point spread function and taking into account the relevant global inter-order flux information across the image region.

Telemetry dropouts are flagged in the two-dimensional images as MMFs, but it is important to translate this information into how these dropouts affect the extracted spectral data and extracted background. In essence, the MMF flag is split into two values for the one-dimensional ν flag vector which accompanies the extracted data. The first flag retains the -8192 value and is used to represent the critical information of missing pixels in the spectral data. The second flag has the value of -4 and is used to denote missing pixels in the extracted background. Since the background is fit with a Chebyshev polynomial, missing pixels in the extracted background potentially play a very small role in the computation of the net flux. The much smaller absolute value of the second flag reflects the much less crucial nature of the condition.

The uncalibrated data flag is found only in the extracted spectrum and indicates wavelength regions which have been extracted from the SILO/HI image, but whose absolute flux calibration has not been defined.

Because the ν flags are stored as negative integers, it is necessary to warn the user on how to interpret these data properly. Negative integers are stored in two's complement form by most computer systems. This means that the internal bit settings for negative values are derived by subtracting the desired value from 2^{15} or 2^{31}, for 2 or 4 byte integers respectively. Hence, many more bits are turned on (set to 1) to represent the negative integer than just the bits for the actual digit. Consequently, if intrinsic bit decoding functions are used to decode the ν flag values as is, the wrong answer will be derived. It is most straightforward to first take the absolute value of the ν flag image or vector before attempting to interpret the data.

Chapter 6

Photometric Correction

Non-linear photometric response and spatial sensitivity variations in the detectors are present in all raw data and must be taken into consideration before the data can be utilized for scientific purposes. In accounting for the detector response, the photometric correction procedure converts the raw Data Numbers (DN) into normalized Flux Numbers (FN) which are linearly related to the incident photon flux. The photometric correction is performed on a pixel-by-pixel basis in the two-dimensional image.

The photometric correction procedure in NEWSIPS differs in two fundamental ways from the correction performed in IUESIPS. The Intensity Transfer Functions (ITFs) (*i.e.*, graded ultraviolet floodlamp exposures used to linearize and normalize the camera response) are constructed in a manner which eliminates the necessity to resample, and consequently degrade, the data and preserves the inherent characteristics of the detector. In addition, a more precise image registration technique (Chapter 4) is used to align accurately the raw science data with the ITFs (Shaw 1990, De La Peña *et al.* 1990).

6.1 Construction of the ITFs

6.1.1 Images

The modern epoch ITF series used for the Final Archive (LWP:1992, LWR:1983, and SWP:1985) were obtained in a closely monitored and stable satellite configuration such that any parameters known to affect the image quality (*e.g.*, camera temperature) were carefully controlled. These improved acquisition procedures ensured that the constituent ITF images at each exposure level have little geometric distortion relative to each other. The ITFs for the Final Archive have been constructed in raw space with no attempt to align geometrically the images, because some smoothing of the ITF data is inherent in such an alignment. The raw images for each level were averaged on a pixel-by-pixel basis to form a mean level. If the intensity level of a pixel from one of the component images varied from the mean intensity value for that pixel by more than 2.5 sigma for the SWP and LWR ITFs and 1.4 sigma for the LWP 1992 ITF, the deviant pixel was excluded from the sum. In this way it was

51

possible to use images with missing minor frames in the construction of the ITF. Each level of the ITF is constructed with at least 4 images; the null level was typically constructed with many more images. The resulting ITF for each camera is a 3-dimensional file of dimensions $768 \times 768 \times 12$ pixels.

The lowest level of the ITF is a zero exposure or null level which is the background left by the standard camera flood/erase preparation procedure. Correspondingly, the highest level of the ITF has a long enough exposure time to allow the detector to achieve its saturation limit of 255 DN over a majority of the image. The intermediate ITF levels map the camera response through the mid-range of DN values. The 12 level ITF provides sufficient granularity in intensity to allow linear interpolation between the levels.

6.1.2 SWP ITF

At the time of construction of the SWP ITF for use in the Final Archive, two ITF series had been acquired for that camera. The images that comprise the ITF acquired in 1978 were not acquired under stable spacecraft conditions and are geometrically dissimilar to each other. These images cannot be used to construct a raw space ITF, which requires minimal distortion among the images. The images acquired for the 1985 ITF comprise a geometrically homogeneous group. Therefore, the images acquired for the 1985 ITF were used to construct the raw space ITF for the Final Archive processing. In 1992, a new ITF for the SWP camera was acquired, but there are no current plans for use of this ITF in the Final Archive processing.

6.1.3 LWP ITF

The ITF originally acquired for the LWP camera in 1978–1980 was a "mini-ITF" with one image for most of the levels. These images were taken under widely varying spacecraft conditions, with some images taken during optimization testing when camera parameters were deliberately modified. The ITF taken in 1984 was taken under controlled conditions and the images are geometrically similar, allowing the construction of a raw space ITF. However, it was discovered during testing of this ITF that the LWP dataset of science images divide generally into two subgroups. Images taken before 1984 tend to have similar geometric distortions to one another, and images taken after 1984 tend to have similar geometric distortions, but the two subgroups are not geometrically similar to each other. Clearly, there was a discrete change in the camera operating parameters in 1984, probably in the voltages set in the camera, but the information available via telemetry is not sufficient to identify the exact nature of the change. Unfortunately, images taken before the 1984 ITF (a very small percentage of the total LWP dataset) are geometrically similar to the LWP ITF (Epoch 1984). Images taken after the 1984 ITF are not well aligned with the 1984 ITF. This situation prompted the acquisition of a new ITF for the LWP camera in 1992.

The LWP ITF acquired in 1992 is virtually always better aligned in raw space with the science images acquired since 1984 than the 1984 ITF. However, the bimodal nature of

the image distortion for the LWP camera manifested itself in the null images acquired for the 1992 ITF. The null level images formed two discrete groups. Approximately half the null images are geometrically similar to each other and form an internally consistent group (Null A). The other group of null images (Null B) are geometrically similar to each other in raw space, but the two groups are not sufficiently aligned geometrically to be co-added without loss of accuracy in the photometric correction. While somewhat more than half of the science images acquired with the LWP camera are better aligned with Null B than Null A, the intensity level of Null B is higher than that of Null A, resulting in the science data not being fully bracketed by the calibration ITF data in intensity when Null B is used. The Final Archive processing uses the 1992 LWP ITF constructed with Null A.

6.1.4 Periodic Noise

All raw *IUE* images suffer from periodic noise (Nichols-Bohlin 1988, Shaw 1989) which is constant in raw space. The noise has been found to be multiplicative in nature and ranging from 1% to 8% in amplitude; however, the particular periodicities present and the amplitude of the noise are camera specific. Due to geometric distortion, the periodic noise in the ITF will not, in general, align with the noise present in the science image, and therefore, the periodic noise has been filtered from the ITF images using a Fourier-filtering technique. For the SWP camera, noise spikes were filtered every 192 points in the line direction and every 16 points in the sample direction in frequency space. For the LWP camera, noise spikes were filtered every 12 points in the line direction and every 16 points in the sample direction. The noise features in the LWR camera are much larger (8%) than the other cameras; noise spikes every 192 points are filtered in both the line and sample directions.

6.2 Determination of the Effective Exposure Times

The effective exposure times for the 1983–1985 Epoch ITFs were derived by Imhoff (1984b and 1986) and by De La Peña (1992a) for the 1992 Epoch LWP ITF. During the creation of the 1983–1985 ITFs in their own geometric space for the NEWSIPS system, if additional images were deemed usable in contrast to those originally chosen by Imhoff, the effective exposure times were modified to reflect the use of additional images.

6.2.1 Effective Exposure Times

Table 6.1 lists the effective exposure times (FN exposure values) for each level of the ITFs used in the Final Archive. These exposure values have been normalized to an arbitrary scale such that the FN associated with the lowest level of an ITF is 0.0.

Table 6.1: ITF Effective Exposure Times (seconds)

Level	SWP Epoch 1985	LWP Epoch 1992
1	0.000	0.000
2	32.919	38.750
3	67.946	78.737
4	104.147	121.868
5	131.397	168.958
6	166.296	200.756
7	223.034	237.941
8	269.680	278.107
9	340.471	341.073
10	408.490	396.582
11	473.749	483.497
12	575.995	561.518

6.3   Description of the Photometric Correction

The actual pixels photometrically corrected in high dispersion reside within a region defined by edge-detection algorithms on raw, well-exposed UV Flood images. These pseudo-circular regions coincide with the target boundary. For low dispersion, only a diagonal swath of data encompassing both the large and small apertures, as well as a generous portion of the background, is photometrically corrected.

The photometric correction procedure accesses *explicitly* determined displacements between the raw science image and the ITF to align the two images and to convert the DN to FN. These displacements have been derived using the image registration technique as described in Chapter 4.

6.3.1   Determination of the ITF Pixels

Displacement vectors calculated in the image-registration step map each pixel in the raw science image to the geometric space of the ITF, where the final displacement coordinates are floating point coordinates. If the final coordinates for the science pixel are within 0.125 pixel (in either the line or sample direction) of the integer coordinates of an ITF pixel, the science image pixel is assumed to be coincident with the ITF pixel and the FN computed will be based upon data contributed only from the single ITF pixel. If the science image pixel is displaced by more than 0.125 pixel from the integer coordinates of any ITF pixel, the FN computed will be based upon data contributed from a 4×4 matrix of ITF pixels surrounding the final position in question. Both of these scenarios will be described in further detail in the next section.

6.3.2 Determination of the Flux Values

In contrast to the original IUESIPS photometric correction, the raw DN values are converted to linearized FN values directly from the effective exposure time associated with each level of the ITF. For a given pixel the FN associated with level i of the ITF is:

$$FN_i = T(i)$$

where $T(i)$ is the effective exposure time in seconds for level i.

There are four basic methods for the determination of the FN of a raw science image pixel from a single ITF pixel (for the case where the displacement coordinates of the science image are ≤ 0.125 pixel from the ITF pixel coordinate). Where $DN(ITF_1)$ equals the DN level of the relevant pixel in the first ITF level; $DN(ITF_{12})$ equals the DN level of the relevant pixel in the twelfth ITF level; DN_{raw} equals the DN level of the science image pixel; and DN_{sat} equals the DN level of saturation for the relevant pixel, the four options are:

- **Fully calibrated data:** When $DN(ITF_1) \leq DN_{raw} \leq DN(ITF_{12})$, the FN is determined with a linear interpolation algorithm. The interpolation is performed between the two ITF levels that bound the input DN in intensity.

- **Saturated data:** When $DN_{raw} \geq DN(ITF_{12})$ and $DN_{raw} \geq DN_{sat}$, the FN is set to a constant (the FN exposure value) which is defined to represent the top level of the ITF (see Table 6.1). This raw image DN not only exceeds the intensity of the 12th level of the ITF, but it is also found to possess a saturated DN. The saturation DN has been determined on a pixel-by-pixel basis through analysis of the individual ITF curves. Saturation has been defined to be the DN at which the slope of the ITF curve (DN versus exposure level) approaches zero. Since ITF curves vary considerably from pixel to pixel, the ITF reference saturation limit varies from pixel to pixel. If a science image pixel is deemed saturated (by the above definition), that pixel is set to the saturated DN value for that pixel, unless the value is > 251 DN, whereupon the value is set to 251 DN. In all other instances (non-saturated pixels, pixels which achieve 255 DN before level 12 of the ITF), the saturation limit is defined to be 251 DN. The 251 DN represents the limit in the Analog-to-Digital converter, plus or minus some uncertainty due to the fact that the ITF is an average of several images. These pixels are flagged with the saturation flag of -1024. In the case where $DN_{raw} > DN(ITF_{12})$, the pixels are flagged with both the saturation flag of -1024 and the positive extrapolation flag of -256.

- **Positively extrapolated data:** When $DN_{raw} > DN(ITF_{12})$ and $DN_{raw} < DN_{sat}$, the FN is computed by a two-point extrapolation from the top two levels of the ITF. These pixels are flagged with the positive extrapolation flag of -256.

- **Negatively extrapolated data:** When $DN_{raw} < DN(ITF_1)$, the FN is computed with a two-point extrapolation from the bottom two levels of the ITF. However, the pixel is only flagged with an indication of negative extrapolation if the extrapolation is

considered excessive. For this purpose, the negative extrapolation reference image has been created by determining the 50% intensity level of the ITF null image, and smoothing these data with a 5-point boxcar in two-dimensions. Consequently, negative extrapolations are only considered excessive and flagged if $DN_{raw} < DN_{neg.\ ext.\ ref.\ image}$. Excessive negative extrapolations are flagged with a value of -128.

When there is significant misalignment (>0.125 pixel) between the raw science image and the ITF, a 4×4 matrix of ITF pixels surrounding the location in question is used to compute the relevant FN. Using the raw science image DN, an FN value is computed at each of the 4×4 locations in the matrix, using the above described single pixel scenarios. The median FN in the matrix is computed, and then deviant values are eliminated from the FN matrix and replaced with the median FN. FN values are considered to be deviant if they are different from the median by more than 100 FN. Once the FN matrix has been defined and deviant values replaced, the matrix is fit with a spline surface which is evaluated at the final coordinate location desired for the final FN value.

The FNs determined during the photometric correction procedure have values which range between ± 1024. Any FN values originally exceeding these limits are clipped and set to the respective limit value.

6.4   Associated ν Flags and Reference Images

A major difference between the IUESIPS processing and the NEWSIPS processing, which will be quite apparent to the user, is that the NEWSIPS photometrically corrected FN values in the Linearized Image (LI) file are not encoded with error condition information. Error conditions are represented by ν flags and are recorded in a separate image flag file (LIF).

6.4.1   Non-photometrically Corrected Image Regions

As discussed in Chapter 4, the regions defined for photometric correction either reside within an approximately circular boundary for high dispersion, or a diagonal swath encompassing the location of both apertures and a large area of background for low dispersion. All pixel locations which do not reside within these defined boundaries are not photometrically corrected and are flagged in the LIF file as -16384.

6.4.2   Warning Track

In order to alert the user that data being analyzed are spatially close to the edge of the region of photometric correction and/or near the target ring, a warning zone approximately five pixels deep has been established on the photometrically corrected data side of the boundary. Pixel locations determined to be in the warning track are flagged in the LIF file as -512.

6.4.3 ITF Artifacts

6.4.3.1 Permanent Artifacts and Reseaux

The permanent ITF artifacts have been cataloged and both the artifacts and reseaux have been removed from the ITF images with a bi-linear interpolation scheme. The location of the specific pixels affected by either an artifact or reseau mark have been preserved in an ITF-dependent "permanent blemish" reference image. This image is used in the pipeline processing during the photometric correction step to flag pixels in the science image whose location is coincident to those of the ITF blemishes. The ν flag values corresponding to permanent ITF artifacts and reseaux are -2048 and -4096, respectively. Because the ITF has been spatially interpolated in these regions, the accuracy of the photometric correction is somewhat degraded.

6.4.3.2 The 1515Å Artifact

Analyses of presumably featureless SWP spectral data of white dwarfs have revealed a distinctive absorption artifact at 1515Å. Although this "feature" is now known to be present in a variety of the SWP spectra, its presence in the featureless white dwarf spectra analyzed for flux calibration studies was the catalyst for further investigation and allowed the absolute determination of this "feature" as an artifact (De La Peña 1992b).

Figure 6.1 is a plot of the SWP spectrum of the white dwarf, G191-B2B, a featureless continuum source. The spectra were produced with the standard extraction method of the NEWSIPS image processing system, a Signal Weighted Extraction Technique (SWET).

Upon further investigation, the 1515Å feature was found to be present in both NEWSIPS and IUESIPS data. Recall that NEWSIPS is using a SWET extraction and the SWP ITF (Epoch 1985) was constructed in raw space. IUESIPS uses a standard boxcar extraction and the SWP ITF (Epoch 1978) was constructed in geometrically corrected space. Therefore, this artifact is independent of the extraction method, and both the ITF epoch and creation method. Despite the major differences in the image processing techniques employed by the two systems, the feature is apparent in both datasets. In addition, not only is this artifact found in these recently obtained white dwarf observations (1991), but it also can be found in extracted spectra acquired as early as 1978.

Using the data from a specific SWP image in which this absorption feature is present, the vector displacement information was used to trace the pixels in the extracted/resampled (MXLO/SILO) images back to the linearized (LI) and raw (RI) images, and ultimately back to the ITF. There appears to be a group of "lazy" pixels in the ITF at the computed location. These pixels lack sensitivity in the lowest levels of the ITF in that they require more illumination than their neighbors before they "react." Unfortunately, there are several adjacent pixels along the edge of the low-dispersion spectral swath which appear to be less sensitive than the neighboring pixels at low illumination levels. It is simply an unfortunate circumstance that these pixels reside along the edge of the spectral swath, and therefore, manifest themselves as a flux deficit in the extracted data. Because of the difficulty in accu-
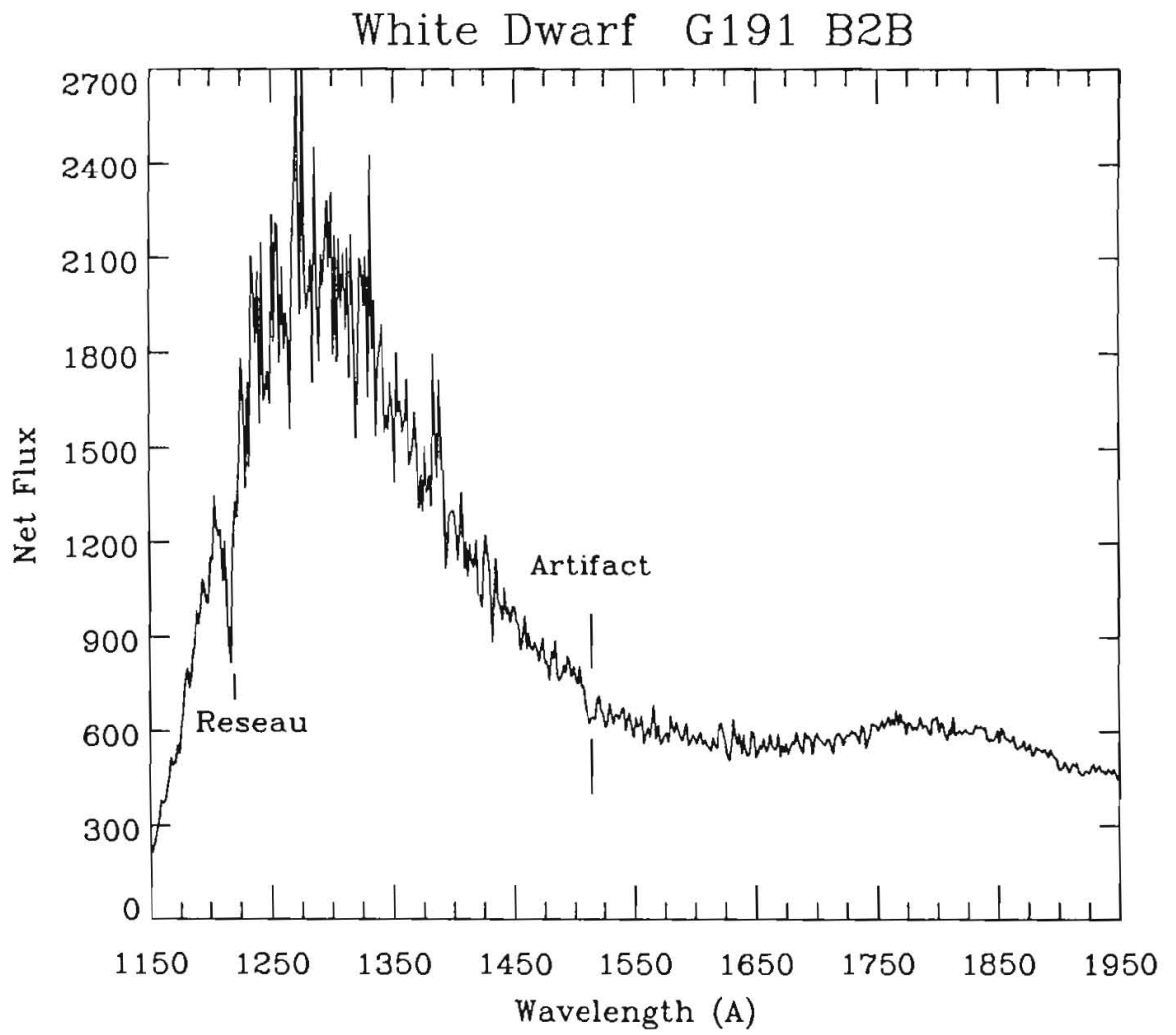
Figure 6.1: White Dwarf SWP spectra showing the 1515Å artifact.

rately identifying the pixels contributing to the 1515Å artifact due to the variable placement of the spectrum on the image, this artifact is not flagged.

6.5 Photometric Correction Output

There are two main output data products produced during the photometric correction stage of image processing: the LI image and corresponding LIF image. For both low and high dispersion, the LI and LIF files are full 768×768 images. The LI image contains FN values in raw image space for the data which have been photometrically corrected. Since the LI image was created by overwriting a copy of the raw image, the remainder of the data in the LI frame outside the photometrically corrected region are the raw data scaled down by a factor of 32.0. The LIF image contains the ν flags associated with the pixels in the LI image; the photometric correction error conditions have been combined with the conditions determined during the raw image screening portion of the image processing. The intensity data (LI) are output as a FITS image, and the associated ν flags (LIF) are output as the corresponding FITS image extension.

The photometric correction module writes information to the HISTORY portion of the image label for each raw science image processed:

- ITF used for the photometric correction, camera and year of ITF image acquisition

- Mean THDA of ITF

- ITF UVC voltage

- UV Flood wavelength

- ITF SEC voltage

- Characteristics of the ITF construction and construction date

Chapter 7

Image Resampling

Raw *IUE* images suffer from spatial distortions introduced by the SEC Vidicon cameras. The electrostatically-focused image section of the camera produces a pincushion distortion, while the magnetically-focused readout section produces an S-distortion. Furthermore, the dispersion direction lies at an angle of approximately 45 degrees relative to the image axes and the dispersion function is not linear within the spectral orders. The combination of these effects can make the task of spectral extraction and subsequent analysis very difficult. Therefore, our goal is to create a geometrically corrected and rotated *IUE* image in which the spectral orders are parallel to one image axis and the dispersion is linear within each order, thus providing an image format that is best suited to scientific analysis.

Our approach to producing a geometrically corrected *IUE* image is to construct a vector field that maps each pixel from its instrumental raw space to a geometrically rectified space. These vectors include: the displacements between the science image and the Intensity Transfer Function (ITF), the displacement of the reseau pattern (camera fiducials) in the ITF from its original square grid, the rotation of the spectral format to lie along image rows, the small change of scale needed to linearize the dispersion, the alignment of the two spectrograph apertures in wavelength space for low-dispersion mode, corrections for the spatial deviations (cross-dispersion "wiggles") for the LWP and LWR low-dispersion data, and shifts in both the wavelength and spatial directions to maintain a fixed wavelength zeropoint and spatial position in the resampled low-dispersion (SILO) image. In addition, low-dispersion images of extended sources receive a correction to account for the fact that the major axis of the large aperture is not exactly perpendicular to the dispersion direction. Resampled high-dispersion (SIHI) images will also include corrections for the echelle order splaying and for the cross-dispersion spectral wiggles.

7.1 Geometric Distortion Corrections

7.1.1 Measurement of Distortions

7.1.1.1 Mapping of Raw Science Image to ITF Space

The first correction for image distortion maps the science image to the geometric space of the relevant ITF. This correction utilizes the displacement vectors determined for each pixel during the raw image registration step (Chapter 4). These vectors are unique for each science image and can be recovered from the information in the binary 3-D table extension to the final vector displacement file.

7.1.1.2 Mapping of ITF Space to Geometrically Rectified Space

Laboratory measured positions of the fiducial marks (reseaux) are used to map the distortion of the null-subtracted 20% level of the ITF in order to compensate for the geometric distortions in the ITF images. The faceplate of each camera is etched with a square-grid pattern of 169 reseau marks arranged in 13 rows and 13 columns. The reseaux appear on images as occulted areas approximately 2-3 pixels wide, spaced approximately 55 pixels apart for LWP and LWR and 56 pixels apart for SWP. Of the 169 reseau marks embedded in the fiber-optic coupling, approximately 129 fall within the camera target area. According to the design specifications of the scientific instrument (GSFC System Design Report for the *IUE*, 1976), the placement of the reseau marks in a true square grid is accurate to within ±0.005 mm, which corresponds to ±0.138 pixels for LWP/LWR and ±0.14 pixels for SWP.

In order to refine the true locations of the reseau marks, laboratory measurements were made of the reseau grid on an SEC Vidicon tube which was deposited around the same time as those on the *IUE* flight tubes, and therefore, the same deposition mask was used. This work was done by the Metrology Department at Rutherford Appleton Laboratory (Didcot, U.K.) in late 1990. The measurements were obtained in an X/Y reference frame in millimeters with a demonstrated repeatability of ±0.003 millimeters. It was then necessary to derive the scale factor to convert the millimeter measurements to "true" pixel locations for the reseaux. Note that the NEWSIPS true reseau positions may be very different from the positions quoted for IUESIPS. The IUESIPS reseau positions are *not* laboratory measurements, but rather a square grid construct based upon the definitions of a central reseau mark and mean reseau spacing. The NEWSIPS true reseau positions are listed in Tables 7.1–7.6.

The observed positions of the reseau marks are determined per ITF, and the departures of the observed positions from their true locations are used to characterize the geometric distortion of the camera system. A vector field defining the displacement of each pixel in the null-subtracted 20% level of the ITF from geometrically rectified space is derived using a bi-cubic spline interpolation between the reseau marks.

Table 7.1: LWP True Reseau Positions in X Direction

	1	2	3	4	5	6	7
1	80.39	135.37	190.32	245.29	300.11	355.10	410.15
2	80.39	135.35	190.26	245.25	300.17	355.11	410.18
3	80.33	135.32	190.32	245.25	300.17	355.10	410.20
4	80.39	135.39	190.33	245.24	300.20	355.18	410.18
5	80.39	135.40	190.32	245.25	300.20	355.15	410.21
6	80.39	135.30	190.26	245.20	300.17	355.09	410.18
7	80.41	135.33	190.33	245.22	300.20	355.15	410.21
8	80.39	135.24	190.26	245.13	300.13	355.07	410.18
9	80.39	135.25	190.25	245.13	300.09	355.09	410.20
10	80.37	135.22	190.22	245.11	300.09	355.10	410.14
11	80.36	135.20	190.18	245.03	300.02	355.00	410.09
12	80.33	135.26	190.24	245.18	300.10	355.13	410.15
13	80.36	135.26	190.22	245.13	300.07	355.10	410.14

	8	9	10	11	12	13
1	465.00	520.00	574.88	629.81	684.67	738.86
2	465.04	520.06	574.88	629.88	684.73	738.93
3	465.04	520.04	574.92	629.84	684.77	739.14
4	465.06	520.06	574.93	629.71	684.76	739.15
5	465.07	520.06	574.99	629.78	684.76	739.25
6	465.03	520.02	574.92	629.70	684.73	739.32
7	465.10	520.10	574.95	629.76	684.67	739.36
8	465.04	520.09	574.91	629.70	684.56	739.29
9	465.03	520.04	574.93	629.70	684.55	739.34
10	465.00	520.04	574.93	629.63	684.52	739.34
11	464.96	519.92	574.81	629.54	684.38	739.32
12	465.04	520.03	574.88	629.70	684.36	739.45
13	465.03	520.03	574.89	629.74	684.51	739.54

Table 7.2: LWP True Reseau Positions in Y Direction

	1	2	3	4	5	6	7
1	60.40	60.32	60.29	60.39	60.32	60.33	60.29
2	115.35	115.22	115.44	115.44	115.39	115.40	115.33
3	170.20	170.21	170.30	170.50	170.30	170.36	170.18
4	225.21	225.22	225.41	225.46	225.41	225.30	225.24
5	280.18	280.13	280.36	280.43	280.32	280.36	280.21
6	335.20	335.13	335.32	335.32	335.30	335.21	335.11
7	390.14	390.07	390.24	390.32	390.22	390.14	390.04
8	445.04	445.09	445.18	445.35	445.29	445.28	445.07
9	500.21	500.09	500.18	500.33	500.17	500.21	500.10
10	555.10	555.13	555.22	555.30	555.25	555.15	554.98
11	610.00	610.07	610.04	610.29	610.15	610.09	609.93
12	664.93	665.05	665.03	665.30	665.14	665.13	664.98
13	719.96	720.15	720.13	720.20	720.04	720.11	719.98

	8	9	10	11	12	13
1	60.36	60.26	60.32	60.30	60.29	60.29
2	115.26	115.29	115.32	115.25	115.22	115.22
3	170.33	170.30	170.33	170.13	170.24	170.17
4	225.30	225.20	225.26	225.17	225.11	225.32
5	280.29	280.20	280.24	280.18	280.25	280.33
6	335.29	335.22	335.21	335.14	335.17	335.29
7	390.18	390.11	390.17	390.06	390.15	390.24
8	445.22	445.11	445.18	445.17	445.14	445.29
9	500.15	500.13	500.25	500.13	500.09	500.22
10	554.98	555.04	555.18	555.03	555.06	555.29
11	610.09	609.99	610.03	609.99	609.92	610.17
12	665.04	665.00	664.93	664.89	664.92	665.13
13	720.04	719.93	719.87	719.93	719.98	720.20

Table 7.3: LWR True Reseau Positions in X Direction

	1	2	3	4	5	6	7
1	80.39	135.37	190.32	245.29	300.11	355.10	410.15
2	80.39	135.35	190.26	245.25	300.17	355.11	410.18
3	80.33	135.32	190.32	245.25	300.17	355.10	410.20
4	80.39	135.39	190.33	245.24	300.20	355.18	410.18
5	80.39	135.40	190.32	245.25	300.20	355.15	410.21
6	80.39	135.30	190.26	245.20	300.17	355.09	410.18
7	80.41	135.33	190.33	245.22	300.20	355.15	410.21
8	80.39	135.24	190.26	245.13	300.13	355.07	410.18
9	80.39	135.25	190.25	245.13	300.09	355.09	410.20
10	80.37	135.22	190.22	245.11	300.09	355.10	410.14
11	80.36	135.20	190.18	245.03	300.02	355.00	410.09
12	80.33	135.26	190.24	245.18	300.10	355.13	410.15
13	80.36	135.26	190.22	245.13	300.07	355.10	410.14

	8	9	10	11	12	13
1	465.00	520.00	574.88	629.81	684.67	738.86
2	465.04	520.06	574.88	629.88	684.73	738.93
3	465.04	520.04	574.92	629.84	684.77	739.14
4	465.06	520.06	574.93	629.71	684.76	739.15
5	465.07	520.06	574.99	629.78	684.76	739.25
6	465.03	520.02	574.92	629.70	684.73	739.32
7	465.10	520.10	574.95	629.76	684.67	739.36
8	465.04	520.09	574.91	629.70	684.56	739.29
9	465.03	520.04	574.93	629.70	684.55	739.34
10	465.00	520.04	574.93	629.63	684.52	739.34
11	464.96	519.92	574.81	629.54	684.38	739.32
12	465.04	520.03	574.88	629.70	684.36	739.45
13	465.03	520.03	574.89	629.74	684.51	739.54

Table 7.4: LWR True Reseau Positions in Y Direction

	1	2	3	4	5	6	7
1	60.40	60.32	60.29	60.39	60.32	60.33	60.29
2	115.35	115.22	115.44	115.44	115.39	115.40	115.33
3	170.20	170.21	170.30	170.50	170.30	170.36	170.18
4	225.19	225.22	225.41	225.46	225.41	225.30	225.24
5	280.18	280.13	280.36	280.43	280.32	280.36	280.21
6	335.20	335.13	335.32	335.32	335.30	335.21	335.11
7	390.14	390.07	390.24	390.32	390.22	390.14	390.04
8	445.04	445.09	445.18	445.35	445.29	445.28	445.07
9	500.21	500.09	500.18	500.33	500.17	500.21	500.10
10	555.10	555.13	555.22	555.30	555.25	555.15	554.98
11	610.00	610.07	610.04	610.29	610.15	610.09	609.93
12	664.93	665.05	665.03	665.30	665.14	665.13	664.98
13	719.96	720.15	720.13	720.20	720.04	720.11	719.98

	8	9	10	11	12	13
1	60.36	60.26	60.32	60.30	60.29	60.29
2	115.26	115.29	115.32	115.25	115.22	115.22
3	170.33	170.30	170.33	170.13	170.24	170.17
4	225.30	225.20	225.26	225.17	225.11	225.32
5	280.29	280.20	280.24	280.18	280.25	280.33
6	335.29	335.22	335.21	335.14	335.17	335.29
7	390.18	390.11	390.17	390.06	390.15	390.24
8	445.22	445.11	445.18	445.17	445.14	445.29
9	500.15	500.13	500.25	500.13	500.09	500.22
10	554.98	555.04	555.18	555.03	555.06	555.29
11	610.09	609.99	610.03	609.99	609.92	610.17
12	665.04	665.00	664.93	664.89	664.92	665.13
13	720.04	719.93	719.87	719.93	719.98	720.20

Table 7.5: SWP True Reseau Positions in X Direction

	1	2	3	4	5	6	7
1	74.41	130.48	186.50	242.55	298.45	354.51	410.65
2	74.41	130.45	186.45	242.51	298.50	354.53	410.68
3	74.36	130.42	186.50	242.51	298.50	354.51	410.69
4	74.41	130.49	186.52	242.50	298.53	354.60	410.68
5	74.41	130.51	186.50	242.51	298.53	354.57	410.70
6	74.41	130.41	186.45	242.45	298.50	354.50	410.68
7	74.44	130.44	186.52	242.48	298.53	354.57	410.70
8	74.41	130.34	186.45	242.38	298.46	354.48	410.68
9	74.41	130.35	186.43	242.38	298.42	354.50	410.69
10	74.40	130.32	186.40	242.37	298.42	354.51	410.63
11	74.39	130.30	186.36	242.29	298.35	354.41	410.58
12	74.36	130.36	186.42	242.44	298.43	354.54	410.65
13	74.39	130.37	186.40	242.38	298.41	354.51	410.63

	8	9	10	11	12	13
1	466.57	522.65	578.60	634.61	690.55	745.80
2	466.61	522.71	578.60	634.68	690.61	745.87
3	466.61	522.69	578.64	634.64	690.65	746.08
4	466.63	522.71	578.66	634.51	690.63	746.10
5	466.64	522.71	578.71	634.58	690.63	746.19
6	466.60	522.66	578.64	634.50	690.61	746.26
7	466.67	522.75	578.67	634.55	690.55	746.31
8	466.61	522.73	578.63	634.50	690.44	746.24
9	466.60	522.69	578.66	634.50	690.42	746.29
10	466.57	522.69	578.66	634.43	690.39	746.29
11	466.53	522.57	578.53	634.33	690.25	746.26
12	466.61	522.68	578.60	634.50	690.23	746.40
13	466.60	522.68	578.62	634.54	690.38	746.49

Table 7.6: SWP True Reseau Positions in Y Direction

	1	2	3	4	5	6	7
1	54.43	54.34	54.32	54.41	54.34	54.36	54.32
2	110.45	110.32	110.55	110.55	110.49	110.51	110.44
3	166.38	166.39	166.49	166.68	166.49	166.54	166.36
4	222.47	222.48	222.68	222.72	222.68	222.57	222.50
5	278.52	278.46	278.70	278.77	278.66	278.70	278.55
6	334.61	334.54	334.74	334.74	334.72	334.62	334.53
7	390.63	390.56	390.73	390.82	390.72	390.63	390.54
8	446.61	446.66	446.75	446.92	446.87	446.85	446.64
9	502.86	502.73	502.83	502.99	502.82	502.86	502.75
10	558.83	558.85	558.95	559.04	558.98	558.88	558.70
11	614.81	614.88	614.85	615.10	614.96	614.89	614.74
12	670.82	670.93	670.91	671.19	671.03	671.01	670.86
13	726.92	727.12	727.09	727.16	727.01	727.08	726.94

	8	9	10	11	12	13
1	54.39	54.29	54.34	54.33	54.32	54.32
2	110.37	110.39	110.42	110.35	110.32	110.42
3	166.52	166.49	166.52	166.31	166.42	166.35
4	222.57	222.45	222.52	222.43	222.37	222.58
5	278.63	278.53	278.57	278.52	278.59	278.67
6	334.71	334.64	334.62	334.55	334.58	334.71
7	390.68	390.61	390.66	390.55	390.65	390.73
8	446.80	446.68	446.75	446.74	446.71	446.87
9	502.80	502.78	502.90	502.78	502.73	502.87
10	558.70	558.77	558.91	558.76	558.78	559.02
11	614.89	614.79	614.83	614.79	614.72	614.97
12	670.93	670.89	670.82	670.77	670.80	671.01
13	727.01	726.89	726.82	726.89	726.94	727.16

7.1.2 Image Rotation

The image rotation is not, strictly speaking, a distortion correction, but rather is performed to simplify the extraction of spectral data from the SILO/SIHI image. The purpose of the rotation is to align the spectral order(s) horizontally along the geometrically rectified image.

7.1.3 Wavelength Linearization in Low Dispersion

As discussed in Chapter 8.3, the dispersion solutions for SILO images are not precisely linear; significant second- and third-order terms are present. The non-linearities which exist in the dispersion solutions for the SILO image can, if not accounted for, lead to wavelength errors on the order of several Angstroms in some regions of the spectrum. Therefore, a remapping of the SILO image data is necessary to force the dispersion solution onto a linear scale. The high-order terms for a given camera are quite stable over time and camera temperature (THDA) so that a single third-order correction can be applied to the all of the data for a given camera. The derivation of the corrections is discussed in detail in Chapter 8.3. The form of the corrections is shown in Figure 7.1. This figure shows the amount by which each pixel in the SILO image must be shifted along the dispersion direction from its original uncorrected position in order to achieve a linear dispersion solution. This correction is applied uniformly throughout the spatial direction of the image so that entire image columns (*i.e.*, lines of constant wavelength) are shifted by the same amount.

7.2 Additional Corrections for Low Dispersion

7.2.1 Aperture Alignment

The SILO image includes the spectral data for both the large and small apertures. Because the centers of the two apertures are not aligned along a line of constant wavelength in the rotated image space, it would be impossible to have a single dispersion solution apply to the entire image. Therefore, a shift along the dispersion direction is introduced for the small-aperture spectra so that both apertures are on a common wavelength scale. The small-aperture data for SWP are shifted by 0.8 pixels in the dispersion direction towards longer wavelengths, and for LWP and LWR the small-aperture data are shifted by 2.3 pixels towards shorter wavelengths. The shift is applied uniformly to all pixels within the small-aperture region of the SILO image, which is defined to extend from row 1 through row 33 of the image.

7.2.2 Wiggle Corrections

The LWP and LWR cameras are known to exhibit localized discontinuities in the spectral format which are believed to be due to slight misalignments between neighboring fiber optic bundles in the output stage of the ultraviolet converter (UVC) portion of the cameras. These misalignments are seen as abrupt changes in the spatial centroid of the spectrum of up to

65
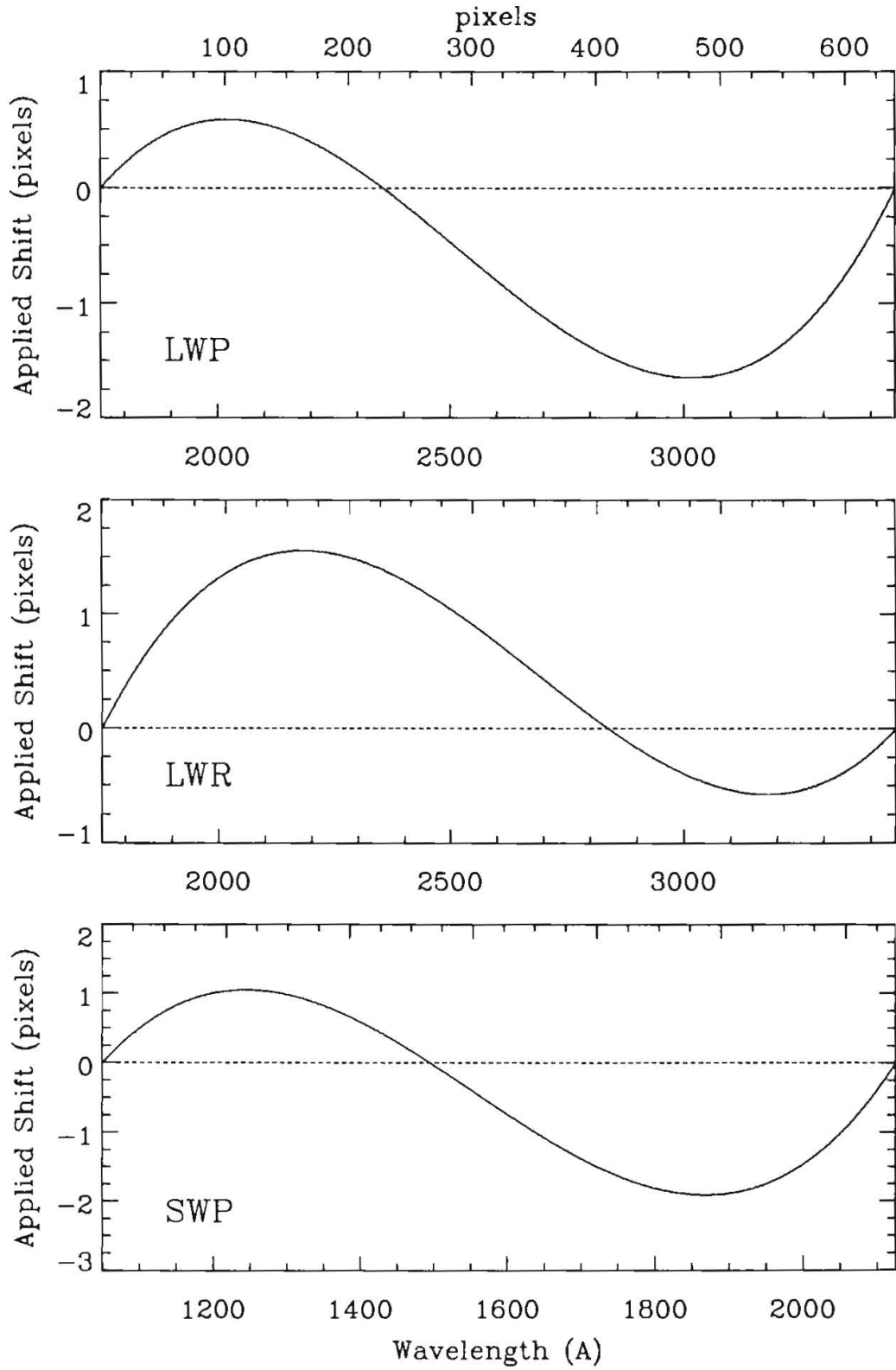
Figure 7.1: Wavelength linearization correction vectors.

1 pixel. In addition to these abrupt changes, there also exist more slowly varying "wiggles" in the spectral format. These wiggles can have peak-to-peak amplitudes of 1 pixel or more within the space of a few dozen pixels along the dispersion direction. Figures 7.2 and 7.3 show the locations of the spectral centroid as a function of wavelength for the LWP and LWR cameras, respectively. Note the sharp discontinuites at ~3290Å in the large aperture (the feature at ~3100Å is a reseau) and at ~2780Å and ~3290Å in the small aperture for the LWP. The LWR shows similar discontinuities at ~2450Å and ~2830Å in the large aperture. The existence of these wiggles complicates the task of spectral extraction since it is necessary to have the extraction slit follow the changing spectral centroid in order to ensure that all of the spectral flux is extracted at a given wavelength.

To compensate for these wiggles, the spectral centroid as a function of wavelength has been measured from approximately 30 SILO images for each of the LWP and LWR cameras and the average deviations have been incorporated into the resampling step of the image processing system as an additional geometric correction vector. These corrections affect only the spatial dimension of SILO images. Separate deviation vectors are applied for the large- and small-aperture regions of the LWP and LWR SILO images. As Figures 7.2 and 7.3 show, the deviation vectors for the two apertures are qualitatively similar, but differ in detail, due to the fact that they are imaged onto different portions of the camera faceplate. Figures 7.4 and 7.5 show examples of the measured centroid locations for "dewiggled" versions of LWP and LWR images.

7.2.3   Large-Aperture Tilt Correction

The major axis of the large aperture in low-dispersion data is not precisely perpendicular to the direction of dispersion. The major axis is at an angle, called the ω angle, with the dispersion direction, which is slightly different for each of the three cameras. The geometry of the entrance apertures in relation to the image scan lines and dispersion directions as they appear in SILO images is shown in Figure 7.6. The left side of each figure shows the intrinsic geometry with no corrections applied, the middle portion shows the resulting geometry after applying the aperture alignment correction only, and the right side shows the results after applying both alignment and tilt corrections. Note that the major axis of the large aperture in high-dispersion data is very nearly coincident with the direction of dispersion so no tilt correction is necessary.

The error introduced by extracting extended spectral data (data that fills the large aperture) which has not been tilt corrected, by summing the flux perpendicular to the dispersion can be calculated as follows. The maximum tilt of the large aperture with respect to the dispersion direction occurs in the SWP camera, with an ω angle of 81°. If the length of the large aperture is taken to be 14.3 pixels (based on a plate scale factor of 1.51 arcsec/pixel), then the displacement from the line perpendicular to the dispersion direction is 1.1 pixels at each end of the aperture, or approximately 1.9Å. Spectral features will show some broadening if extracted perpendicular to the dispersion ($\omega = 90°$), which will amount to a broadening of the base of the point spread function by 3.8Å. The overall effect is in reality not as severe
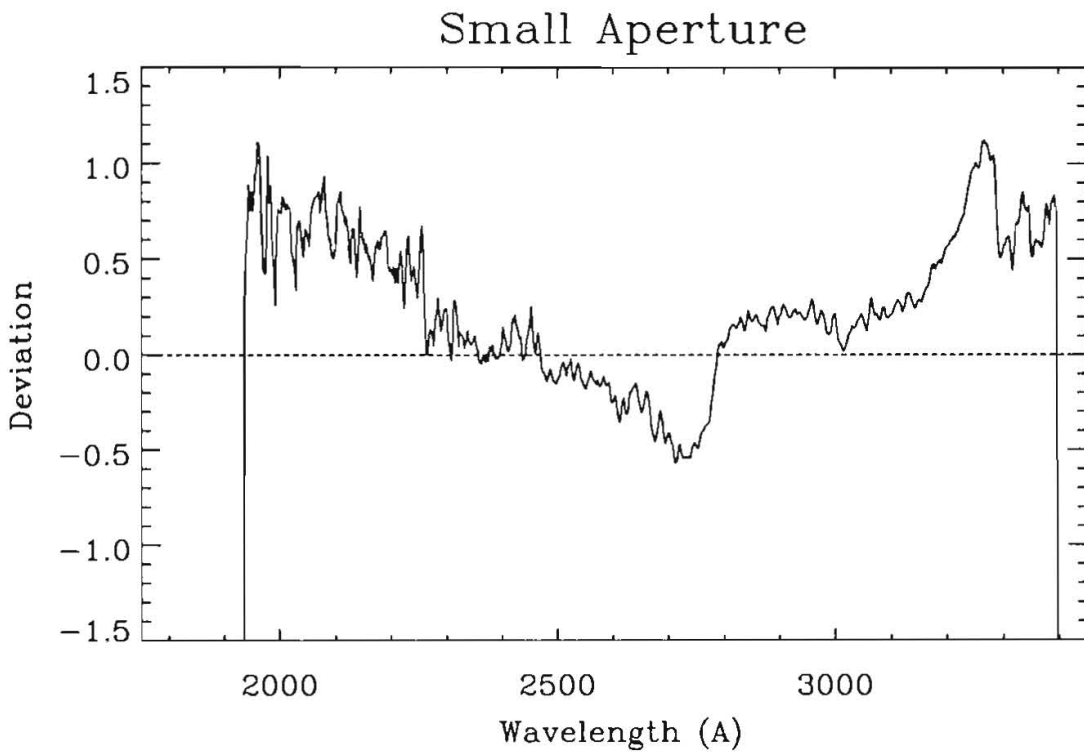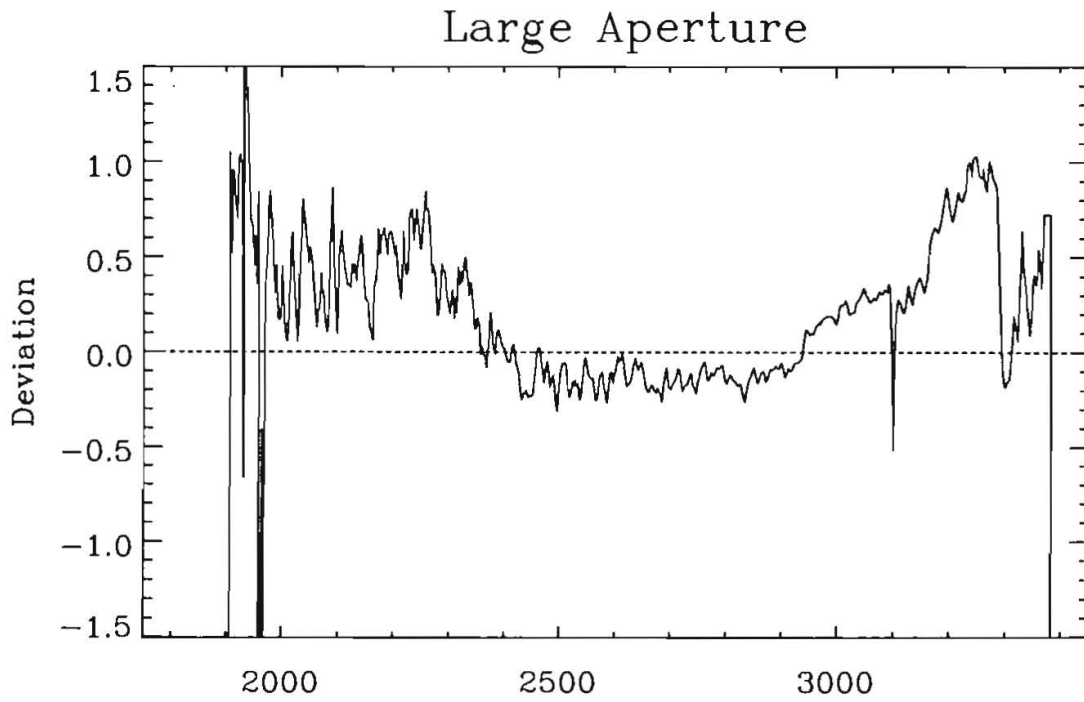
Figure 7.2: Spectrum centroid location in LWP SILO images.

Large Aperture

Small Aperture
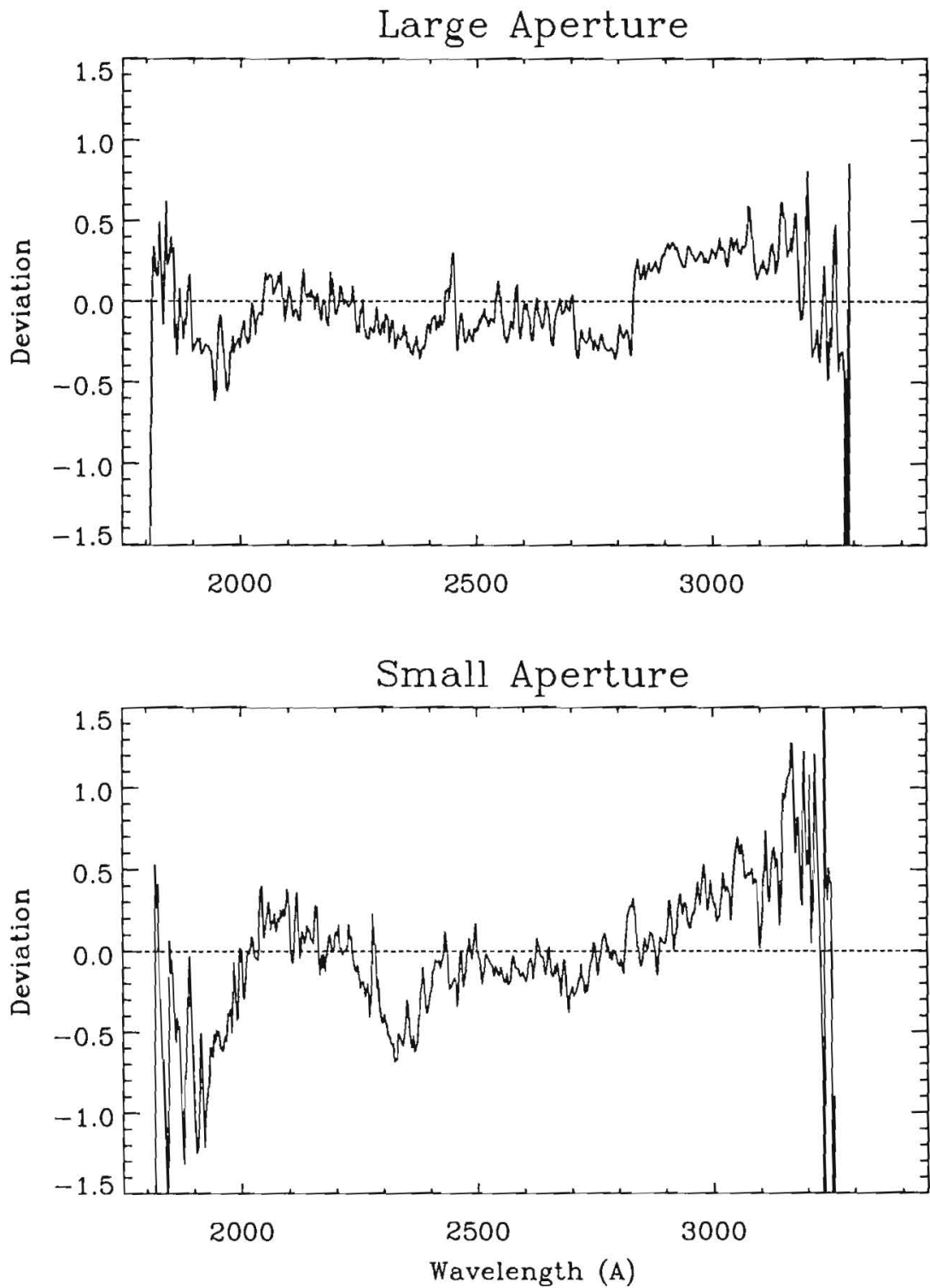
Figure 7.3: Spectrum centroid location in LWR SILO images.
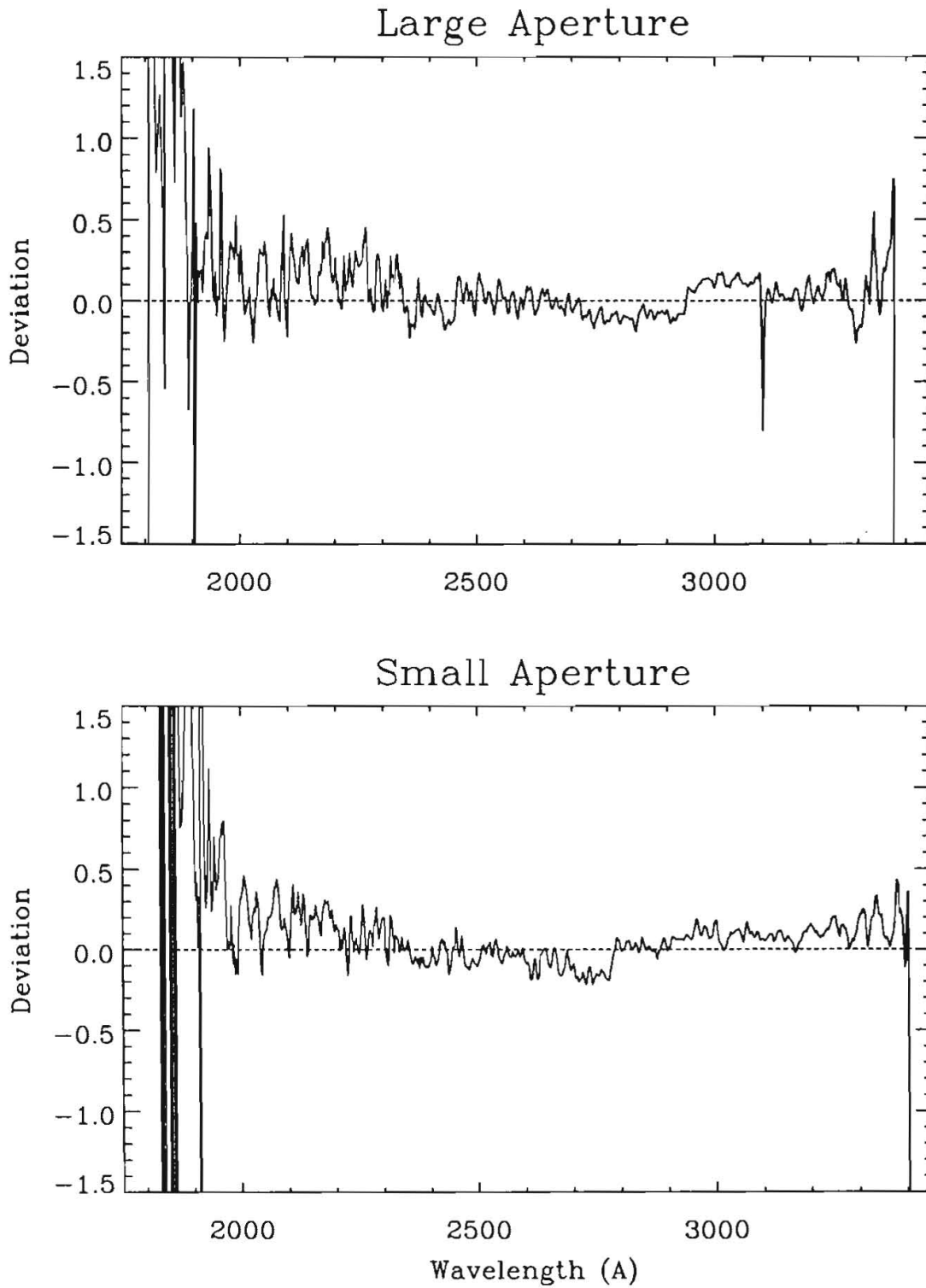
Figure 7.4: Spectrum centroid location in "dewiggled" LWP SILO images.
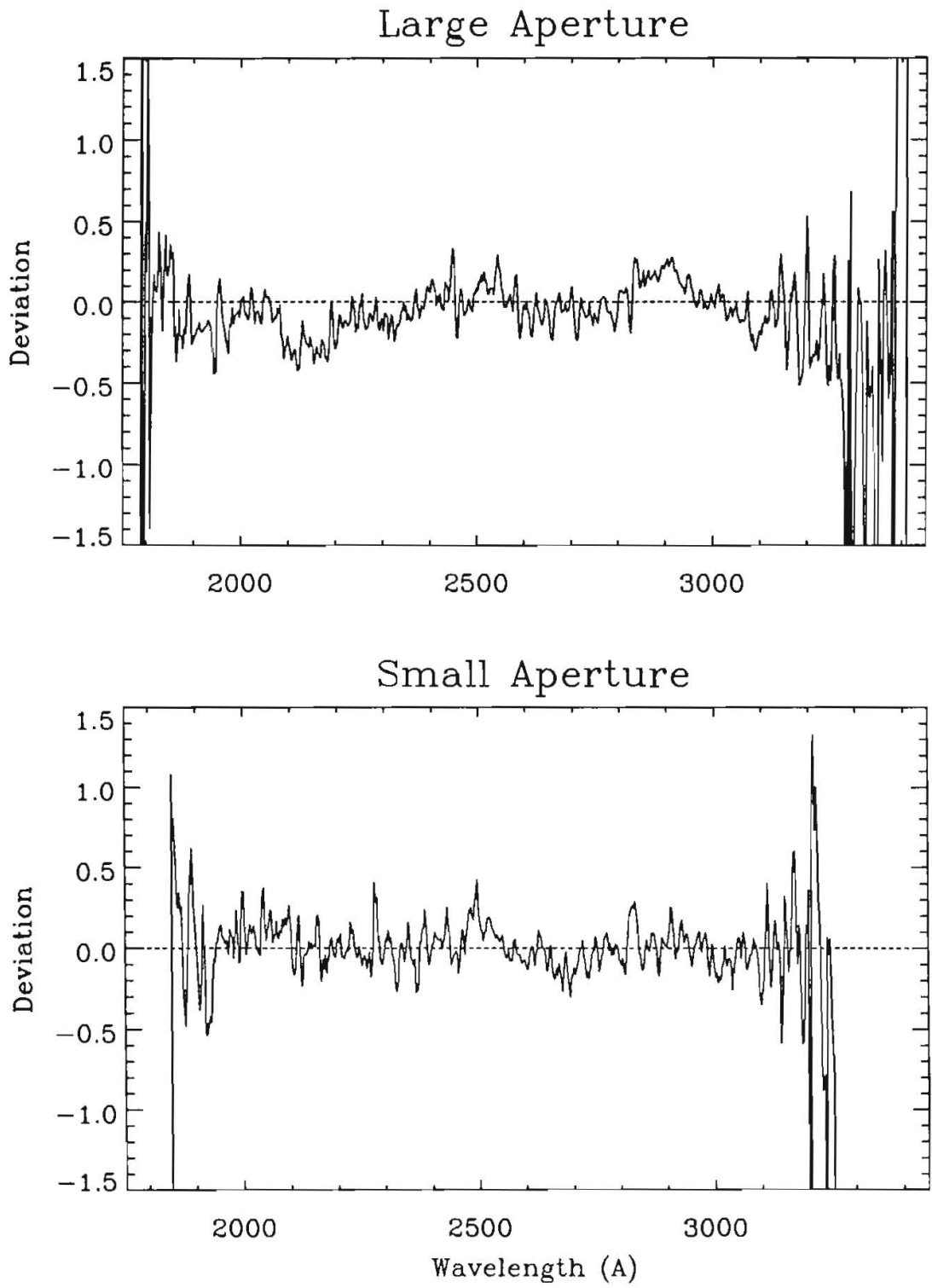
Figure 7.5: Spectrum centroid location in "dewiggled" LWR SILO images.
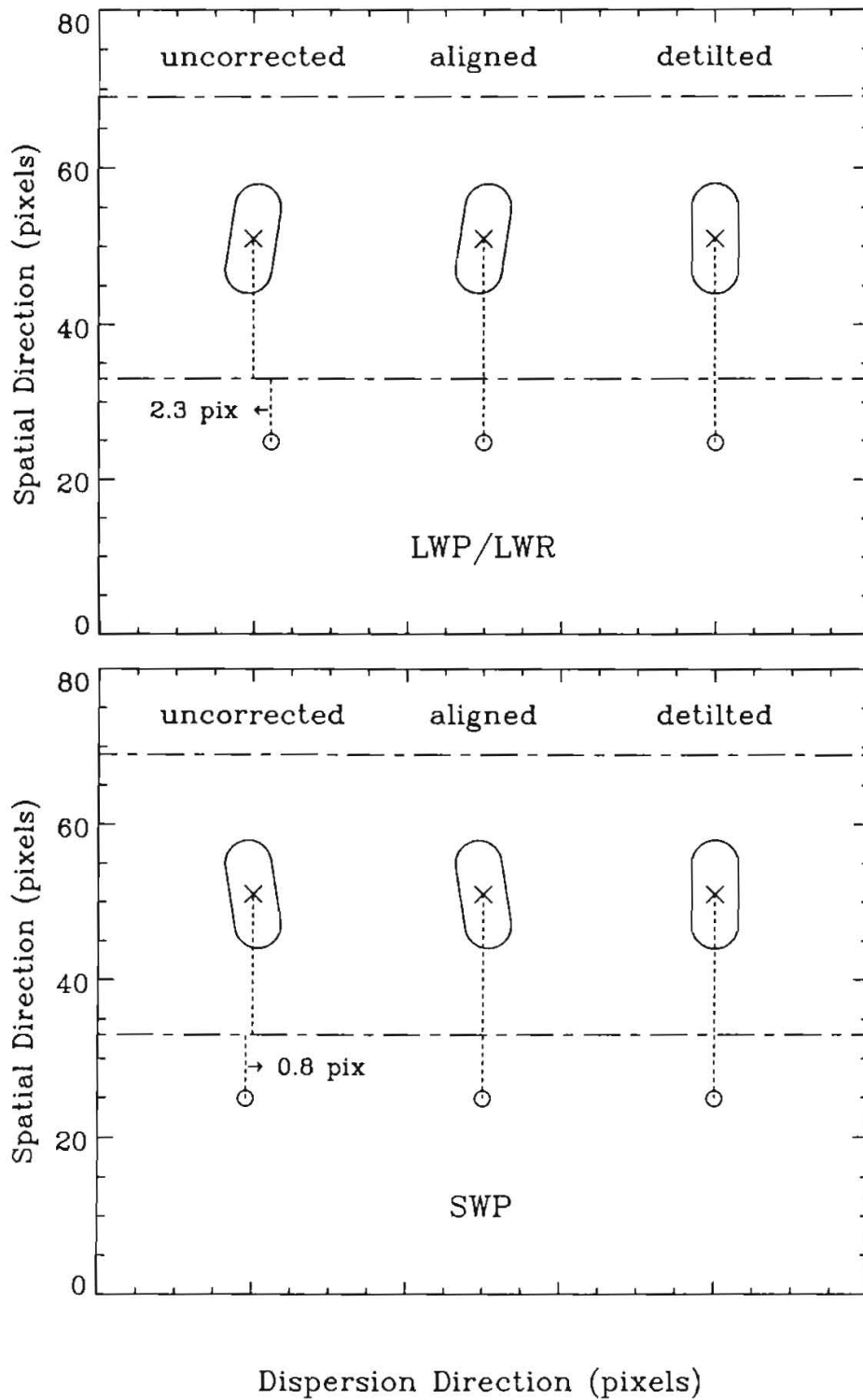
Figure 7.6: Geometry of the spectrograph apertures as they appear in SILO images.

as a simple convolution of the data with a 3.8Å wide slit, because the part of the signal extracted near the slit center is not really being degraded. A more precise approximation to the error is to think of the 11Å slit width as being convolved with a triangular function with FWHM of 2Å and a base width of 4Å, which will result in a degradation in resolution of 20–25%.

Since this is a significant effect, a correction is made to "detilt" the large-aperture data for observations that result in the detection of spatially extended spectra. This correction is obviously not necessary for point source spectra, nor is it appropriate for most trailed or multiple observations because in these types of observations the source is moved along the FES x-axis which is nearly perpendicular to the dispersion direction. Multiple spectra acquired along the major axis of the FES, however, are tilt corrected. The tilt correction is not applied to any spectrum having object class designation 10–57 (stellar sources), regardless of whether the spectrum is determined to be point or extended. Presumably a stellar spectrum measured to be extended is saturated.

The tilt correction is only applied to a region of the SILO image that extends for 18 image lines on either side of the predicted center of the large aperture, thus leaving the small-aperture data intact. The extent of the correction region was chosen so as to include the areas on either side of the aperture which are used for background subtraction in the subsequent extraction step of the image processing. The actual correction is accomplished by simply shifting each image line in the dispersion direction by an amount given by

$$\Delta x = \Delta y \times \tan(\omega_t)$$

where Δy is the number of spatial image lines between the center of the large aperture and the image line under consideration, and ω_t is the tilt angle of the aperture. The correction is a projection of the aperture onto the spatial axis of the image, as opposed to a rotation about the center of the aperture, since the latter would result in a slight remapping of the spatial character of the data.

7.2.4 Wavelength and Spatial Normalization

As discussed in Chapter 8.2, global shifts in the location of the spectral format occur as a function of time and camera temperature. Because the SILO image boundaries are fixed in rotated image space, the global movements of the spectral format appear as displacements of the spectrum in both the spatial and dispersion directions of the SILO image. The resulting change in the wavelength zeropoint (*i.e.* the wavelength value assigned to column 1 of the SILO image) is compensated for through the application of zeropoint corrections derived from wavelength calibration (WAVECAL) images (Chapter 8.2). While this results in the assignment of the correct wavelength zeropoint for each SILO image, it also results in the assignment of a *different* zeropoint for each image. Having spectra with different wavelength scales would severely complicate subsequent data analysis. To coadd properly multiple images of a given source, for example, would require first resampling the individual spectra to a common wavelength scale.

To alleviate this problem, zeropoint shifts in both the spatial and dispersion directions are applied to the image resampling vectors so that all spectra for a given camera have the same wavelength zeropoint and the same spatial location within the SILO image. The spatial centroid of large-aperture spectra is chosen to lie on or about line 51 of the SILO image for all cameras. The resulting centroid of small-aperture spectra is approximately at line 25. The common wavelength zeropoints are 1050 and 1750Å for the short and long wavelength cameras, respectively. The amount of the zeropoint shift to be applied to each image is computed from the difference between the desired zeropoints and those predicted from the time- and temperature-corrected dispersion constants (Chapter 8.2). Image-to-image scatter in the precise location of the spectral format leads to 1-sigma errors in the predicted wavelength and spatial zeropoints of $\sim$0.3Å and 0.26 pixels, respectively, for the SWP and $\sim$0.6Å and 0.35 pixels, respectively, for the LWP.

7.3   Flux Resampling Algorithm

The final coordinate mapping is derived by adding the individual geometric corrections in a vectorial fashion. Consequently, the transformation from raw image space to geometrically rectified space necessitates the use of a sophisticated resampling algorithm because the raw image pixels must be resampled from the irregular grid resulting from the vector mapping to a regular grid to produce the SILO image. This type of two-dimensional interpolation is mathematically challenging and particularly difficult to solve satisfactorily. The intensity values (FNs) in the linearized (LI) image are resampled to the geometrically corrected space of the SILO/SIHI image using a modified Shepard method, an algorithm found in the NAG (1990) library. The interpolant for the modified Shepard method is continuous and also possesses first derivative continuity. The method is local in that the output flux value is dependent only upon data in a surrounding neighborhood.

7.4 ν Flag Resampling

Since the intensity values are resampled in the mapping from the raw space of the LI file to the geometrically rectified space of the SILO/SIHI file, the ν flag values must also be appropriately mapped into this new space. However, in order to map the flag values from raw space to the new geometric space, a "resampling" algorithm is clearly *not* desired as the ν flags have a very specific meaning which must be maintained. The flag values need to be mapped to their new coordinates such that they retain their initial values, but also are appropriately assigned to additional locations in the remapped space in accordance to the distribution of intensities.

The residuals from integer coordinates are computed for the sample and line final floating-point geometric coordinates. These residuals are then evaluated in combination against a pre-defined threshold of 0.25. This threshold represents an "in-between" region which determines if the ν flags should be mapped to 1, 2, 3, or 4 pixels in the final geometric space.

7.5　Image Resampling Output

There are three main output data products produced during the image resampling stage: the SILO/SIHI, SILOF/SIHIF, and the VD file. The SILO/SIHI image contains the geometrically resampled intensity values; the SILOF/SIHIF is the "resampled" ν flag image corresponding to the intensity data. The intensity data are output as a FITS image, and the associated ν flags are output as the corresponding FITS image extension. The 3-D VD FITS image produced is the summation of all the geometric corrections implemented to perform the single image resampling and gives, for each pixel in LI space, the final x and y coordinate in SI space. As discussed in Chapter 4, the raw cross correlation data are, after resampling, retained as a binary 3-D table extension to the VD FITS image.

The image resampling module writes information to the HISTORY portion of the image label for each raw science image processed:

- The four Chebyshev coefficients used to define the wavelength linearization,

- The tilt angle (applied only for extended sources),

- Wavelength zeropoint and spatial shifts,

- Final time/temperature corrected dispersion constants, and

- Predicted center line of the large and small apertures.

Chapter 8

Wavelength Calibration

High- and low-dispersion small-aperture spectra of the on-board hollow cathode platinum-neon (Pt-Ne) calibration lamp are used to determine wavelength as a function of position in *IUE* images. These wavelength calibration (WAVECAL) exposures are obtained once a month for each camera and are usually a combination of the calibration spectrum and a tungsten flood lamp (TFLOOD) exposure. The TFLOOD exposure was originally added to raise the DN level of the fainter emission lines and was also used to allow reseau marks to be located on the low-dispersion WAVECAL images; these reseau positions were used by IUE-SIPS to perform geometric corrections, but are not needed in the NEWSIPS system. Since approximately mid-1992 WAVECAL images have been obtained without the superimposed TFLOOD exposures, as it was found that the NEWSIPS wavelength calibration analysis was more accurate without them. Instead, the TFLOOD is taken as a separate exposure.

8.1 Calculation of Dispersion Relations

Each set of calibration images is processed to provide analytic relations between wavelength and pixel position in the geometrically-corrected, rotated, and resampled image (SILO/SIHI) space. The derivation of these dispersion relations is a multi-step process. First, the pixel locations of the Pt-Ne emission lines in the WAVECAL SILO/SIHI image are measured interactively. The measured Pt-Ne line positions are then combined with laboratory values for the wavelength and order number of each emission line (stored in a line library) and used in a regression analysis to determine a set of dispersion constants relating wavelength and order number to pixel location. The line libraries are based on the Pt-Ne line positions measured by Reader *et al.* (1990) at the National Institute of Standards and Technology (NIST). Figure 8.1 shows low-dispersion WAVECAL spectra for the LWP and SWP cameras and indicates the features included in the low-dispersion libraries. Table 8.1 contains listings of the low-dispersion line libraries. The line positions for all cameras, and therefore the dispersion solutions, are expressed in *vacuum* wavelengths.

Because the geometric correction and resampling step of the image processing rotates both high- and low-dispersion images so that the dispersion direction is parallel to the
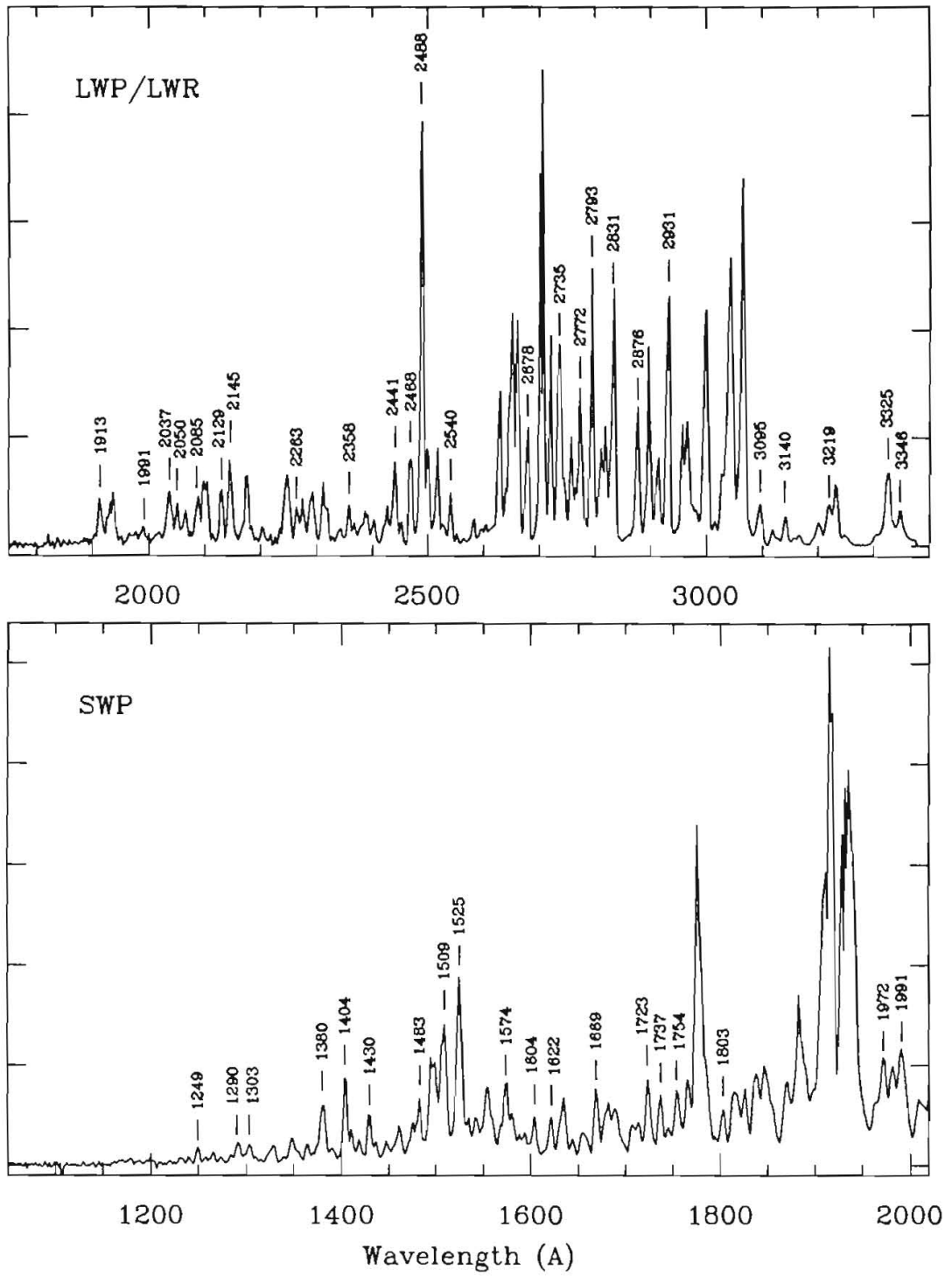
Figure 8.1: Short and long wavelength low-dispersion WAVECAL spectra. Pt-Ne features included in the low-dispersion line libraries are marked.

Table 8.1: Low-Dispersion Pt-Ne Line Libraries

Short Wave Camera (Å)	Long Wave Cameras (Å)
1248.61	1913.23
1289.95	1990.58
1302.79	2037.12
1380.49	2050.05
1403.90	2085.26
1429.52	2129.31
1482.83	2144.92
1509.29	2263.42
1524.73	2357.83
1574.31	2440.80
1604.01	2468.15
1621.65	2487.92
1669.23	2539.97
1723.13	2677.94
1736.52	2734.77
1753.83	2772.48
1802.94	2792.84
1971.54	2831.13
1990.58	2876.48
	2930.65
	3094.90
	3140.30
	3219.12
	3324.69
	3346.42

horizontal or x-axis of the SILO/SIHI image and corrects for the splaying of high-dispersion orders so that the orders are parallel to one another, the terms of the dispersion solutions for the two image dimensions are completely decoupled. The parameterization of the dispersion solutions is as follows:

$$x = A_1 + A_2 m\lambda$$

$$y = B_1 + B_2 m^{-1}$$

where x and y are the image pixel locations, m is the order number, and A_1, A_2, B_1, and B_2 are the dispersion constants. For resampled low-dispersion (SILO) images $m = 1$ and the y dimension of the image contains spatial information only. In this case the B coefficients simply give the image line number at which the spectrum centroid is located.

8.2   Application of the Dispersion Relations

The dispersion solutions derived for individual WAVECAL images are not implemented directly into the production processing system as this would produce a discontinuity in wavelength assignments due to small variations in the dispersion constants derived from individual WAVECALs. These variations arise from two sources, the first of which is simply the measurement uncertainties involved in locating the Pt-Ne emission features in the WAVECAL images and the uncertainties in the coefficients of the derived dispersion solutions. Second, global shifts in the location of the spectral format within individual images are known to occur as a function of camera temperature (THDA) and time (see *e.g.* Thompson 1988 and Garhart 1993). These shifts occur both parallel and perpendicular to the dispersion direction and consequently result in changes to the wavelength zeropoint (A_1) as well as the spatial location (B_1) of spectra within SI images. These format shifts appear to be a translational shift only, with no change in image scale, and as a result the higher order dispersion terms remain constant.

The dispersion solutions for individual WAVECAL images are stored in a master dispersion constant table for each camera. Mean dispersion constants and the temporal and THDA correlations with the zeropoint terms are determined via a regression analysis of the individual solutions stored in this database. The dispersion coefficients, as actually applied to science images, are determined by adding corrections to the mean zeropoint terms appropriate for the observation date and THDA of the particular image. The correction terms W_λ and W_s, which represent the offset that is added to the mean wavelength and spatial zeropoints, are defined by the following general expressions:

$$W_\lambda = W_{1\lambda} + W_{2\lambda}T + W_{3\lambda}t + W_{4\lambda}t^2 + W_{5\lambda}t^3$$

$$W_s = W_{1s} + W_{2s}T + W_{3s}t + W_{4s}t^2 + W_{5s}t^3$$

where W_λ and W_s are the corrections to be added to the A_1 and B_1 terms of the mean dispersion relation, respectively, T is the THDA at the end of exposure, and t is time expressed as the total number of elapsed days since 1 January 1978.

Table 8.2: Time and Temperature Zeropoint Coefficients

	LWP	SWP
A_1 (Å)	1711.6597	1032.4392
A_2 (Å/pix)	2.6626680	1.6763376
B_1 (pix)	23.61	21.97
$W_{1\lambda}$	4.4345033	-2.3252555
$W_{2\lambda}$	4.0537516e-4	3.5285037e-3
$W_{3\lambda}$	-6.0635105e-1	-2.6882430e-1
$W_{4\lambda}$	0.0	-6.1677609e-7
$W_{5\lambda}$	0.0	4.2678509e-11
W_{1s}	-4.3763553	4.3991865
W_{2s}	2.8160580e-4	-3.2833262e-3
W_{3s}	3.6686645e-1	-1.0900706e-1
W_{4s}	0.0	8.2522805e-7
W_{5s}	0.0	-7.1718122e-11

A first-order (*i.e.* linear) fit is sufficient to characterize the correlation between THDA and zeropoint for all cameras. The correlation between time and zeropoint, however, has second- and third-order dependencies for some cameras. The W_λ and W_s coefficients currently in use for the low-dispersion mode of the LWP and SWP cameras are listed in Table 8.2. The zeropoint shifts and corresponding polynomial fits are illustrated graphically for each camera in Figures 8.2–8.3.

8.3 Non-Linearities

Due to residual small-scale geometric distortions introduced by the *IUE* SEC Vidicon cameras, the dispersion solutions for SILO images are not precisely linear in nature. Residuals from a linear fit to the emission-line positions in low-dispersion WAVECAL spectra show significant second- and third-order terms. These distortions lead to wavelength errors on the order of several Angstroms in some regions of SILO images. A remapping (along the dispersion direction) of SILO image data is necessary to eliminate these distortions and allow the use of a linear dispersion relation. This remapping has been incorporated into the resampling (GEOM) step of the image processing system as another vector field that is added to the existing vector fields that describe the image rotation and geometric rectification (Chapter 7.1.3).

Analysis of many WAVECAL spectra has shown that the first-, second-, and third-order dispersion terms for SILO images which have not been linearized are very uniform over time and THDA. This allows the use of a single third-order remapping vector for all images from a
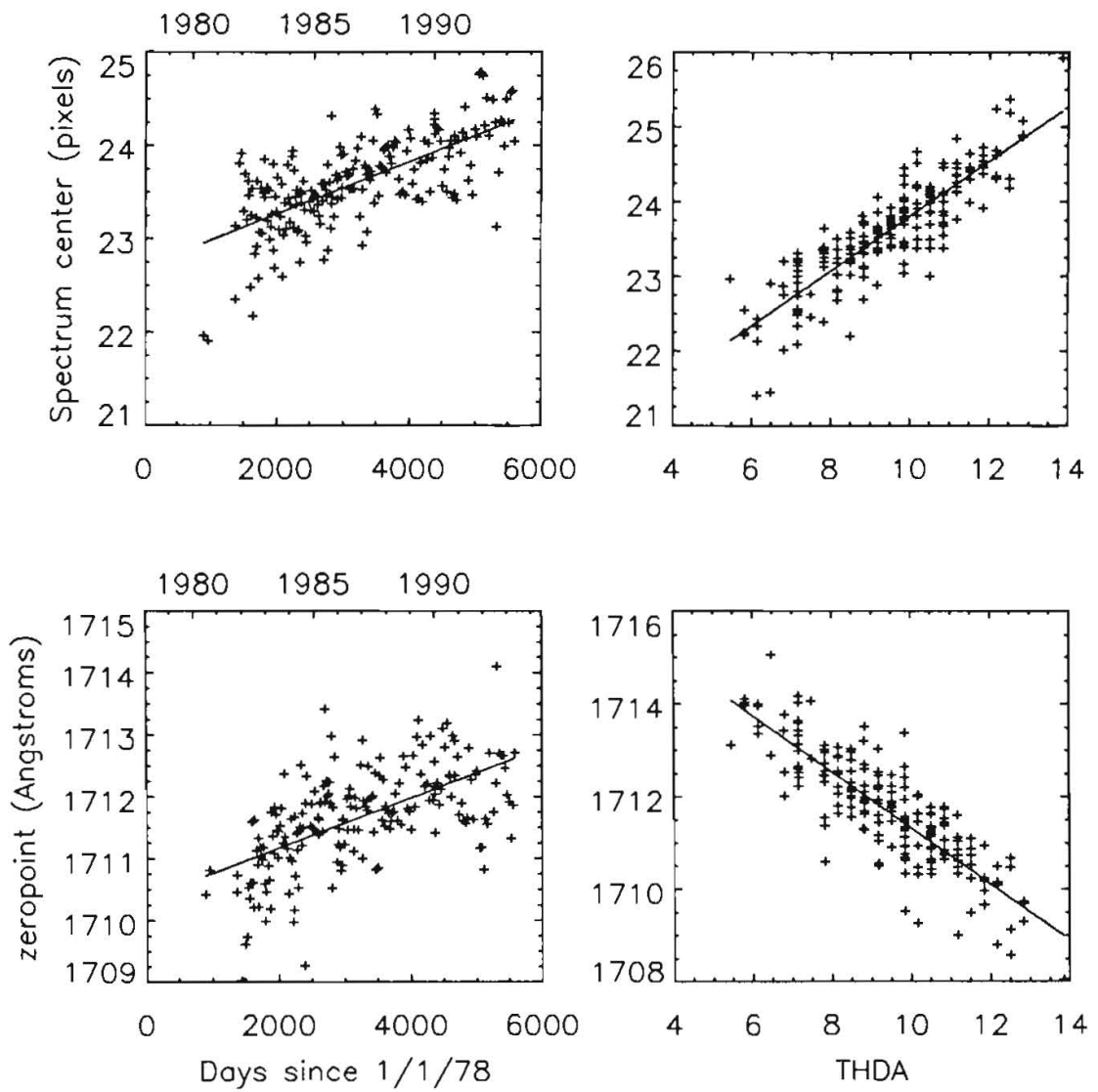
Figure 8.2: Time and temperature correlations with wavelength and spatial zeropoints for the LWP camera.
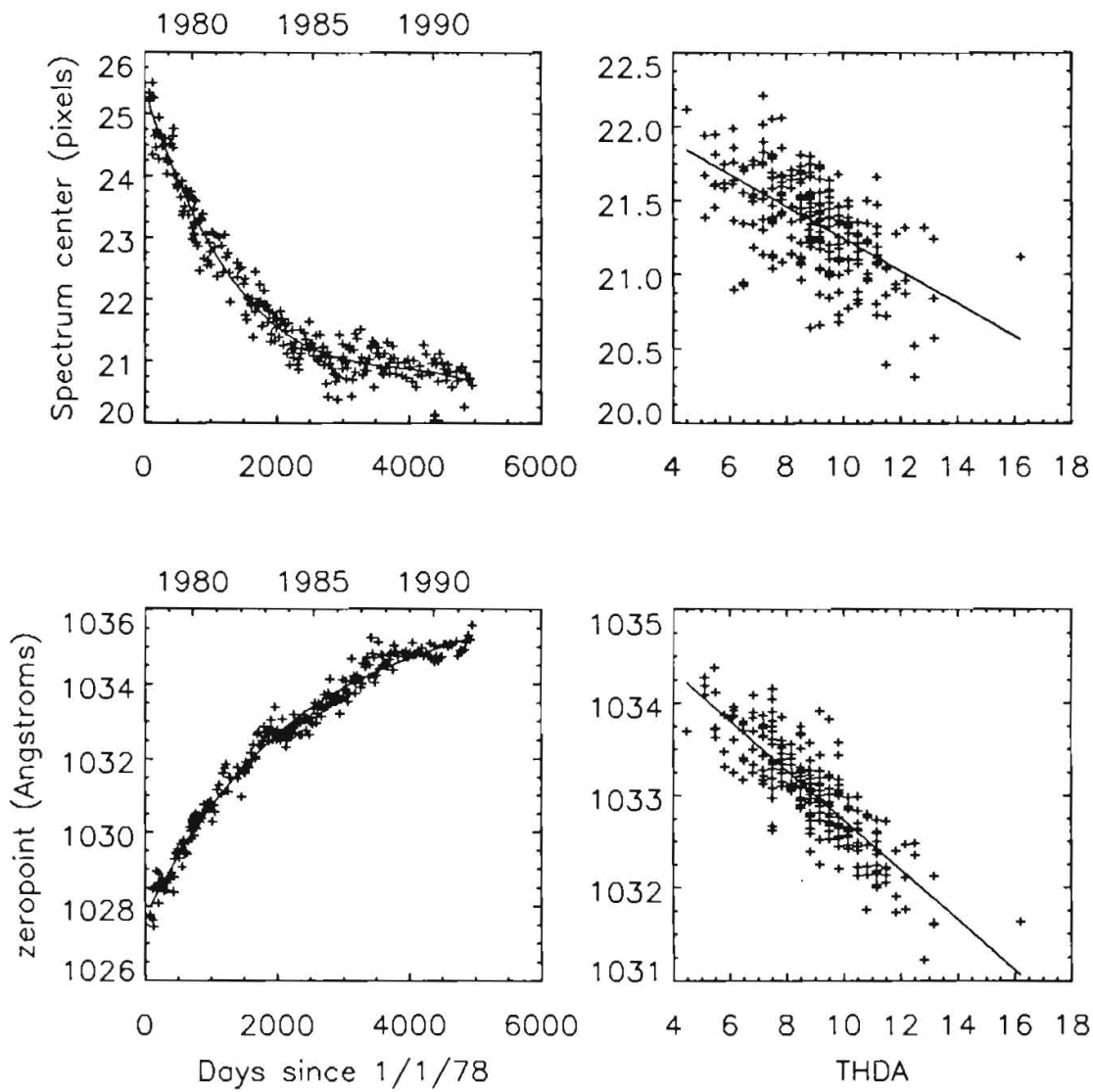
Figure 8.3: Time and temperature correlations with wavelength and spatial zeropoints for the SWP camera.

given camera. The exact form of the correction for each camera is derived as follows. First, a representative sample of WAVECAL images covering the extremes in both observation date and THDA is chosen for analysis. The number of images is typically on the order of 80–90. This sample of images is processed without any attempt to apply the (as yet unknown) linearization correction in the GEOM step. Third-order Chebyshev dispersion solutions are derived for each of these uncorrected images and the mean dispersion coefficients for the entire sample are calculated on a term-by-term basis. The mean dispersion coefficients are converted into equivalent pixel-space coefficients, at which point they can be used within the GEOM processing step to compute the appropriate linearization correction vector to apply to all subsequent images. The resulting linearization correction displacements for each camera are shown graphically in Figure 7.1.

After the linearization correction is determined for a given camera, all WAVECAL images for that camera are processed with the correction applied so that mean linear dispersion solutions and corresponding zeropoint dependencies with time and THDA can be derived as described in the previous sections.

Chapter 9

Extraction of Spectral Flux

9.1   Low-Dispersion Data

Spectral data are extracted from the low-dispersion resampled images (SILO) using a signal weighted extraction technique (SWET). This technique provides an increase in the signal-to-noise ratio of the extracted spectrum, as compared to simple "boxcar" extractions, by utilizing information on the cross-dispersion spectral profile, while preserving the total flux. The output of this technique also includes an error estimate associated with each point in the extracted spectrum and cosmic ray hits are, in many cases, automatically rejected from the calculation of extracted fluxes. The technique, which has been developed for low-dispersion *IUE* data, is based on the weighted slit extraction code originally developed by Horne (1986) for use with optical CCD data. A detailed explanation of the adaptation of this software for use with *IUE* data processed using IUESIPS is given by Kinney *et al.* (1991) who supplied the software to the *IUE* Project. Various threshold values in the code were modified by the *IUE* Project to account for the very different flux scales of NEWSIPS and IUESIPS.

Briefly, the processing steps involved in the weighted extraction of a one-dimensional spectrum from a SILO image are as follows:

- The background flux as a function of wavelength in the SILO image is characterized by a sixth-order Chebyshev polynomial.

- The spectral signal is located within the image and the average signal strength is evaluated in order to determine whether or not a spectral profile can be computed empirically.

- If there is sufficient signal strength, the cross-dispersion instrumental flux profile is derived for each wavelength sample. A default profile shape is used for spectra that are too faint to allow an empirical determination.

- The cross-dispersion profile is used in combination with a model of the detector noise characteristics to identify anomalous data points which are to be excluded from the computation of extracted fluxes.

- The good data points are weighted according to their positions on the cross-dispersion profile and according to their relative noise in order to calculate the total net flux and its associated one-sigma uncertainty at each wavelength sample.

- A one-dimensional ν flag spectrum is calculated to show where flagged pixels may have precluded the calculation of a reasonable flux value.

9.1.1 Noise Models

Two portions of the extraction procedure rely upon an estimate of the detector noise in order to perform their functions. First, the cross-dispersion profile fitting routine utilizes the estimated signal-to-noise ratios of each wavelength sample in order to calculate appropriately weighted spline fits to the data. Second, the extraction procedure uses the noise model information to derive an error estimate for each point in the extracted spectrum. The noise models are derived empirically for each camera by measuring the scatter in the flux numbers (FN) around the mean FN in the background regions of several hundred science and flat-field images taken at a variety of exposure levels. Since the sigma as a function of FN is wavelength-dependent, the analysis is performed within 20 equal-sized wavelength bins (∼54Å wide for the SWP and ∼85Å wide for the long wavelength cameras) in SILO images. For each wavelength bin the standard deviation in FN versus mean FN is represented by a third-order polynomial. The wavelength-dependence of the four coefficients of this polynomial are then each represented with a third-order polynomial to allow a determination of the expected standard deviation of any pixel given its wavelength and observed FN. All images that are used to create the noise models are identified in the Final Catalog as utilized in the Final Archive calibration.

9.1.2 Background Flux

The background that is present on *IUE* images is composed of contributions from several sources, including the null, particle radiation, radioactive decays within the detector phosphor, halation within the UV converter, background skylight, and scattered light. The integrated effect of the last three sources varies in a complicated manner across the target depending on the spectral flux distribution of the object observed, whereas the general radiation and null components vary slowly across the vidicon tube. In practice, the average background flux in the SILO image is computed within two regions on either side of the spectrum and this average flux as a function of wavelength is fitted with a sixth-order Chebyshev polynomial.

The two background regions that are examined are each 7 pixels wide and, for large-aperture data, begin at a distance of 13 pixels from the predicted center location of the spectrum. For small-aperture data the two regions begin at a distance of 8 pixels from the center of the spectrum (see Figure 9.1). The narrow large-aperture extraction region corresponds to the 13 pixel point source slit height, while the broad region is the 23 pixel extended, trailed, multiple, and flat-field source slit height. The entire wavelength space of

the SILO image is included in the analysis. Before calculating the average flux as a function of wavelength for each of the two regions, each spatial image line within the two regions is examined individually in order to identify flagged pixels. The FN values of flagged pixels are temporarily replaced with the FN value of the closest unflagged pixel. Telemetry dropouts in the background regions are identified during this process and ν flag values of -4 are set in the output one-dimensional flag spectrum as well as retroactively set in the two-dimensional SILOF image. This flag replaces the original value of -8192.

At this point a difference spectrum is computed from the average FN as a function of wavelength for each of the two background regions. This difference spectrum is used to detect the presence of cosmic ray hits that may occur in either of the two regions. The Chebyshev polynomial that will be fitted to the background data is sensitive to broad features such as grazing cosmic ray hits. Since we are only concerned with relatively broad features, the difference spectrum is smoothed with a 7 pixel wide boxcar function. The mean and standard deviation of the smoothed difference spectrum is then computed and any pixel locations that deviate by more than 2σ from the mean have their weights for the polynomial fitting step set to zero. All remaining good pixel locations are given equal non-zero weights in the polynomial fit. Pixel locations that are beyond the long wavelength edge of the camera target area are also excluded from the polynomial fit. Once the Chebyshev fit has been calculated, the values in the one-dimensional background spectrum that correspond to locations outside the camera target area are replaced with the fitted value of the last valid pixel.

9.1.3   Spectrum Location and Signal Level

The location of the spectrum in the SILO image (in the cross-dispersion direction) is found by computing the wavelength-averaged flux-weighted centroid of the sky-subtracted flux levels within a search region that is centered on the predicted spectrum location. For SWP images the region of the SILO image below 1233Å is excluded from this calculation so as to avoid contamination from geocoronal Lyα. If insufficient signal exists from which to determine reliably a location for the spectrum, the predicted center position is used instead and a warning message to this effect appears in the processing history log.

If the spectrum centroid can be determined empirically, then the dispersion line that contains the maximum net flux (summed over wavelength) is also determined and is referred to as the spectrum peak location. The wavelength-averaged net flux of this dispersion line is computed and compared against the threshold value of 5 FN in order to determine whether the spectral signal is strong enough to attempt an empirical profile fit. For the SWP camera, the region below 1233Å is excluded from this computation so as to avoid contamination from geocoronal Lyα. If the image is processed as a point source, then a warning message appears if the location of the spectrum peak is found to be more than one image line away from the spectrum centroid, since this may indicate that the spectrum is not characteristic of a point source but rather may be spatially extended.

If the average FN of the peak line of the spectrum is below the threshold value, then an empirical fit is not attempted. Instead, a default profile shape is used to compute the
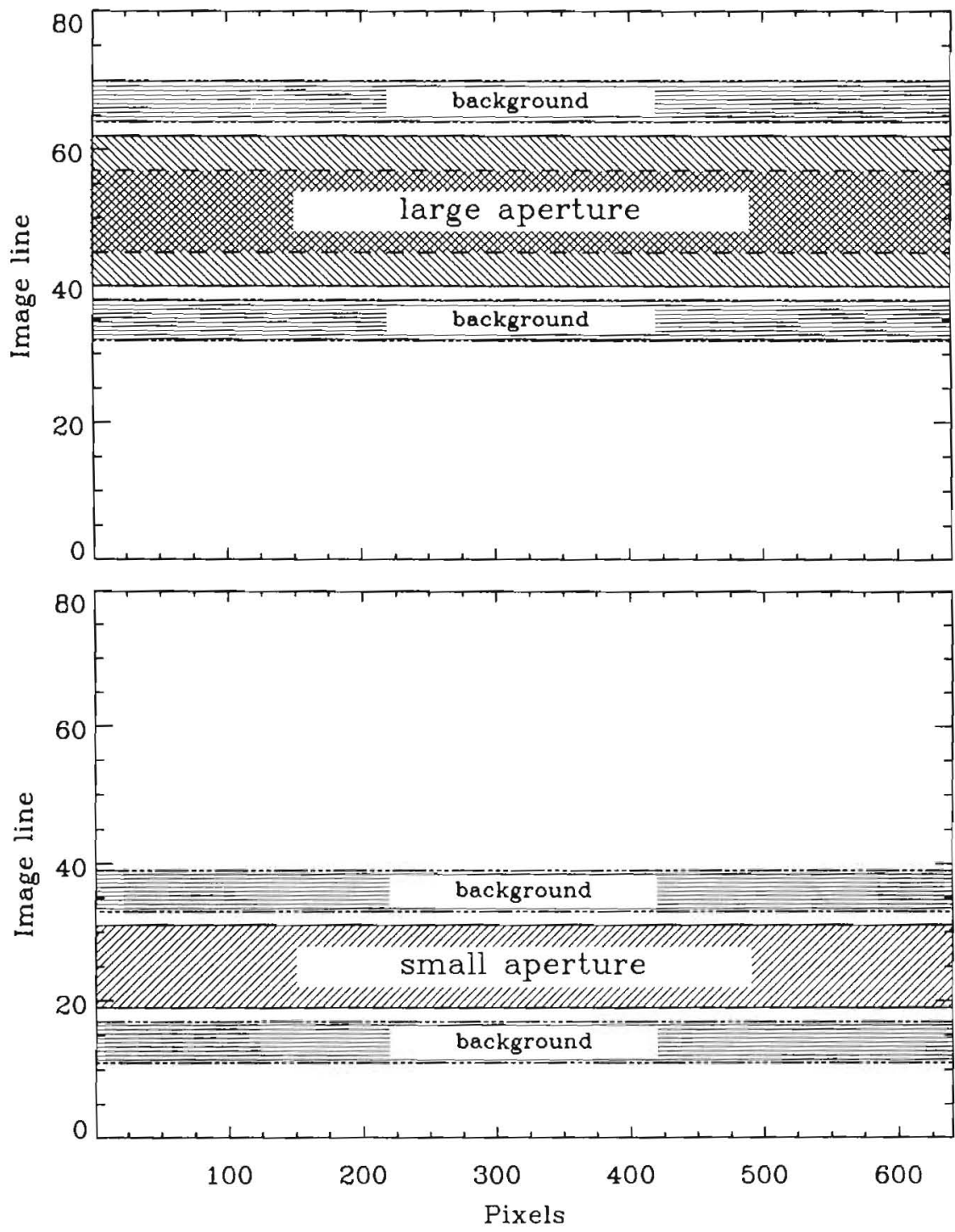
Figure 9.1: Locations of the extraction and background fitting regions within SILO images.

extracted fluxes. There are three default profiles for point sources, one for each camera. Each default profile has been derived from well-exposed observations of *IUE* standard stars, by averaging the profile fits for these observations over wavelength and renormalizing, thus producing a profile that is constant in wavelength. Since the spectral profile for *IUE* data is not repeatable from image to image, this average profile provides a rough weighting that is useful in very low signal images and provides a lower noise spectrum than attempting to fit the profile from the image. For extended and trailed sources, the default profile has a boxcar-like shape where all spatial image lines receive equal weights. Warning messages appear in the processing history log when a default profile is used.

A warning message is also issued if the location of the spectrum centroid is found to be more than two image lines away from the predicted spectrum center. This situation may arise if the location of the spectral format within the raw image space does not follow, for whatever reason, the normal behavior of the spectral format as a function of time (observation date) and camera temperature (THDA) as may be the case for objects poorly centered in the aperture. If this is the case, then the time and temperature-corrected dispersion constants that are computed for this particular image may be called into question. Note, however, that this warning only indicates that the location of the spectrum in the cross-dispersion (*i.e.* spatial) direction has been found to be unusual. We have no information as to whether or not a similar shift may have occurred in the dispersion direction of the image.

The search for the spectrum center and the determination of the average peak FN is skipped entirely for images classified as flat-field (*i.e.* nulls and other floodlamp only images), since they contain no spectral data. In this case the predicted spectrum center location and the default profile for extended/trailed sources are used to perform the computation of extracted fluxes.

9.1.4   Profile Fitting

The cross-dispersion profile is determined from the background-subtracted net flux data. Each line of data in the SILO image that is contained within the spatial limits of the extraction slit (13 lines for point sources, 23 lines for extended, trailed, multiple, and flat-field sources) is temporarily binned in wavelength according to the signal-to-noise ratio, with bin sizes typically ranging from 1 to 10 pixels. A warning is issued if the bin size exceeds 4 pixels since this may indicate either weak or noisy spectral data or that a large fraction of the data is unusable due to conditions such as saturation or telemetry dropouts. The area under the cross-dispersion profile at each wavelength bin is then normalized to one to divide out the spectral information. After normalizing, the fraction of flux in each line of data (relative to the total flux in each wavelength bin) is smoothed by fitting splines with anywhere from 2 to 15 nodes in each line.

The number of spline nodes is determined dynamically based on the total of the square of the signal-to-noise ratio (S/N) of the spectral data. The placement of the nodes in wavelength space is also determined dynamically so that the data located between each pair of nodes have an equal total of $(S/N)^2$. Thus regions of higher S/N have more spline nodes placed

more closely together than regions with lower S/N. All lines of data in the cross-dispersion direction use the same number and placement of spline nodes and there is always a minimum of two nodes placed at either end of the spectrum. The spline fits for each line of data are computed iteratively, rejecting data bins that have residuals to the fit greater than 3.5σ. The iteration cycle ends when no new bins are rejected.

In the procedure outlined above, those wavelength bins that have negative or zero total flux are rejected from the computation of the spline fits. If bins on either end of the spectrum are rejected, they are replaced by the average fraction of light values for the last 10 good bins closest to the end. This is done to avoid extrapolation of the high order splines into wavelength regions that have no constraining data. Rejected bins that are not at either end of the spectrum but are located in the interior of spectrum are simply excluded from the computation of the spline fit and are therefore essentially interpolated over. This extrapolation/interpolation process provides a means of dealing with discontinuous data.

The cross-dispersion profile at each wavelength sample is constructed by evaluating the splines, clipping the negative values that may occur in the wings of the profile, and renormalizing to ensure a sum of unity at each wavelength. Thirteen splines are used to specify the cross-dispersion profile for point source data, and 23 are used for extended, trailed, or multiple sources. This profile is used when computing the extracted fluxes to weight the data so that the pixels with the largest fraction of light are given the most weight. Because the profile is derived by fitting each spatial line of data independently of other lines, a wide variety of profiles can be accommodated. Specifically, the algorithm is very capable of handling spectra obtained through either the large or small spectrograph apertures, trailed sources, and extended objects with complicated source structures which may cause the profile to vary dramatically as a function of wavelength. However, because the algorithm produces a single output spectrum, spectra of several sources in the aperture (multiple spectra) will not be separated. Such images will require custom extraction.

9.1.5 Extraction of Flux and Cosmic Ray Removal

The computation of the extracted flux and corresponding identification and rejection of bad pixels is performed iteratively. The total flux at each wavelength is found by performing a weighted sum of all good (*i.e.* unflagged) pixels at the given wavelength according to:

$$FN_{total} = \frac{\sum FN(i) \times p(i)/\sigma(i)^2}{\sum p(i)^2/\sigma(i)^2}$$

where $FN(i)$ is the net flux of the ith spatial pixel at this wavelength, and $p(i)$ and $\sigma(i)$ are the corresponding profile and estimated noise values for that pixel. Similarly, the estimated error in the extracted flux is:

$$error(i) = \sqrt{\frac{1}{\sum p(i)^2/\sigma(i)^2}}$$

which is hereafter referred to as the "sigma" spectrum. Because the sum of the profile values is involved in the calculation of the total flux, individual bad pixels can be excluded from the

sum so that a reliable estimate of the total flux can be obtained based on only the remaining good pixels.

Pixels which have already been assigned ν flags by the earlier processing stages are excluded from the extracted flux computation. Pixels having anomalous FN values but which were not flagged previously (hereafter referred to generically as cosmic ray pixels) are also identified and excluded during calculation of extracted fluxes. This is accomplished by rejecting the most extreme outlying pixel at each wavelength sample if the value of that pixel is greater than a predetermined sigma level from the scaled profile at that wavelength. The threshold values for this rejection are 6, 5, and 4σ for the LWP, LWR, and SWP cameras, respectively. The rejection thresholds for each camera were determined empirically so that most cosmic ray pixels are removed without removing good data points. When such a pixel is identified, it is assigned a ν flag value of -32 which is written back into the SILOF image. Each time a new cosmic ray pixel is identified and excluded, an updated value for the total flux at that wavelength is computed. This process is repeated until no more pixels are rejected or until less than 30% of the flux in the profile at that wavelength sample remains.

The total numbers of pixels excluded as bad because they had already been assigned ν flags before the extraction procedure and those excluded as cosmic ray pixels by this routine are reported to the processing history log. In the event that either of these values exceeds 10% of the total number of pixels available to the extraction process, a warning message is issued in the processing history log.

9.1.6   One-Dimensional ν Flag Spectrum

In deriving the one-dimensional ν flag spectrum, the cross-dispersion profile and the flag values in the SILOF image are examined. For each wavelength sample the contribution to the spectral profile from unflagged pixels is calculated. If this contribution amounts to at least 45% of the total flux (as represented by the associated profile values), the wavelength sample will contain no flags in the output spectrum. If less than 45% of the total flux in the profile is from unflagged pixels, then each flag value is examined individually to determine what fraction of the total contribution from all pixels is due to one particular flag condition. For each flag condition that affects pixels representing more than 15% of the spectral profile, that flag value will appear in the output flag spectrum.

Situations can exist in which the contribution by pixels with one particular flag condition account for 45% of the flux at a given wavelength, for example, and a second flag condition is associated with pixels that account for only 11%. Here the total contribution from flagged pixels exceeds the 55% threshold, but only the flag value corresponding to the first condition will appear in the output flag spectrum. The threshold values were determined empirically so that problem conditions that definitely have an adverse affect on the computation of extracted fluxes are always flagged in the output spectrum, while, at the same time, conditions that only have a marginal impact are not flagged. Note that in marginal cases where only one or perhaps a few pixels that contribute in a relatively minor way to the total flux at a given wavelength are flagged and hence excluded from the computation of the extracted

flux, the associated error estimate for that extracted flux value will be increased accordingly even though no flags will appear in the output spectrum. Thus the sigma spectrum serves as an additional indicator of the relative accuracy of the extracted fluxes.

9.1.7 MXLO File Contents

The MXLO file contains the net (sky-subtracted) integrated flux spectrum, the Chebyshev characterized background spectrum, the ν flag spectrum, the absolutely calibrated net flux spectrum, and the calibrated sigma spectrum. The net flux and background spectra are in units of FN, the flag spectrum is in the normal bit-encoded unitless values, and the calibrated flux and sigma spectra are in physical units of ergs sec^{-1} cm^{-2} Å^{-1}. The sigma spectrum, originally computed in FN units, undergoes identical calibration steps (including all corrections for sensitivity degradation, etc.) as the net flux spectrum. The next chapter details the process of absolute flux calibration.

The background flux spectrum is scaled to the same integrated slit length as the net flux spectrum and is evaluated over the entire wavelength space of the camera target region as contained in the SILO image (1050 to ~2000Å for SWP and 1750 to ~3400Å for LWP and LWR). The values of pixel locations past the long wavelength end of the camera target are replications of the last valid pixel value. The net flux and sigma spectra are computed over the entire wavelength space of the SILO image, but locations that are outside the camera target area will have net fluxes equal to zero because these regions do not contain any valid image data. The edge of the camera target areas are encountered at wavelengths greater than (approximately) 3395, 3425, and 2000Å for the LWP, LWR, and SWP cameras, respectively, for large-aperture spectra. Due to the curvature of the target boundary, small-aperture spectra reach the target edge at different wavelengths: 3380, 3400, and 2015Å for the LWP, LWR, and SWP cameras. The absolute calibrations are valid over wavelength limits of 1150–1980Å for SWP and 1850–3350Å for LWP and LWR. Beyond these limits the calibrated net flux and sigma spectra are set to values of 0 and −1, respectively and have a ν flag value of −2. The valid wavelength limits of the calibrated spectra are consequently somewhat truncated as compared to the net flux spectrum.

Chapter 10

Calibration of the Net Flux Data

10.1 Absolute Flux Calibration

10.1.1 Zero-Epoch Point Source Calibrations

Absolute flux calibrations have been derived for the low-dispersion modes of the IUE cameras through observations of ultraviolet photometric standard stars, as well as observations and models of the white dwarf star, G191-B2B. All spectra used in the determination of the absolute flux calibration are identified in the Final Catalog as utilized in the Final Archive calibration. The wavelength-dependence of the inverse sensitivity function (S_λ^{-1}) for each camera has been determined by comparison of IUE observations of the white dwarf star with model atmosphere calculations that were provided to the IUE project by D. Finley. The overall zeropoint of the calibration curves has been set by applying the white dwarf derived S_λ^{-1} values to IUE observations of ultraviolet photometric standard stars and comparing these results with OAO-2 measurements in the 2100–2300Å band (see González-Riestra, Cassatella, and de la Fuente 1992 for details regarding the calibration procedures).

The final S_λ^{-1} curves for the LWP and SWP, evaluated in 15Å and 10Å bins, respectively, are listed in Tables 10.1–10.2. The absolute flux at a given wavelength, F_λ (ergs sec^{-1} cm^{-2} Å^{-1}), is computed as follows:

$$F_\lambda = FN_\lambda \times S_\lambda^{-1}/t_{eff}$$

where FN_λ is the extracted net flux in FN units, S_λ^{-1} is the inverse sensitivity value at that wavelength, and t_{eff} is the effective exposure time in seconds. The inverse sensitivity value at a particular wavelength is determined by quadratic interpolation of the tabulated values for a given camera.

The effective exposure time for point sources is derived from the original commanded exposure time, t_{com}, and takes into account the effects of On-Board Computer (OBC) tick rounding and the camera rise time, t_{rise}, as follows:

$$t_{eff} = 0.4096 \times INT(t_{com}/0.4096) - t_{rise}$$

where the values of t_{rise} for each camera are taken from González-Riestra (1991) and are

92

0.123, 0.126, and 0.130 for the LWP, LWR, and SWP cameras, respectively. Tick rounding results from the integer arithmetic used by the OBC in commanding exposures. Effective exposure times for large-aperture trailed observations are determined according to:

$$t_{TR} = Trail\ length/Trail\ rate \times Passes$$

where $Trail\ length$ is the trail path length of the aperture in arcsec, $Trail\ rate$ is the effective trail rate in arcsec/sec, and $Passes$ is the number of passes across the aperture. Because the OBC uses integer arithmetic in calculating fixed rate slews, there is a truncation in the commanded trail rate. This "rounding off" is similar to the OBC quantitization of point source exposure times. The effective trail rate is calculated using the following equation:

$$TR_{eff} = \sqrt{(LSB \times INT(0.4695 \times TR_{com}/LSB))^2 + (LSB \times INT(0.8829 \times TR_{com}/LSB))^2}$$

where LSB is the least significant bit (0.03001548/32 arcsec/sec) and TR_{com} is the commanded trail rate.

10.1.2   Aperture Response Corrections

The S_λ^{-1} functions described above apply only to point source observations acquired through the large aperture. The small-aperture and trailed observing modes are known to have different relative responses as compared to large-aperture point spectra (*e.g.* Harris and Cassatella 1985, Bohlin 1986, Crenshaw and Park 1989). This effect has been ascribed to several sources, including vignetting effects of the entrance apertures in trailed and small-aperture spectra and spatial inhomogeneities in the UVC efficiency (Cassatella 1990). Application of the large-aperture point source calibration to spectra obtained either in trail mode or through the small aperture will introduce photometric errors of at least 5–7% in the regions near the detector edge and of 1–2% in regions where the camera response is flatter.

Calibration corrections for small-aperture and for large-aperture trailed observations have been derived and are applied by the processing system when necessary. *IUE* standard-star observations from the 1984–1985 epoch have been used to calculate the wavelength-dependent flux ratios of small- and large-aperture point sources, and of large-aperture point source and trail mode observations. Observations from the 1984–1985 epoch were chosen so as to match the large-aperture point source calibration epoch. Also, by limiting the range of time over which the observations were obtained, effects due to sensitivity degradation in the cameras are minimized.

Optimal exposure level observations of the four TD1 standard stars BD+28° 4211, HD 93521, HD 60753, and BD+75° 325 were used to compute the small-to-large aperture (S/L) ratios and the large-aperture trailed-to-point source (T/L) ratios. The effective exposure times of the trailed observations were determined using a value of 21.48 arcseconds for the SWP major-axis trail path length (Garhart 1992b) and 21.84 arcseconds for the LWP major-axis trail path length. The ratios of pairs of observations of the same object obtained through the small and large apertures, or in point and trail modes were averaged together

to determine the mean S/L and T/L spectral ratios. Approximately 20 pairs of spectra were used to determine each of the two response ratios. The mean spectral ratios were resampled into the bin size of the appropriate inverse sensitivity function and a spline fit to the binned ratios was calculated. Tabulated values of the spline fits for each camera are listed in Tables 10.3–10.4.

Because centering errors in the small aperture can lead to large variations in the overall observed flux level for individual spectra, it is impossible to determine an absolute S/L ratio. Therefore, the average of S/L over all wavelengths is normalized to unity. *As a result, the small-aperture fluxes are known in a relative sense but not in an absolute one.* The relative small- and absolute large-aperture inverse sensitivities are related by

$$S_\lambda^{-1}(S) = S_\lambda^{-1}(L)/(S/L).$$

Investigators should be aware that absolute fluxes for small-aperture data are significantly less reliable than those of large-aperture data. For the ratio of trailed response to point sources in the large aperture, the absolute calibrations are related by

$$S_\lambda^{-1}(T) = S_\lambda^{-1}(L)/(T/L).$$

Only trailed large-aperture spectra are calibrated with the T/L ratio applied. Images processed as extended sources are calibrated as point source observations.

10.1.3 Gain Factors

The S_λ^{-1} function for the LWR camera will be derived from observations obtained at a UVC voltage setting of -5.0 kV. Therefore all LWR observations that have been obtained at the reduced voltage setting of -4.5 kV have an absolute calibration gain correction factor of 1.37 applied by the processing system (Harris 1985). A message to this effect is included in the processing history log. In the event that an observation for any camera has been obtained at non-standard settings of either the exposure gain (normally MAXIMUM) or the camera read gain (normally LOW), an additional absolute flux scaling factor is multiplicatively applied as follows (cf. Coleman *et al.* 1977):

- Exposure Gain Corrections

  Maximum: Correction = 1.0
  Medium: Correction = 3.0
  Minimum: Correction = 10.0

- Read Gain Corrections

  High: Correction = 0.33
  Low: Correction = 1.0

Corrections are also applied to the absolute flux spectrum to take into account changes in camera sensitivity as a function of time (observation date) and camera temperature (THDA). The derivation and application of these corrections are detailed in the following sections.

Table 10.1: LWP Absolute Calibration

λ	S^{-1}[a]	λ	S^{-1}	λ	S^{-1}
1850	93.736	2360	6.108	2870	2.823
1865	62.950	2375	5.855	2885	2.877
1880	45.372	2390	5.560	2900	2.925
1895	35.791	2405	5.221	2915	2.998
1910	30.233	2420	4.918	2930	3.135
1925	25.704	2435	4.699	2945	3.314
1940	21.886	2450	4.498	2960	3.414
1955	18.946	2465	4.221	2975	3.686
1970	16.467	2480	3.902	2990	3.911
1985	14.460	2495	3.892	3005	4.132
2000	13.095	2510	3.892	3020	4.465
2015	12.447	2525	3.650	3035	4.868
2030	12.234	2540	3.460	3050	5.326
2045	12.084	2555	3.222	3065	5.972
2060	11.730	2570	3.173	3080	6.614
2075	11.326	2585	3.162	3095	7.318
2090	11.123	2600	3.010	3110	8.075
2105	11.227	2615	2.904	3125	9.101
2120	11.355	2630	2.853	3140	10.060
2135	11.266	2645	2.801	3155	11.577
2150	11.174	2660	2.739	3170	13.041
2165	11.127	2675	2.673	3185	14.704
2180	11.095	2690	2.635	3200	16.832
2195	11.050	2705	2.666	3215	19.605
2210	10.963	2720	2.726	3230	23.110
2225	10.806	2735	2.633	3245	27.069
2240	10.533	2750	2.636	3260	31.107
2255	10.026	2765	2.618	3275	35.122
2270	9.261	2780	2.648	3290	40.094
2285	8.657	2795	2.759	3305	47.271
2300	8.456	2810	2.702	3320	57.623
2315	7.974	2825	2.705	3335	71.007
2330	7.225	2840	2.729	3350	87.001
2345	6.560	2855	2.769		

[a]Inverse sensitivity in units of 10^{-13} ergs cm^{-2} Å^{-1} FN^{-1}.

Table 10.2: SWP Absolute Calibration

λ	S^{-1a}	λ	S^{-1}	λ	S^{-1}
1150	10.60	1440	1.491	1730	1.269
1160	7.032	1450	1.535	1740	1.226
1170	4.666	1460	1.568	1750	1.185
1180	3.204	1470	1.593	1760	1.149
1190	2.377	1480	1.616	1770	1.117
1200	1.921	1490	1.642	1780	1.089
1210	1.614	1500	1.677	1790	1.067
1220	1.396	1510	1.721	1800	1.049
1230	1.249	1520	1.766	1810	1.035
1240	1.153	1530	1.798	1820	1.025
1250	1.090	1540	1.808	1830	1.019
1260	1.045	1550	1.805	1840	1.017
1270	1.012	1560	1.798	1850	1.019
1280	0.991	1570	1.789	1860	1.025
1290	0.980	1580	1.778	1870	1.034
1300	0.977	1590	1.764	1880	1.046
1310	0.981	1600	1.745	1890	1.059
1320	0.992	1610	1.729	1900	1.071
1330	1.008	1620	1.706	1910	1.081
1340	1.030	1630	1.681	1920	1.086
1350	1.057	1640	1.652	1930	1.084
1360	1.089	1650	1.620	1940	1.073
1370	1.125	1660	1.584	1950	1.054
1380	1.166	1670	1.544	1960	1.038
1390	1.213	1680	1.501	1970	1.040
1400	1.265	1690	1.456	1980	1.075
1410	1.322	1700	1.409		
1420	1.381	1710	1.362		
1430	1.439	1720	1.315		

[a]Inverse sensitivity in units of 10^{-12} ergs cm^{-2} $\mathrm{\AA}^{-1}$ FN^{-1}.

Table 10.3: LWP S/L and T/L Relative Sensitivities

λ	S/L	T/L	λ	S/L	T/L	λ	S/L	T/L
1850	1.0487	0.9892	2360	1.0247	1.0036	2870	0.9982	0.9957
1865	1.0263	0.9897	2375	1.0212	1.0000	2885	0.9977	0.9951
1880	1.0059	0.9898	2390	1.0174	0.9965	2900	0.9963	0.9947
1895	0.9894	0.9896	2405	1.0135	0.9935	2915	0.9940	0.9944
1910	0.9786	0.9891	2420	1.0098	0.9909	2930	0.9909	0.9942
1925	0.9734	0.9884	2435	1.0067	0.9888	2945	0.9873	0.9942
1940	0.9725	0.9877	2450	1.0044	0.9872	2960	0.9834	0.9945
1955	0.9747	0.9868	2465	1.0031	0.9859	2975	0.9796	0.9951
1970	0.9787	0.9860	2480	1.0028	0.9850	2990	0.9761	0.9960
1985	0.9832	0.9853	2495	1.0032	0.9845	3005	0.9733	0.9973
2000	0.9869	0.9848	2510	1.0042	0.9844	3020	0.9714	0.9990
2015	0.9888	0.9845	2525	1.0055	0.9845	3035	0.9706	1.0012
2030	0.9890	0.9845	2540	1.0070	0.9850	3050	0.9714	1.0040
2045	0.9879	0.9848	2555	1.0084	0.9857	3065	0.9738	1.0075
2060	0.9859	0.9856	2570	1.0096	0.9867	3080	0.9776	1.0116
2075	0.9834	0.9870	2585	1.0104	0.9878	3095	0.9827	1.0165
2090	0.9809	0.9889	2600	1.0104	0.9891	3110	0.9886	1.0223
2105	0.9786	0.9914	2615	1.0097	0.9904	3125	0.9951	1.0290
2120	0.9770	0.9946	2630	1.0084	0.9918	3140	1.0020	1.0367
2135	0.9766	0.9983	2645	1.0065	0.9932	3155	1.0089	1.0454
2150	0.9776	1.0022	2660	1.0042	0.9945	3170	1.0156	1.0549
2165	0.9804	1.0062	2675	1.0018	0.9957	3185	1.0218	1.0644
2180	0.9848	1.0100	2690	0.9993	0.9968	3200	1.0271	1.0731
2195	0.9902	1.0136	2705	0.9970	0.9976	3215	1.0314	1.0801
2210	0.9965	1.0167	2720	0.9950	0.9982	3230	1.0348	1.0845
2225	1.0031	1.0192	2735	0.9935	0.9985	3245	1.0372	1.0856
2240	1.0097	1.0208	2750	0.9926	0.9987	3260	1.0389	1.0824
2255	1.0160	1.0213	2765	0.9925	0.9987	3275	1.0400	1.0742
2270	1.0215	1.0208	2780	0.9929	0.9985	3290	1.0405	1.0601
2285	1.0258	1.0193	2795	0.9938	0.9982	3305	1.0405	1.0392
2300	1.0287	1.0171	2810	0.9950	0.9978	3320	1.0403	1.0120
2315	1.0297	1.0142	2825	0.9961	0.9974	3335	1.0398	0.9804
2330	1.0292	1.0109	2840	0.9972	0.9968	3350	1.0392	0.9466
2345	1.0274	1.0073	2855	0.9979	0.9963			

Table 10.4: SWP S/L and T/L Relative Sensitivities

λ	S/L	T/L	λ	S/L	T/L	λ	S/L	T/L
1150	0.970	1.000	1440	1.020	0.981	1730	0.997	0.994
1160	0.974	0.995	1450	1.020	0.984	1740	0.996	0.995
1170	0.977	0.991	1460	1.020	0.986	1750	0.995	0.995
1180	0.981	0.986	1470	1.020	0.988	1760	0.993	0.995
1190	0.984	0.982	1480	1.020	0.990	1770	0.992	0.995
1200	0.987	0.977	1490	1.019	0.991	1780	0.991	0.996
1210	0.990	0.973	1500	1.019	0.992	1790	0.990	0.996
1220	0.992	0.969	1510	1.019	0.992	1800	0.988	0.996
1230	0.995	0.965	1520	1.018	0.992	1810	0.987	0.996
1240	0.997	0.962	1530	1.018	0.992	1820	0.986	0.997
1250	1.000	0.959	1540	1.017	0.993	1830	0.984	0.997
1260	1.002	0.956	1550	1.016	0.992	1840	0.983	0.997
1270	1.004	0.953	1560	1.016	0.992	1850	0.982	0.998
1280	1.006	0.951	1570	1.015	0.993	1860	0.981	0.998
1290	1.007	0.949	1580	1.014	0.993	1870	0.980	0.998
1300	1.009	0.947	1590	1.013	0.993	1880	0.979	0.998
1310	1.010	0.947	1600	1.012	0.993	1890	0.977	0.999
1320	1.012	0.946	1610	1.011	0.993	1900	0.976	0.999
1330	1.013	0.947	1620	1.010	0.993	1910	0.975	0.999
1340	1.014	0.948	1630	1.009	0.993	1920	0.974	1.000
1350	1.015	0.949	1640	1.008	0.993	1930	0.973	1.000
1360	1.016	0.952	1650	1.007	0.993	1940	0.972	1.000
1370	1.017	0.955	1660	1.006	0.993	1950	0.971	1.001
1380	1.018	0.958	1670	1.005	0.993	1960	0.971	1.001
1390	1.018	0.962	1680	1.004	0.993	1970	0.970	1.001
1400	1.019	0.965	1690	1.003	0.994	1980	0.969	1.002
1410	1.019	0.970	1700	1.001	0.994			
1420	1.020	0.973	1710	1.000	0.994			
1430	1.020	0.977	1720	0.999	0.994			

10.2 Camera Sensitivity Degradation Correction

The sensitivity of the SEC Vidicon camera is known to degrade with time, hence the need for a method to correct for this loss. One of the fundamental requirements of the *IUE* Final Archive is that the dataset be fully intercomparable. The sensitivity degradation correction is essential in satisfying this requirement and allowing full utilization of the remarkably long timeline of *IUE* observations. The broad-band sensitivity analysis (Garhart 1992a) that monitors the degradation effects on the optical coatings of the camera caused by exposure to radiation is of insufficient resolution to provide a proper correction algorithm. The analysis described herein was motivated as a result of this concern.

10.2.1 Database

The database employed in the analysis contains the same images used for quick-look sensitivity monitoring and consists of several hundred point source and trailed observations distributed amongst the sensitivity monitoring standard stars. The photowrite for each image was carefully examined for defects such as data dropouts, cosmic ray hits, etc. and any corrupted spectra were discarded. All of the data were uniformly reprocessed using the prototype final archive processing software (Nichols-Bohlin 1990) and the updated line library and wavelength calibration (Bushouse 1991a). The spectra used in this analysis are identified in the Final Catalog as utilized in the Final Archive calibrations.

10.2.2 Analysis

The analysis was done on the extracted net spectra, before application of the absolute calibration (*i.e.*, in flux numbers), and the data sets for each standard star were treated separately. The spectra were corrected for camera head amplifier temperature (THDA) induced sensitivity variations (Garhart 1991) and sections of the spectra affected by camera reseaux were interpolated across using adjacent good data points. Several absorption features (*e.g.*, Si IV, C IV, and geocoronal Ly α,) were also interpolated across by applying the same technique. Each spectrum was then normalized by dividing by an average of several spectra taken in a six month time period centered on the time of the ITF. The normalized data were then binned in 5Å intervals (low dispersion) using the standard IUE Data Analysis Center (IUEDAC) procedure BINS and a set of degradation ratios was produced by performing a final binning of the data at six month intervals. The ratios derived from each standard star were compared and found to be in good agreement, so the last step of the process was repeated using all the data and a combined set of degradation ratios was derived. The same analysis was performed on low-dispersion trailed data and a separate set of degradation ratios was produced.

10.2.3 Fits to Ratios

10.2.3.1 LWP

The LWP camera appears to have two behavioral trends in sensitivity degradation (Teays and Garhart 1990). The division occurs at approximately 1984.5, which corresponds to the time this camera became the default camera. Data taken after this date are corrected using a linear fit (Bevington 1969) to the post 1984.5 ratios, while images taken prior to this point in time are corrected using a linear interpolation between each pre-1984.5 degradation ratio. The fluxes of corrected pre-1984.5 data will be less accurate than the fluxes of corrected post-1984.5 data due to the higher uncertainty in the degradation ratios for the early data. Fortunately little science data (except for calibration images) were taken using this camera during the pre-1984.5 time period, so the impact on the entire archive is minimal.

10.2.3.2 LWR

As is the case with the LWP camera, the LWR exhibits two trends with the dividing point occurring at approximately the same time. However unlike the LWP, enough data exists to provide linear fits to the ratios in both time periods.

10.2.3.3 SWP

The SWP sensitivity degradation for the post-1979.5 epoch can also be adequately represented by a linear relationship. The 1978.5 to 1979.5 epoch degradation ratios, which exhibit a behavior unlike the post-1979.5 epoch, were fit using a linear interpolation between each discrete point (Garhart 1992c).

10.2.4 Application of Degradation Correction

The degradation ratio at 1985.0, which corresponds to the mean time of the ITFs, was calculated for each wavelength bin using the linear fits. A zeropoint correction was then applied to the y-intercepts in order to force the degradation ratios to be one. This ensures that no degradation correction will be applied to data near the 1985.0 fiducial date.

The ratios are applied to the net flux spectra using a nearest neighbor wavelength interpolation scheme along with the inverse sensitivity function so as to provide absolutely calibrated and degradation corrected flux data. Extended-source images are corrected using the point source ratios. The correction is performed in the following manner:

1. The appropriate slopes and y-intercepts which correspond to the epoch of the observation in question are identified.

2. A correction ratio for each wavelength is calculated in the following manner:

$$R_\lambda = Intercept_\lambda + Slope_\lambda \times Date$$

where *Date* is the observation date in decimal years (*e.g.*, 1984.3).

3. The correction ratio is applied as follows:

$$Corrected\ Flux_\lambda = Flux_\lambda / R_\lambda$$

where λ is the closest 5Å bin.

10.3 Temperature-Dependent Correction

IUE flux values are corrected for variations in camera sensitivity as a function of THDA using the temperature-dependent coefficients as derived from the sensitivity monitoring analysis (see *e.g.* Garhart 1991 for more details). This correction is applied to the net flux along with the absolute calibration and sensitivity degradation corrections according to:

$$R_{THDA} = \frac{1}{(1 + C(THDA - ref.\ THDA))}$$

and

$$Corrected\ Flux = Flux \times R_{THDA}$$

where *Flux* is the net flux, *C* is the temperature coefficient and *ref. THDA* is the reference THDA. The reference THDA was calculated by taking an average of the THDAs for the sensitivity monitoring data which were used to derive the temperature coefficients. Table 10.5 contains the correction values, as used in the above equation.

Table 10.5: Temperature Coefficients and Reference THDAs

	LWP	LWR	SWP
Temp. Coef. (%/°C)	-0.19 ± 0.03	-0.88 ± 0.04	-0.46 ± 0.03
Ref. THDA (°C)	9.5	14.0	9.4

10.4 Application of Calibrations and Corrections

It is important to note that, as implemented in the image processing software, the interpolated inverse sensitivity values, time- and temperature-dependent sensitivity corrections, effective exposure time normalization, and any overall gain correction factor (for non-standard exposure or read gain or LWR UVC voltage settings) are computed as independent correction factors and then all applied simultaneously to the net flux and sigma spectra to result in fully calibrated and corrected spectra in absolute flux units. The net flux spectrum (in FN units), as determined by SWET, that is retained in the MXLO file does not have any of these correction factors applied to it. The calibrations and corrections are applied as follows:

$$F_{calib}(\lambda) = F_{FN}(\lambda) \times S_\lambda^{-1} \times gain \times R_{THDA} / R_\lambda / t_{eff}$$

$$\sigma_{calib}(\lambda) = \sigma_{FN}(\lambda) \times S_{\lambda}^{-1} \times gain \times R_{THDA}/R_{\lambda}/t_{eff}$$

where S_{λ}^{-1} is the inverse sensitivity (including any necessary S/L or T/L response corrections), *gain* is the cumulative UVC voltage and gain correction factor (if necessary), R_{λ} and R_{THDA} are the time- and temperature-dependent sensitivity correction factors, respectively, and t_{eff} is the effective exposure time. The values for S_{λ}^{-1} and R_{λ} are evaluated at the wavelength of each pixel through quadratic and nearest neighbor interpolation, respectively, of their tabulated values. The resulting absolutely calibrated units are $ergs/cm^2/\text{Å}/sec$.

Chapter 11

IUE Final Archive Data Products

The output files for the *IUE* Final Archive are fundamentally different in content, quantity, size, and format from those of the current IUESIPS. We have given a brief description of each file below along with a definition of the associated FITS format. All output data from the Final Archive will be available only in FITS format. Table 11.1 lists the output files that will be available only for low-dispersion data, along with the file ID, file size, and an indication of the type of FITS file to be used. Table 11.2 gives the same data for the files which will be available for high-dispersion images. Table 11.3 lists the FES data to be included in the Final Archive.

11.1 File Naming Conventions

The file names are defined so as to allow the unique identification of the information stored in the file. It is expected that the FITS reader will assign the file names according to the keyword **FILENAME**. Files with extensions include the keyword both for the main data set and for the extensions so that the FITS reader could either store the information in a single file or store the main data set and the extension in different files. There are three possible combinations of data files: (1) main data set with extension (*e.g.*, resampled image with resampled flag image), (2) main data set with no extension (*e.g.*, raw image), and (3) extension with no main data set (*e.g.*, extracted image).

The file name is formed by the concatenation of the following codes:

- Camera: 3 letter code (LWP, LWR, SWP, SWR).

- Image number: 5 digits.

- File type: 2 letter code as:

  RI raw image

  VD vector displacement

  XC cross correlation coefficients (binary table extension of the VD file)

103

LI linearized image

LF flags associated with the linearized image (image extension of the LI file)

SI resampled image

SF flags associated with the resampled image (image extension of the SI file)

SW wavelengths associated with the high-dispersion resampled image

MX merged extracted spectrum (large, small or both apertures)

WH whole high-dispersion extracted spectrum

- Dispersion: 2 letter code (**HI**, **LO**).

For example the files generated for LWP 12345, low-dispersion image, are the following

```
main data set      extension
LWP12345.RILO        -
LWP12345.VDLO      LWP12345.XCLO
LWP12345.LILO      LWP12345.LFLO
LWP12345.SILO      LWP12345.SFLO
     -             LWP12345.MXLO
```

The files generated for SWP 9876, high-dispersion image, are

```
main data set      extension
SWP09876.RIHI        -
SWP09876.VDHI      SWP09876.XCHI
SWP09876.LIHI      SWP09876.LFHI
SWP09876.SIHI      SWP09876.SFHI, SWP09876.SWHI
     -             SWP09876.MXHI
     -             SWP09876.WHHI
```

Images which are processed as both high dispersion and low dispersion will therefore have both sets of files in the archive. Note that in this case two copies of the raw image will appear in the archives, due to the dispersion dependent Core Data Items (CDIs) assigned during processing.

11.2 Raw Image (RILO/RIHI)

The *IUE* raw image is the fundamental input file for the *IUE* image processing system. Except for the conversion from VICAR format to FITS format (including the addition of the CDIs as FITS keywords), the data remain unaltered.

The RILO/RIHI FITS file contains a two-dimensional primary array consisting of 768 × 768 pixels, with no group structure or extensions. Each pixel is a data number (DN), coded as an 8 bit unsigned integer ranging from 0 to 255. The Basic Keywords are shown in Table 11.4.

Table 11.1: File Formats for *IUE* Final Archive (Low Dispersion)

File Name	File ID	File Size	Format	FITS Type
Raw Image	.RILO	768x768	8-bit	primary array
Linearized Image	.LILO	768x768	I*2	primary array
LI Flag Image	.LFLO	768x768	I*2	image extension
Resampled Low-Disp Image	.SILO	640x80	I*2	primary array
SILO Flag Image	.SFLO	640x80	I*2	image extension
Vector Displacement	.VDLO	2x768x768	R*4	primary array
Cross-correlation Coefficients	.XCLO	7x~140	R*4	table extension
Extracted Low-Disp Spectra	.MXLO	640x5	8-bit	binary table extension

Table 11.2: File Formats for *IUE* Final Archive (High Dispersion)

File Name	File ID	File Size	Format	FITS Type
Raw Image	.RIHI	768x768	8-bit	primary array
Linearized Image	.LIHI	768x768	I*2	primary array
LI Flag Image	.LFHI	768x768	I*2	image extension
Resampled High-Disp Image	.SIHI	768x768	I*2	primary array
SIHI Flag Image	.SFHI	768x768	I*2	image extension
Vector Displacement	.VDHI	2x768x768	R*4	primary array
Cross-correlation Coefficients	.XCHI	7x~500	R*4	table extension
Extracted High-Disp Spectra	.MXHI	TBD	8-bit	binary table extension
Concatenated High-Disp Spectra	.WHHI	TBD	8-bit	binary table extension

Table 11.3: File Formats for *IUE* Final Archive (FES Images)

File Name	File ID	File Size	Format	FITS Type
FES Image	FES	81x81	I*2	primary array
		7x7		
		113x113		
		127x127		
		other		

Table 11.4: RILO/RIHI File - Basic FITS Keywords

Keyword and value		Description
SIMPLE =	T	Standard FITS Format
BITPIX =	8	8-bit integer pixels
NAXIS =	2	Two-dimensional image
NAXIS1 =	768	Dimension along x-axis
NAXIS2 =	768	Dimension along y-axis
CTYPE1 = 'SAMPLE '		x-axis
CTYPE2 = 'LINE '		y-axis
BUNIT = 'DN '		Data Numbers
TELESCOP= 'IUE '		International Ultraviolet Explorer
FILENAME= 'AAAnnnnn.RIdd'		Filename (camera)(number).RI(disp)
DATE = 'dd/mm/yy'		Date file is written
ORIGIN = 'VILSPA '		Institution generating the file
DATAMIN =	nnn.0	Minimum pixel value
DATAMAX =	nnn.0	Maximum pixel value

11.3 Linearized Image (LILO/LIHI)

The linearized image is a primary array containing linearized (photometrically-corrected) pixels in FN units (I*2). Only the pixels inside the target ring in high dispersion, or in a swath including the spectrum in low dispersion, have been photometrically corrected. The actual FN values have been scaled up by a factor of 32 for storage. The scale factor of 32 will automatically be applied by standard FITS readers; the FITS keyword "BSCALE" is equal to 1/32.

The LILO/LIHI file will contain the linearized image as a two-dimensional primary array consisting of 768×768 pixels, with each pixel value coded as 16 bits, two's complement integers with bits stored in decreasing order of significance. The associated pixel quality flags are stored as an image extension using 16-bit, two's complement integers. Basic Keywords in the main header and the image extension header are shown in Table 11.5.

11.4 Linearized Flag Image (LFLO/LFHI)

This image extension is the same size as the LILO/LIHI file. For every pixel that is photometrically corrected, this file contains a ν flag for specific error conditions in the corresponding pixel in the LILO/LIHI image. The values are stored as integer. The ν flags are inherently 2 bytes (negative values). Pixels which suffer from saturation, are close to the edge of the photometric correction region, or require ITF curve extrapolation to compute an FN value are flagged in the LFLO/LFHI file. In addition, all pixels on the target region which have not been photometrically corrected but are known to suffer from bright spots, reseaux, microphonics, and missing minor frames are appropriately flagged. Flagging for microphonic noise is performed over the entire 768×768 image for the LWR camera only.

11.5 Resampled Image (SILO/SIHI)

The resampled image is a primary array produced by resampling the photometrically corrected portion of the LILO/LIHI image using the modified Shepard algorithm taken from the Numerical Algorithms Group (NAG) software package. Each pixel is resampled to the position determined by the summation of the vectors needed for:

1. shift to photometric correction (ITF) raw space,

2. shift from ITF space to geometrically-rectified space,

3. rotation such that orders are horizontal,

4. wavelength linearization,

5. detilting of large-aperture spectra for low-dispersion extended sources only,

Table 11.5: LILO/LIHI File - Basic FITS Keywords

Keyword and value	Description
SIMPLE = T	Standard FITS Format
BITPIX = 16	16-bit, 2's complement pixels
NAXIS = 2	Two-dimensional image
NAXIS1 = 768	Dimension along x-axis
NAXIS2 = 768	Dimension along y-axis
EXTEND = T	Extensions are present
CTYPE1 = 'SAMPLE '	x-axis
CTYPE2 = 'LINE '	y-axis
BUNIT = 'FN '	Flux Numbers
BSCALE = 3.1250E-02	real=tape*bscale+bzero
BZERO = 0.	offset
TELESCOP= 'IUE '	International Ultraviolet Explorer
FILENAME= 'AAAnnnnn.LIdd'	Filename (camera)(number).LI(disp)
DATE = 'dd/mm/yy'	Date file is written
ORIGIN = 'VILSPA '	Institution generating the file
DATAMIN = nnnnn.n	Minimum pixel value
DATAMAX = nnnnn.n	Maximum pixel value
XTENSION= 'IMAGE '	Image extension
BITPIX = 16	16-bit, 2's complement pixels
NAXIS = 2	Two-dimensional image
NAXIS1 = 768	Dimension along x-axis
NAXIS2 = 768	Dimension along y-axis
PCOUNT = 0	number of bytes following data matrix
GCOUNT = 1	number of groups
CTYPE1 = 'SAMPLE '	x-axis
CTYPE2 = 'LINE '	y-axis
BUNIT = ' '	unitless
FILENAME= 'AAAnnnnn.LFdd'	Filename (camera)(number).LF(disp)
EXTNAME = 'LIF '	LILO/LIHI pixel quality flags

6. alignment of the low-dispersion apertures for constant wavelength in the line direction,

7. adjustment so that both LW cameras provide coverage of the same spectral range,

8. adjustment to maintain the spectrum at approximately the same location in the file in the spatial direction (low dispersion only),

9. adjustment to LWP data to put the large-aperture data at the top of the file,

10. corrections for the spatial deviations (cross-dispersion wiggles) for the LWP and LWR low-dispersion data,

11. heliocentric velocity correction for high dispersion,

12. de-splaying correction for high-dispersion data, and

13. order centroiding for high-dispersion data.

The resampled image (SILO/SIHI) is I*2, in scaled FN units, with the y coordinate in pixels and the x coordinate in angstroms (Å). Starting wavelength and wavelength increment are stored in the FITS header for low dispersion. Both large- and small-aperture data are present in one resampled image for low-dispersion data. The FITS header will indicate predicted line center for large-aperture and for small-aperture data.

The SILO image is stored as a two-dimensional primary array consisting of 640×80 pixels, while the SIHI is 768×768 pixels. Each pixel represents a flux number (FN) scaled by a factor of 32 for storage purposes. The pixels are coded as 16 bits, two's complement integers, with the bits stored in decreasing order of significance. The associated pixel quality flags are stored as an image extension which has the same dimensions as the primary array. Table 11.6 shows the basic FITS Keywords for the main header and the image extension header.

11.6 Resampled Flag Image (SFLO/SFHI)

This image extension is the same size as the resampled image. Like the linearized flag image, it contains the ν flag for specific error conditions for the corresponding pixel in the SILO/SIHI image. The values are stored as I*2.

11.7 Vector Displacement File (VDLO/VDHI)

The vector displacement file is a primary array that provides, for each pixel in the LILO/LIHI file, the final coordinate values in the x (wavelength) and in the y (spatial) directions in the resampled space. "Resampled space" is defined to be a geometrically corrected 768×768

Table 11.6: SILO/SIHI File - Basic FITS Keywords

Keyword and value	Description
SIMPLE = T	Standard FITS Format
BITPIX = 16	16-bit, 2's complement pixels
NAXIS = 2	Two-dimensional image
NAXIS1 = nnn	Dimension along x-axis
NAXIS2 = nnn	Dimension along y-axis
EXTEND = T	Extensions are present
CRPIX1 = 1.	x reference pixel
CRPIX2 = 1.	y reference pixel
CRVAL1 = nnnn.nn	Wavelength at reference pixel
CRVAL2 = 1.	Coordinate of CRPIX2
CDELT1 = nn.nnnn	Increment in wavelengths
CDELT2 = 1.	Increment unit along y-axis
CTYPE1 = 'WAVELENGTH'	x-axis
CTYPE2 = 'SCAN '	y-axis
BUNIT = 'FN '	Flux Numbers
BSCALE = 3.1250E-02	real=tape*bscale+bzero
BZERO = 0.	Pixel offset
TELESCOP= 'IUE '	International Ultraviolet Explorer
FILENAME= 'AAAnnnnn.SIdd'	Filename (camera)(number).SI(disp)
DATE = 'dd/mm/yy'	Date file is written
ORIGIN = 'VILSPA '	Institution generating the file
DATAMIN = nnnnn.n	Minimum pixel value
DATAMAX = nnnnn.n	Maximum pixel value
XTENSION= 'IMAGE '	Image extension
BITPIX = 16	16-bit, 2's complement pixels
NAXIS = 2	Two-dimensional image
NAXIS1 = nnn	Dimension along x-axis
NAXIS2 = nnn	Dimension along y-axis
PCOUNT = 0	number of bytes following data matrix
GCOUNT = 1	number of groups
CRPIX1 = 1.	x reference pixel
CRPIX2 = 1.	y reference pixel
CRVAL1 = nnnn.nn	Coordinate of CRPIX1
CRVAL2 = 1.	Coordinate of CRPIX2
CDELT1 = nn.nnnn	Increment unit along x-axis
CDELT2 = 1.	Increment unit along y-axis
CTYPE1 = 'WAVELENGTH'	x-axis
CTYPE2 = 'SCAN '	y-axis
BUNIT = ' '	unitless
FILENAME= 'AAAnnnnn.SFdd'	Filename (camera)(number).SF(disp)
EXTNAME = 'SIddF '	SILO/SIHI pixel quality flags

image. In order to determine the final coordinates in the "resampled image" (the SILO/SIHI file) for any photometrically corrected pixel in the LILO/LIHI file:

$$Fin\_coord(x) = VD(i,j,1) - offset(x, cam, disp)$$

$$Fin\_coord(y) = VD(i,j,2) - offset(y, cam, disp)$$

where i and j range from 1 to 768 and

	Offset X		Offset Y	
	disp=L	H	L	H
LWP	100	0	297	0
LWR	~100	0	~250	0
SWP	130	0	490	0

The displacement vectors are recoverable by:

$$DELTA_x = VD(i,j,1) - i$$

and

$$DELTA_y = VD(i,j,2) - j,$$

where i and j range from 1 to 768. $Fin\_coord(x)$ contains the final x coordinate in the SILO/SIHI file and $Fin\_coord(y)$ contains the final y coordinate in the SILO/SIHI file. The final coordinate values are coded as 32 bits, R*4 numbers.

Basic Keywords in the VDLO/VDHI file header and in the table extension are shown in Table 11.7.

11.8   Cross-Correlation Coefficients (XCLO/XCHI)

This file allows the user to recover the calculated displacement vectors which produced the mapping from science image raw space to the ITF. For each of the approximately 500 (140 for low-dispersion) points used to obtain the displacement between the science image and the corresponding level of the ITF, this file contains (1) science image x-position (I*2), (2) science image y-position (I*2), (3) ITF x-position at position of best match (R*4), (4) ITF y-position at position of best match (R*4), (5) cross-correlation coefficient (R*4), (6) number of points used to calculate the coefficient (I*2), and (7) the ITF level used in the correlation (I*2). The x and y positions correspond to the sample and line numbers in the raw image. The resulting ITF positions of the best match are pre-filtered positions (before bogus matches have been identified and deleted), and will not necessarily correspond exactly to the photometric registration displacement components utilized to create the final displacement vector.

Note: The keyword NAXIS1 of the table extension has a value of 20 corresponding to the number of bytes in a row of the table.

Table 11.7: VDLO/VDHI File - Basic FITS Keywords

Keyword and value			Description
SIMPLE	=	T	Standard FITS Format
BITPIX	=	-32	IEEE single precision floating point
NAXIS	=	3	Three-dimensional image
NAXIS1	=	2	Dimension along x-axis
NAXIS2	=	768	Dimension along y-axis
NAXIS3	=	768	Dimension along z-axis
EXTEND	=	T	Extensions are present
CTYPE1	= '	'	Units along x-axis
CTYPE2	= 'PIXEL	'	Units along y-axis
CTYPE3	= 'PIXEL	'	Units along z-axis
BUNIT	= 'PIXEL	'	Pixel units
BZERO	=	nnnn.	Pixel offset
BSCALE	=	nn.n	Scale factor
TELESCOP= 'IUE		'	International Ultraviolet Explorer
FILENAME= 'AAAnnnnn.VDdd'			Filename (camera)(number).VD(disp)
DATE	= 'dd/mm/yy'		Date file is written
ORIGIN	= 'VILSPA	'	Institution generating the file
DATAMIN =		nnnnn.n	Minimum pixel value
DATAMAX =		nnnnn.n	Maximum pixel value
XTENSION= 'BINTABLE'			Table extension
BITPIX	=	8	binary data
NAXIS	=	2	Two-dimensional image
NAXIS1	=	20	width of table in bytes
NAXIS2	=	nnn	number of entries in table
PCOUNT	=	0	number of bytes following data matrix
GCOUNT	=	1	number of groups
TFIELDS	=	7	number of fields in each row
TFORM1	= '1I	'	16-bit integer
TTYPE1	= 'XRAW	'	science image x-position
TUNIT1	= 'PIXEL	'	unit is pixel
TFORM2	= '1I	'	16-bit integer
TTYPE2	= 'YRAW	'	science image y-position
TUNIT2	= 'PIXEL	'	unit is pixel
TFORM3	= '1E	'	single precision float
TTYPE3	= 'XITF	'	ITF x-position of best match
TUNIT3	= 'PIXEL	'	unit is pixel
TFORM4	= '1E	'	single precision float
TTYPE4	= 'YITF	'	ITF y-position of best match
TUNIT4	= 'PIXEL	'	unit is pixel
TFORM5	= '1E	'	single precision float
TTYPE5	= 'XCOEFF	'	cross correlation coefficient
TUNIT5	= '	'	unitless
TFORM6	= '1I	'	16-bit integer
TTYPE6	= 'NPOINTS	'	number of points used
TUNIT6	= '	'	unitless
TFORM7	= '1I	'	16-bit integer
TTYPE7	= 'ITFLEVEL'		ITF level
TUNIT7	= '	'	unitless
FILENAME= 'AAAnnnnn.XCdd'			Filename (camera)(number).XC(disp)
EXTNAME = 'XCOEF	'		cross correlation coefficients

11.9 Extracted Low-Dispersion Spectra (MXLO)

The extracted low-dispersion file uses the binary 3-D table extension with fixed-length floating point vectors to contain the extracted fluxes and associated data quality flags. Since no primary data are included, the extension header immediately follows the primary FITS header. Each row of the binary table includes the following columns:

1. Aperture designation as 'LARGE' or 'SMALL', stored in 5 ASCII characters.

2. Number of extracted points, one 16-bit integer. The number of extracted points is 640.

3. Starting wavelength, one single precision floating point value.

4. Wavelength increment, one single precision floating point value.

5. Net flux spectrum, array with 640 single precision floating point values.

6. Background flux spectrum, array with 640 single precision floating point values.

7. Sigma vector, array with 640 single precision floating point values.

8. Data quality flags, array of 640 16-bit integers.

9. Absolutely calibrated net flux spectrum, array with 640 single precision floating point values.

Wavelengths are linearly sampled, and referenced to vacuum. Double aperture low-dispersion spectra will contain two rows in the above format, with one row for each aperture. Table 11.8 shows the basic FITS Keywords for the MXLO file.

Note: The keyword NAXIS1 in the table extension defines the number of bytes per row in the table, computed as $15 + 18 \times 640$.

11.10 FES Image File

The Fine Error Sensor (FES) is an image dissector with an S-20 photocathode sensitive in the wavelength range from 4000–7000Å. Although not routinely archived, FES images are frequently read down from the satellite and stored in a format similar to the raw image file. The FES image size can range from 1×1 to 127×127 pixels, but they are generally archived in sizes of 7×7, 81×81, 113×113, or 127×127 pixels. Although this file is converted from VICAR to FITS format, with the VICAR label and appropriate CDIs stored as keywords in the FITS header, the FES data remain unaltered.

The FES file is stored as a two-dimensional primary array, with no group structure or extensions. Each pixel is coded as 16 bits, two's complement integers. Basic Keywords are shown in Table 11.9.

Table 11.8: MXLO File - Basic FITS Keywords

Keyword and value		Description
SIMPLE =	T	Standard FITS Format
BITPIX =	8	8 bits ASCII
NAXIS =	0	No image data
EXTEND =	T	Extensions are present
TELESCOP= 'IUE '		International Ultraviolet Explorer
DATE = 'dd/mm/yy'		Date file is written
ORIGIN = 'VILSPA '		Institution generating the file
XTENSION= 'BINTABLE'		Table extension
BITPIX =	8	Binary data
NAXIS =	2	Two-dimensional table array
NAXIS1 =	11535	With of the table row in bytes
NAXIS2 =	n	Number of apertures (1-single, 2-both)
PCOUNT =	0	Number of bytes following data matrix
GCOUNT =	1	Only one group
TFIELDS =	9	Number of column in the table
TFORM1 = '5A '		character string
TTYPE1 = 'APERTURE'		aperture type (large or small)
TUNIT1 = ' '		unitless
TFORM2 = '1I '		16-bit integer
TTYPE2 = 'NPOINTS '		number of points
TUNIT2 = ' '		unitless
TFORM3 = '1E '		single precision
TTYPE3 = 'WAVELENGTH'		starting wavelength
TUNIT3 = 'ANGSTROM'		unit is angstrom
TFORM4 = '1E '		single precision
TTYPE4 = 'DELTAW '		wavelength increment
TUNIT4 = 'ANGSTROM'		unit is angstrom
TFORM5 = '640E '		single precision array
TTYPE5 = 'NET '		net flux array
TUNIT5 = 'FN '		unit is IUE FN
TFORM6 = '640E '		single precision array
TTYPE6 = 'BACKGROUND'		background flux array
TUNIT6 = 'FN '		unit is IUE FN
TFORM7 = '640E '		single precision array
TTYPE7 = 'SIGMA '		sigma
TUNIT7 = 'ERG/CM2/S/A'		unit is erg/cm2/sec/angstrom
TFORM8 = '640I '		16-bit integer array
TTYPE8 = 'QUALITY '		data quality flag
TUNIT8 = ' '		unitless
TFORM9 = '640E '		single precision array
TTYPE9 = 'FLUX '		calibrated flux
TUNIT9 = 'ERG/CM2/S/A'		unit is erg/cm2/sec/angstrom
FILENAME= 'AAAnnnnn.MXLO'		Filename (camera)(number).MXLO
EXTNAME = 'MXLO '		name of table

113

Table 11.9: FES File - Basic FITS Keywords

Keyword and value	Description
SIMPLE = T	Standard FITS Format
BITPIX = 16	16-bit, 2's complement pixels
NAXIS ≃ 2	Two-dimensional image
NAXIS1 = nnn	Dimension along x-axis
NAXIS2 = nnn	Dimension along y-axis
CTYPE1 = 'SAMPLE '	x-axis
CTYPE2 = 'LINE '	y-axis
CUNIT1 = 'PIXEL '	Units along x-axis (8 arcsec/pixel)
CUNIT2 = 'PIXEL '	Units along y-axis (8 arcsec/pixel)
BUNIT = 'COUNTS '	Pixel units
TELESCOP= 'IUE '	International Ultraviolet Explorer
FILENAME= 'AAAnnnnn.FES'	Filename (camera)(number).FES
DATE = 'dd/mm/yy'	Date file is written
ORIGIN = 'VILSPA '	Institution generating the file
DATAMIN = nnn.n	Minimum pixel value
DATAMAX = nnn.n	Maximum pixel value

Chapter 12

Image Header Contents

12.1   Image Header

The structure of each new file header in FITS format will contain:

- Basic FITS keywords.

- Core Data Items.

- Original *IUE* label.

- NEWSIPS Image Processing History.

This header is attached to each of the files stored in the archive. Core Data Items (CDIs), the *IUE* label and the cumulative NEWSIPS Image Processing History will be contained only in the primary FITS header; the extension headers will not duplicate this information.

It should be noted that the structure of the FITS header is such that some information may appear in more than one form. For example, specific information may appear in multiple places in the original *IUE* label as well as in a CDI FITS keyword and/or the processing history. In cases where these entries disagree, the CDIs should always be considered the most reliable source for the specific information.

12.2   VICAR Label Format

Each image has an associated VICAR header which is generated by the *IUE* Operations Control Center software during image acquisition and contains various scientific and engineering data pertinent to the image. This header, called the image label, consists of 72-byte lines containing EBCDIC and binary information. The contents of the image label are shown in Table 12.1.

Note that lines 3–9 are entered by the Telescope Operator (TO) at the console and may occasionally contain errors. Lines 36–37, normally input from the POT (Preplanned

Observation Tape), may be modified by the TO and hence are also subject to errors. The automatic entries on the other lines (10–32) are more accurate but can be affected, for instance, by ground computer problems. The binary-format portion of the image label (located in lines 51–82 and 86–100) is not usefully decoded when interpreted in EBCDIC characters. See Van Steenberg (1989) for translation of the event round robin in *IUE* VICAR image labels.

Table 12.1: *IUE* VICAR Header

Line number	Description	Code
1-2	Image info. written by the system	EBCDIC
3-9	General comments	EBCDIC
10-32	Real-time command buffer	EBCDIC
33-35	Blanks	EBCDIC
36-37	GO information from POT tape	EBCDIC
38-45	Spares	EBCDIC
46	Computer switch info used at GSFC	EBCDIC
47-50	Spares	EBCDIC
51-75	Data quality bits	Binary
76-82	S/C snapshot	Binary
83-85	Orbital elements and S/C info	EBCDIC
86-100	Camera snapshots	Binary

The raw image VICAR header label, as well as any appendages which had been added for database information or label corrections, are stored in the primary FITS header. Each line contains the original label information coded in ASCII, in bytes 9 to 80, with blanks in bytes 1 to 8. Lines originally coded in EBCDIC have been converted to ASCII, and lines containing binary data have been converted into 2 lines containing hexadecimal ASCII characters. (*e.g.*, the unsigned integer byte value 63 will become '3F'). The first line of hexadecimal ASCII characters contain bytes 1 through 33 of the original line of binary data and are stored in columns 9 through 74. The second line contains bytes 34 through 66 in columns 9 through 74. The traditional VICAR line number and continuation character are stored at the end of each line in bytes 75 through 80. In this format, the *IUE* raw-image label generally consists of approximately 150 lines in the FITS header.

Four COMMENT lines precede the *IUE* label and one COMMENT line flags the end of the label.

12.3   NEWSIPS Processing History

The NEWSIPS image processing history includes the cumulative processing information generated by NEWSIPS. The history documents the processing system (software identification, version if required, and hardware platform), and the individual application modules with the

116

corresponding time stamps. Relevant variables used or computed by the various processing routines (*e.g.*, median cross-correlation coefficient, dispersion constants, shifts used during the extraction, etc.) are reported in the history lines.

Each line of the processing history contains the keyword HISTORY in bytes 1 to 8, with processing information stored in bytes 9 to 71. Bytes 73 to 80 are reserved for time stamps, which designate the GMT times at which the individual application modules were executed. Separate lines containing the processing date indicate the start and end of the log. An example of the processing history is outlined in the following section.

12.4 Header Example

The following example shows the FITS header corresponding to a low-dispersion, double aperture raw image. In the case of a single aperture spectral image, the header includes only the corresponding large- (or small-) aperture set.

```
        1         2         3         4         5         6         7         8
12345678901234567890123456789012345678901234567890123456789012345678901234567890
SIMPLE  =                     T / Standard FITS Format
BITPIX  =                     8 / 8-bit integer pixels
NAXIS   =                     2 / Two-dimensional image
NAXIS1  =                   768 / Dimension along x-axis
NAXIS2  =                   768 / Dimension along y-axis
CTYPE1  = 'SAMPLE  '             / x-axis
CTYPE2  = 'LINE    '             / y-axis
BUNIT   = 'DN      '             / Data Numbers
TELESCOP= 'IUE     '             / International Ultraviolet Explorer
FILENAME= 'SWP26067.RILO'        / Filename(camera)(number).RI(disp)
DATE    = '29/10/93'             / Date file was written
ORIGIN  = 'GSFC    '             / Institution generating the file
DATAMIN =                   0.0 / Minimum pixel value
DATAMAX =                 255.0 / Maximum pixel value
COMMENT *
COMMENT * CORE DATA ITEMS - COMMON SET
COMMENT *
CAMERA  = 'SWP     '             / Camera
IMAGE   =                 26067 / Sequential image number
DISPERSN= 'LOW     '             / Spectrograph dispersion mode
APERTURE= 'BOTH    '             / Aperture
DISPTYPE= 'LOW     '             / Dispersion processing type
READMODE= 'FULL    '             / Read mode
READGAIN= 'LOW     '             / Read gain
EXPOGAIN= 'MAXIMUM '             / Exposure gain
UVC-VOLT=                  -5.0 / UVC voltage
ABNNOSTD= 'YES     '             / Non-standard image acquisition
ABNBADSC= 'NO      '             / LWP bad scans
ABNHTRWU= 'NO      '             / LWR heater warmup
ABNREAD = 'NO      '             / Read at other than 20 KB
ABNUVC  = 'NO      '             / Non-standard UVC voltage
ABNHISTR= 'NO      '             / History replay
ABNOTHER= 'NO      '             / Other abnormality
THDAREAD=                  9.17 / THDA at read of image
EQUINOX =               1950.00 / Epoch of coordinates
STATION = 'GSFC    '             / Observing station
ORBEPOCH= '27/05/85'             / Orbital elements epoch
ORBSAXIS=               42171.0 / Semi-major axis in kilometers
ORBECCEN=             0.1993815 / Eccentricity
```

117

```
ORBINCLI=                29.642 / Inclination in degrees
ORBASCEN=               152.284 / Ascending node in degrees
ORBPERIG=               312.282 / Argument of perigee in degrees
ORBANOMA=                84.056 / Mean anomaly in degrees
POSANGLE=                127.21 / Pos angle of the large aperture (deg)
LAMP    = 'NONE    '           / Lamp
PGM-ID  = 'OD58X   '           / Program identification
ABNMINFR= 'NO      '           / Bad/missing minor frames
CC-PERCN=                  94.9 / Cross-correlation % successful
CC-WINDW=                    29 / Cross-correlation window size
CC-TEMPL=                    23 / Cross-correlation template size
CC-MEDN =                 0.656 / Median cross-correlation coefficient
CC-STDEV=                 0.112 / St dev of cross-corr coefficients
SHFTMEAN=                 0.165 / Mean shift between image and ITF
SHFTMAX =                 0.450 / Maximum shift between image and ITF
ITF     = 'SWP85R92A'          / ITF identification
TILTCORR= 'NO      '           / Tilt correction flag
MEANRAT =                 1.002 / SI vs LI mean
STDEVRAT=                 0.977 / SI vs LI standard deviation
COMMENT BY RA: EXP 1 APER L E=242,C=110,B=32
COMMENT BY RA: EXP 2 APER S E=175,C=90,B=32
COMMENT BY RA:    0 MISSING MINOR FRAMES NOTED ON SCRIPT
COMMENT BY RA: EXP 1 TRACKED ON FES
COMMENT BY RA: EXP 2 TRACKED ON FES
COMMENT BY RA: S   PREP USED
COMMENT BY RA: OFFSET 1 FROM: GC 28144
COMMENT BY RA: OFFSET 1 COORDINATES: 20 13 20.0 +23 21 16
COMMENT BY RA: OFFSET 1 MAGNITUDE: 5.400
COMMENT BY RA: LGAP expo started in high disp for 1 min 08 sec, then exposed
COMMENT BY RA: for 15 min in low disp.
COMMENT BY GO: GO has no special comments.
COMMENT BY GO: GO has no special comments.
COMMENT *
COMMENT * CORE DATA ITEMS - LARGE APERTURE SET
COMMENT *
LDATEOBS= '02/06/85'           / Observing date
LTIMEOBS= '13:56:31'           / Observing time
LMJD-OBS=           46218.58091 / Mod. JD start of obs. (JD - 2400000.5)
LEXPTRMD= 'NO-TRAIL'           / Trail mode
LEXPMULT= 'NO      '           / Multiple exposure mode
LEXPSEGM= 'NO      '           / Segmented exposure code
LEXPTIME=               967.755 / Integration time in seconds
LTHDASTR=                  9.20 / THDA at start of exposure
LTHDAEND=                  9.17 / THDA at end of exposure
LRA     =              304.5125 / Homogeneous R.A. in degrees
LDEC    =               20.9450 / Homogeneous Dec. in degrees
LLAPSTAT= 'OPEN    '           / Large aperture status
LFES2MD = 'SO      '           / FES(2) mode
LFES2CN =                   263 / FES(2) counts on target
LTARGET = 'V SGE   '           / Object as given by Guest Observer
LTARGRA =              304.5042 / R.A. in degrees (given by GO)
LTARGDEC=               20.9444 / Dec. in degrees (given by GO)
LOBJECT = 'V*   V SGE'                   / Homogeneous Object ID
LIUECLAS=                    11 / Object class
LFOCUS  =                 -1.73 / Focus
LFPM    =                  0.75 / Flux particle monitor
LGSTAR2X=                   696 / X coordinate of guide star in FES 2
LGSTAR2Y=                   416 / Y coordinate of guide star in FES 2
LGSTAR2C=                   137 / Guide star counts in FES 2
LGSTAR2M= 'FO      '           / Guide star mode FES2
LMJD-MID=           46218.58651 / Mod. JD middle of obs. (JD - 2400000.5)
LHELCORR=               0.00218 / Heliocentric corr to midpoint (days)
LDATABKG=                    24 / Estimated mean background level (DNs)
LDATACNT=                   107 / Estimated maximum continuum level (DNs)
```

```
LCNTRAPR=                 51.0 / Predicted center line of spectrum
LXTRMODE= 'POINT   '           / Extraction mode
LXTRPROF= 'EMPIRICAL'          / Profile used
LXTRASYM= 'NO      '           / Asymmetrical profile in extraction
LXTRCNTR=                 51.0 / Center line of extracted spectrum
LFLUXAVE=                 80.9 / Average flux (FNs)
COMMENT *
COMMENT * CORE DATA ITEMS - SMALL APERTURE SET
COMMENT *
SDATEOBS= '02/06/85'           / Observing date
STIMEOBS= '14:00:13'           / Observing time
SMJD-OBS=          46218.58348 / Mod. JD start of obs. (JD - 2400000.5)
SEXPTRMD= 'NO-TRAIL'           / Trail mode
SEXPMULT= 'NO      '           / Multiple exposure mode
SEXPSEGM= 'NO      '           / Segmented exposure code
SEXPTIME=             1199.588 / Integration time in seconds
STHDASTR=                 9.17 / THDA at start of exposure
STHDAEND=                 9.17 / THDA at end of exposure
SRA     =             304.5125 / Homogeneous R.A. in degrees
SDEC    =              20.9450 / Homogeneous Dec. in degrees
SLAPSTAT= 'OPEN    '           / Large aperture status
SFES2MD = 'SO      '           / FES(2) mode
SFES2CN =                  242 / FES(2) counts on target
STARGET = 'V SGE   '           / Object as given by Guest Observer
STARGRA =             304.5042 / R.A. in degrees (given by GO)
STARGDEC=              20.9444 / Dec. in degrees (given by GO)
SOBJECT = 'V*   V SGE'                 / Homogeneous Object ID
SIUECLAS=                   11 / Object class
SGSTAR2X=                  846 / X coordinate of guide star in FES 2
SGSTAR2Y=                  415 / Y coordinate of guide star in FES 2
SGSTAR2M= 'FO      '           / Guide star mode FES2
SMJD-MID=          46218.59043 / Mod. JD middle of obs. (JD - 2400000.5)
SHELCORR=              0.00218 / Heliocentric corr to midpoint (days)
SDATABKG=                   24 / Estimated mean background level (DNs)
SDATACNT=                   78 / Estimated maximum continuum level (DNs)
SCNTRAPR=                 24.9 / Predicted center line of spectrum
SXTRMODE= 'POINT   '           / Extraction mode
SXTRPROF= 'EMPIRICAL'          / Profile used
SXTRASYM= 'NO      '           / Asymmetrical profile in extraction
SXTRCNTR=                 24.4 / Center line of extracted spectrum
SFLUXAVE=                 51.1 / Average flux (FNs)
COMMENT *
COMMENT * THE IUE VICAR HEADER
COMMENT *
COMMENT IUE-VICAR HEADER START
                    0001000107680768   1 1 013126067          1  C
      6246*   4*IUESOC  *   *   2168*   *  * * * * * *       *  2  C
   SWP 26067, V SGE, 15 MIN LOW DISP & 68 SEC HIGH DISP LGAP    3  C
   ALSO EXPOSED FOR 20 MIN LOW DISP SMALL APERTURE              4  C
                                                                5  C
                                                                6  C
   OBSERVER: KOCH    ID: OD58K1  DAY 153/02 JUNE 1985           7  C
                                                                8  C
                                                                9  C
   85153145015* 9   * 218 *OPSPRC40*125506 S/C READY FOR MANEUVER * 10 C
   144611 TARGET IN LWLA        *125525 READPREP 3 IMAGE 26066  * 11 C
   144801 GDE TRACK X 499  Y 557 *125600 SCAN READLO SS 1 G3 44 * 12 C
   144901 EXPOBC 1 12 0   MAXG NOL *125616 X 60 Y 76 G1 82 HT 105 * 13 C
   144951 TLM,SWPROM        *131624 TLM,FES2ROM               * 14 C
   145022 READ 3 IMAGE 26067    *133318 FESIMAGE 0 0 81        * 15 C
   145058 SCAN READLO SS 1 G3 44 *134037 TARGET IN SWLA        * 16 C
   145118 X 60 Y 76 G1 82 HT 105 *135034 TARGET FROM SWLA      * 17 C
   145050                        *135256 TARGET IN SWLA        * 18 C
   145117                        *135539 GDE TRACK X 697  Y 417 * 19 C
```

119

```
054657 FESCT 1981 IN 3 0 0      *135636 EXPOBC 3 15 0   MAIG NOL * 20  C
054817 GDE TRACK X 687  Y 154   *135751 MODTIME 3 0 0            * 21  C
054919 EXPOBC 3 200 0  MAIG NOL *135821 FIN 3 T 68 S 97 U 109    * 22  C
090740 TLM,SWPROM               *135842 MODE SWL                * 23  C
090921 FIN 3 T 11999 S 97 U 109 *140021 EXPOBC 3 15 0   MAIG NOL * 24  C
090944 READPREP 3 IMAGE 26065   *140112 MODE LWL                * 25  C
091017 SCAN READLO SS 1 G3 44   *141521 FIN 3 T 968 S 97 U 109  * 26  C
091030 X 60 Y 76 G1 82 HT 105   *141616 TARGET FROM SWLA        * 27  C
093022 TLM,FES2ROM              *141953 TARGET IN SWSA          * 28  C
093351 EXPOBC 3 200 0  MAIG NOL *142145 GDE TRACK X 845  Y 418  * 29  C
125303 TLM,SWPROM               *142244 EXPOBC 3 20 0   MAIG NOL * 30  C
125354 FIN 3 T 11999 S 97 U 109 *144251 FIN 3 T 2168 S 97 U 109 * 31  C
125433 TARGET FROM SWLA         *144332 TARGET FROM SWSA        * 32  C
                                                                  33  C
                                                                  34  C
                                                                  35  C
OD58X*1*07*KOCH           * 1*   *0*   V SEG*0*0*1*020            36  C
2018009+205639*  0*WN*0*11.4*99.00*        *    * 999.99*    *    37  C
                                                                  38  C
                                                                  39  C
                                                                  40  C
                                                                  41  C
                                                                  42  C
                                                                  43  C
                                                                  44  C
                                                                  45  C
                                                                  46  C
                                                                  47  C
                                                                  48  C
                                                                  49  C
                                                                  50  C

.
.            (binary portion of the VICAR label)
.

  2446212.5      .0 42171.1 .199381 29.5417152.2832312.2817 84.055  83  C
153042054 1257131-69562511552 2 153050021 2017424+3834233093533     84  C
153131052 2013204+2321163071239 153132820 2018  8+2056393054710     85  C

.
.            (binary portion of the VICAR label)
.

522020482020614820492020202020202020202020202020202020202020203031 100 C
***** RAW IMAGE *** T3LBAC  *****                                     C
*ARCHIVE  10:26Z JUN 03,'86                                          HL
```
COMMENT IUE-VICAR HEADER END
HISTORY IUE-LOG STARTED   29-OCT-1993 06:21:28
HISTORY PROCESSING SYSTEM: NEWSIPS VERSION 2.3
HISTORY ULTRIX VERSION
HISTORY SWP26067
HISTORY PROCESSED AT GODDARD SPACE FLIGHT CENTER
HISTORY **
HISTORY **
HISTORY START RAW_SCREEN   29-OCT-1993 06:22:22
HISTORY   9 BRIGHT SPOTS DETECTED
HISTORY   0 MISSING MINOR FRAMES DETECTED
HISTORY LARGE APERTURE SPECTRUM WILL BE EXTRACTED AS
HISTORY   POINT SOURCE
HISTORY LARGE APERTURE CONTINUUM DN LEVEL = 107
HISTORY SMALL APERTURE CONTINUUM DN LEVEL = 78
HISTORY BACKGROUND DN LEVEL = 24
HISTORY END   RAW_SCREEN   29-OCT-1993 06:22:49
HISTORY **
HISTORY START TTDC   29-OCT-1993 06:22:53
HISTORY TEMPERATURE USED FOR CORRECTING DISPERSION CONSTANTS = 9.17
HISTORY DATE OF OBSERVATION USED FOR CORRECTING

```
HISTORY          DISPERSION CONSTANTS =  2/ 6/85  13:56:31
HISTORY THIRD-ORDER FIT OVER TIME USED
HISTORY FIRST-ORDER FIT OVER TEMPERATURE USED
HISTORY ZERO-POINT CORRECTION =   1.09 ANGSTROMS
HISTORY SPATIAL CORRECTION =  -0.86 PIXELS
HISTORY END   TTDC                          29-OCT-1993 05:22:54
HISTORY ***********************************************************
HISTORY START CROSS-CORR                    29-OCT-1993 05:23:04
HISTORY WINDOW SIZE USED:    29 X  29 PIXELS
HISTORY TEMPLATE SIZE USED:  23 X  23 PIXELS
HISTORY ITF USED: SWP85R92A
HISTORY  95.0  PERCENT SUCCESSFUL CORRELATIONS (132 OUT OF 139)
HISTORY MEDIAN CORRELATION COEFFICIENT: 0.656
HISTORY STANDARD DEVIATION OF CORRELATION COEFFICIENT: 0.112
HISTORY MEAN SHIFT IN PIXELS: 0.165
HISTORY MAXIMUM SHIFT IN PIXELS: 0.450
HISTORY NUMBER OF SUCCESSFUL SHIFTS FILTERED AS UNRELIABLE IN
HISTORY     POST-FILTER ROUTINE:   1
HISTORY END   CROSS-CORR                    29-OCT-1993 05:24:47
HISTORY ***********************************************************
HISTORY START PHOTOM                        29-OCT-1993 05:26:55
HISTORY ITF USED: SWP85R92A
HISTORY MEAN TEMPERATURE OF ITF:  9.3 C
HISTORY ITF UVC=-5.0 KV; UVFLOOD WAVELENGTH = 2536 A; ITF SEC =-6.1 KV
HISTORY ITF CONSTRUCTION: RAW SPACE, FOURIER FILTERED; JAN92
HISTORY END   PHOTOM                        29-OCT-1993 05:27:45
HISTORY ***********************************************************
HISTORY START GEOM                          29-OCT-1993 05:29:01
HISTORY WAVELENGTH LINEARIZATION APPLIED USING CHEBYSHEV COEFFICIENTS:
HISTORY      C(0) = 319.620
HISTORY      C(1) = 318.820
HISTORY      C(2) = 0.87967
HISTORY      C(3) = 0.67988
HISTORY WAVELENGTH ZEROPOINT AND SPATIAL SHIFT APPLIED:
HISTORY      ZERO-POINT SHIFT = -16.47 ANGSTROMS
HISTORY      SPATIAL SHIFT =   3.79 PIXELS
HISTORY FINAL TIME/TEMP CORRECTED DISPERSION CONSTANTS USED:
HISTORY      1050.00 ANGSTROMS, 1.6763 ANGSTROMS/PIXEL
HISTORY PREDICTED CENTER LINE OF LARGE APERTURE = LINE 51.0
HISTORY PREDICTED CENTER LINE OF SMALL APERTURE = LINE 24.9
HISTORY END   GEOM                          29-OCT-1993 05:35:01
HISTORY ***********************************************************
HISTORY START SWET                          29-OCT-1993 05:35:36
HISTORY  NOISE MODEL USED: SWP  VERSION 1.0
HISTORY
HISTORY  *******************LARGE APERTURE DATA*******************
HISTORY
HISTORY  PREDICTED SPECTRUM CENTER AT LINE 51, CENTROID FOUND AT
HISTORY      LINE 51, PEAK AT LINE 52, AVERAGE PEAK FN =    80.9
HISTORY  CROSS-DISPERSION PROFILES BINNED WITH A BLOCKSIZE OF   1 PIXELS,
HISTORY      FOR A TOTAL OF 526 BLOCKS, OF WHICH  71 ARE REJECTED
HISTORY  FIT PROFILE WITH 15 NODES AND  3.50 SIGMA REJECTION
HISTORY  PROFILE CENTROID AT LINE  51.0
HISTORY  EXTRACT FLUX FROM LINES 45 THROUGH  57
HISTORY  REJECT PIXELS DEVIATING BY  4.0 SIGMA
HISTORY  OUT OF   8320 PIXELS      82 REJECTED AS COSMIC RAY HITS,
HISTORY          141 FLAGGED AS BAD
HISTORY  ABSOLUTE FLUX CALIBRATION SWP VERSION 1.2 APPLIED USING:
HISTORY      MODE = LARGE APERTURE POINT SOURCE
HISTORY      CALIBRATION EPOCH = 1985.00
HISTORY      CAMERA RISE TIME = 0.130 SECONDS
HISTORY      EFFECTIVE EXPOSURE TIME =   967.755 SECONDS
HISTORY  TEMPERATURE-DEPENDENT SENSITIVITY CORRECTION APPLIED USING:
HISTORY      THDA OF IMAGE =  9.17
```

121

```
HISTORY        REFERENCE THDA =  9.40
HISTORY        TEMPERATURE COEFFICIENT = -0.0046
HISTORY        TEMPERATURE CORRECTION FACTOR =   0.999
HISTORY  SENSITIVITY DEGRADATION CORRECTION SWP VERSION 1.0 APPLIED USING:
HISTORY        MODE = LARGE APERTURE POINT SOURCE
HISTORY        CALIBRATION EPOCH = 1985.00
HISTORY        OBSERVATION DATE = 1985.419
HISTORY
HISTORY  *********************SMALL APERTURE DATA************************
HISTORY
HISTORY  PREDICTED SPECTRUM CENTER AT LINE 25, CENTROID FOUND AT
HISTORY        LINE 24, PEAK AT LINE 25, AVERAGE PEAK FN =    51.1
HISTORY  CROSS-DISPERSION PROFILES BINNED WITH A BLOCKSIZE OF   1 PIXELS,
HISTORY        FOR A TOTAL OF 526 BLOCKS, OF WHICH  56 ARE REJECTED
HISTORY  FIT PROFILE WITH 15 NODES AND  3.50 SIGMA REJECTION
HISTORY  PROFILE CENTROID AT LINE  24.4
HISTORY  EXTRACT FLUX FROM LINES 18 THROUGH  30
HISTORY  REJECT PIXELS DEVIATING BY  4.0 SIGMA
HISTORY  OUT OF    8320 PIXELS      17 REJECTED AS COSMIC RAY HITS,
HISTORY          101 FLAGGED AS BAD
HISTORY  ABSOLUTE FLUX CALIBRATION SWP VERSION 1.2 APPLIED USING:
HISTORY        MODE = SMALL APERTURE POINT SOURCE
HISTORY        CALIBRATION EPOCH = 1985.00
HISTORY        CAMERA RISE TIME = 0.130 SECONDS
HISTORY        EFFECTIVE EXPOSURE TIME =  1199.588 SECONDS
HISTORY  TEMPERATURE-DEPENDENT SENSITIVITY CORRECTION APPLIED USING:
HISTORY        THDA OF IMAGE =  9.17
HISTORY        REFERENCE THDA =  9.40
HISTORY        TEMPERATURE COEFFICIENT = -0.0046
HISTORY        TEMPERATURE CORRECTION FACTOR =   0.999
HISTORY  SENSITIVITY DEGRADATION CORRECTION SWP VERSION 1.0 APPLIED USING:
HISTORY        MODE = LARGE APERTURE POINT SOURCE
HISTORY              APPLIED TO SMALL APERTURE DATA
HISTORY        CALIBRATION EPOCH = 1985.00
HISTORY        OBSERVATION DATE = 1985.419
HISTORY END   SWET                          29-OCT-1993 05:36:35
HISTORY  ***********************************************************
HISTORY START FITSCOPY                       29-OCT-1993 05:36:41
END
```

Chapter 13

Keys to Assessing the Quality of NEWSIPS Data

The processing techniques described in this manual provide some information on the quality of the image and the extracted spectral data which was not available with the previous IUESIPS processing. This information can be found in the processing HISTORY portion of the FITS label for each image, and in the Final Catalog of *IUE* observations. Each of these parameters is described below. In some cases, these output parameters can alert the user to the fact that the raw image data are corrupted or that the distortion of a particular image with respect to the ITF is unusually severe. Such problems are inherent in the raw data and cannot be overcome with processing techniques. Other parameters alert the user to difficulties with the extraction of the spectral data. In these cases, alternate extraction methods customized by the user may yield better results.

Items 3–6 refer to statistical information based on data obtained from the entire photometrically corrected region of the image. While these numbers can be useful for quick-look evaluations, the spatial data represented must be examined in two dimensions to understand fully the distortion characteristics of a particular image. These four parameters should therefore be used with caution for anything but a gross categorization of image quality.

1. Maximum continuum DN level:

   This parameter gives an estimate of the exposure level of the spectral data. This estimate is determined automatically during the processing, using the algorithm described in Chapter 3, and may differ significantly from the estimate given in the RA comments field in the database, which is based on a manual estimate at the time the exposure was read down. The estimate of the exposure level in the RA comments field is made in slightly different ways at GSFC and at VILSPA and is not necessarily consistent from image to image. The maximum continuum DN level determined during the processing is consistent for the entire archive and can be used to determine relative exposure differences between various observations of the same object. Of course, the spectral morphology of the object must be taken into account in evaluating the exposure level of an image. In particular, one must be careful when using these numbers if they were

123

determined from emission line objects. Contamination of the continuum level reading from an emission feature may occur in some instances when there is a large spectral format shift (*e.g.*, due to target centering errors or objects with large redshifts).

2. Mean Background DN Level:

The mean background DN level for a short exposure taken during a time of low radiation is about 20–40 DN. This is then the minimum background one would expect. Long exposures and exposures taken on high radiation shifts will have higher mean background DN levels. If the maximum continuum DN level is not at least 50 DN above the mean background DN level, the spectrum will most likely contain little useful data unless it is an emission line source.

3. Percent successful cross correlations:

The percent of successful cross correlations for each image is recorded in the HISTORY portion of the FITS header. For most images, greater than 95% of the attempted cross correlations are successful, according to the criteria described in Chapter 4. If less than 90% of the cross correlations were successful, the image either suffers from unusually large local or global distortions, the raw image background is heavily saturated, the image is a partial read, or the raw image data are corrupted.

4. Median cross-correlation coefficient:

The median cross-correlation coefficient for an image is the median of the cross-correlation coefficients for all patches of the image. In general, the best signal-to-noise ratio in the extracted spectrum can be expected when this parameter is greater than 0.7. When this parameter is less than 0.6, the signal-to-noise ratio of the photometrically corrected data, and ultimately the extracted spectrum, may be degraded.

5. Mean shift:

This parameter is the mean of the magnitudes of the shift vectors for all patches used in the cross correlation. In general, the mean shift is inversely correlated with the median cross-correlation coefficient. Mean shifts of less than 0.5 pixel tend to yield the best signal-to-noise ratio.

6. Maximum shift:

The maximum shift is the largest magnitude of a shift vector in the array of patches used for the cross correlation. This value can be misleading as it may represent a correlation with a correspondingly large displacement which, during the filtering portion of the processing, is declared "bogus", *i.e.*, it does not conform to the overall trend of spatial deviations in the data. If this number is more than 1 pixel, the image may suffer from unusual local distortion. Such local distortion can indicate regions of the spectrum which may be degraded in signal-to-noise ratio.

7. Camera Temperature:

It is known that images acquired at camera temperature (THDA) readings of more than a few degrees from the mean THDA of the ITF images almost always suffer from unusually large distortions compared to the majority of the images in the archive. The cross-correlation algorithm has a significantly higher confidence in the pattern recognition and the mean shifts are smaller when the THDA of the image is close to that of the ITF (see Table 13.1). Images with THDAs more than a few degrees from the mean ITF THDA for that camera will probably have a poor signal-to-noise ratio. Note that the THDA is a secondary indicator of image registration quality; the median correlation coefficient is a more direct measure of registration quality.

Table 13.1: Mean ITF THDAs

Camera	LWP	LWR	SWP
ITF	1992	1983	1985
THDA	9.6	14.5	9.3

8. Spectrum peak displacement from the spectrum centroid:

A warning appears in the HISTORY position of the FITS header alerting the user that the peak of the flux in the spectrum was found more than 1 pixel from the centroid of the spectrum, in the direction perpendicular to the dispersion. The spectrum may not be a point source and may benefit from re-extraction with a wider slit.

9. Spectrum centroid displacement from predicted center:

A warning appears in the HISTORY portion of the FITS header alerting the user that the centroid of the spectrum was found more than 2 pixels from the predicted center of the spectrum, based on time and temperature dependencies. In this case, it is likely that the image suffers from unusually large spectral format shifts or that there were large target centering errors. As a result, the wavelength calibration could be in error due to a global displacement along the dispersion or local distortions not corrected for in the wavelength linearization and wavelength calibration.

10. Number of spline nodes:

Spline nodes are used to determine the shape of the spectrum along the dispersion direction. Spectral data which required 3 spline nodes or less have a very low overall signal strength or are quite noisy, and may have significantly lower than average signal-to-noise ratio.

11. Size of wavelength bins:

A large bin size may indicate that a large fraction of the spectral data are bad, missing, or have no flux above the background level. MXLO data should be examined carefully.

12. Extrapolated wavelength calibration and/or sensitivity degradation:

The image was acquired at a time outside the range of the dates used to generate the wavelength calibration and sensitivity degradation correction. These calibrations were extrapolated in time and could be slightly in error.

13. Percent of flagged pixels in the extracted spectrum:

If more than 10% of the extracted pixels in the MXLO file are flagged as either bad or as cosmic ray hits, the error flags and the sigma vector should be examined carefully for the image.

14. ν flags:

These flags indicate abnormal conditions in the data which can range from fairly minor to quite serious situations. The ν flags for the extracted data (MXLO and MXHI files) should be examined carefully in order to ascertain whether or not a particular data point is good or bad. In general, ν flag values of -16 or less (bits 5–15) are indicative of unreliable data.

More error conditions are flagged in NEWSIPS data than were flagged in IUESIPS data. In addition, *all* error conditions that affect a pixel in the two-dimensional data are bit-encoded into the ν flag data, while only the most severe error condition affecting a pixel could be recovered from IUESIPS data. The attentive investigator will have a better understanding of the errors inherent in the NEWSIPS data than was possible with IUESIPS.

It is particularly important to consider the ν flag values when analyzing extracted spectral data. The ν flag associated with each extracted point is determined from statistical considerations and does not represent all error conditions for all pixels used in the calculation of the extracted spectral point. If 45% or more of the pixels used to determine the flux of the extracted point have no error condition in the resampled image (SILO) file, no error flag is assigned to the extracted point. However, in this case, up to 55% of the pixels contributing to the extracted point can have various error conditions (or the same error condition) associated with them which could be important in the analysis of the spectrum. Examination of the resampled image extension, which contains the flag values, allows recovery of this error information.

If less than 45% of the pixels used to determine the flux of the extracted point have no error condition associated with them, the extracted point is assigned a flag which indicates all error conditions which individually occur in at least 15% of the pixels. Thus, error conditions could exist in less than 15% of the pixels and not be represented in the ν flag, but still be relevant to the scientific analysis. The SILO image extension should always be examined to determine the locations and nature of the error conditions as identified on a pixel-by-pixel basis.

Chapter 14

Contents of the IUE Final Catalog and Observing Log

One aspect of the *IUE* Final Archive process is the need for a catalog which documents the observational data available for *IUE* research. The *IUE* Final Catalog was constructed with this purpose in mind and represents a joint effort between the GSFC and VILSPA observing stations. The *IUE* Final Catalog will be available electronically and contains all Core Data Items (CDIs) for each image. To provide a condensed form of this catalog that can easily be printed, the *IUE* Final Observing Log (IUEFOL) will be available. Entries in this catalog have a format similar to that of the current *IUE* Merged Log and are a subset of the CDIs. The log contains a preface with a brief description of the *IUE* instrument, the Final Archive contents, and other relevant information, such as *IUE* Object Classes, Program Identification listings, and journal references. This log is intended for distribution in both electronic and printed forms and for use through a relational database management system.

The following items are included in the IUEFOL:

Object - Target identification.

Right Ascension and Declination - If homogeneous coordinates are not available, GO coordinates will be used (*e.g.*, solar system objects, wavecals, flat-fields). Offsets from a central position will be identified in the comments.

Class - Two digit code indicating *IUE* object classification.

Camera - LWP, LWR, or SWP.

Image - Image sequence number.

Dispersion - High, Low, Both, or Not Applicable (*e.g.*, flat-fields).

Aperture - Large, Small, Both, or Not Applicable. A double entry will be made when 'both' occurs, each of which will be identified by the appropriate aperture designation (L or S).

FES Counts - A five digit number representing the Fine Error Sensor counts of the target at the Reference Point.

FES Mode - FES tracking mode used for the target.

- FU - fast track underlap
- FO - fast track overlap
- SO - slow track overlap

Date of Observation - Starting date (UT) in the form of Year, Month, and Day (YYM-MDD).

Time of Observation - Starting time in the form of Hours, Minutes, and Seconds (HH-MMSS).

Exposure Time - Effective exposure time expressed in seconds to 3 decimal place accuracy.

Exposure Mode - Three letter code indicating exposure type (Trailed, Multiple, or Segmented).

THDA - Camera Head Amplifier Temperature at time of read.

DN Levels - Maximum continuum and mean background DN readings measured from the raw image.

Extraction Mode - Spectral extraction as point or extended source.

ITF - The Intensity Transfer Function used for the photometric correction. This entry will be specified as a camera, observation year, release year, and version (*e.g.*, SWP85R92A - SWP ITF taken in 1985, released in 1992, version A).

Abnormality Code - A warning to the user that the data may be corrupted in some fashion or non-standard in nature (*e.g.*, LWP bad scan, microphonics noise, telemetry dropouts, different exposure gains, etc.).

Program ID - GO program identification.

Comments - Information extracted from the original header and observing scripts.

These CDIs will be arranged in ASCII format with 132 characters per line. Abnormality, Database, and Resident Astronomer (RA) comments will be flagged in the main part of the log, when applicable, and reported in detail in an addendum to the log. The addendum will be formatted in 80 characters per line.

Chapter 15

Core Data Items

15.1 Introduction

To fully and accurately characterize the *IUE* dataset and facilitate future analysis, a group of "core data items" descriptive of each image was identified. These core data items (CDIs) are defined as all parameters related to the acquired images which are either necessary for image processing with the NEWSIPS system or for scientific analysis of the data. This chapter identifies and defines each CDI, indicates valid values for the CDI, the sources used to verify the CDI, and any comments relevant to the use of the CDI.

The CDIs are divided into two groups: input and output CDIs. All input CDIs for each image are verified for accuracy before NEWSIPS processing of the image by the *IUE* Project. Images are verified at the acquiring observation station. Sources for verification of the CDIs include the original observing script at GSFC and the observing log at VILSPA, the original VICAR image label, engineering data, and handwritten records. The output CDIs are generated by the NEWSIPS processing.

15.2 The Sources for Core Data Items

There are three primary sources for the CDIs, the VICAR image label (which contains the Event Round Robin), the GSFC observing scripts or the VILSPA observing log, and the NEWSIPS processing system. The image label is machine readable and was used as the initial source when possible. The observing scripts are more accurate and were used to verify the accuracy of the data taken from the image label. The output CDIs are determined as part of the image processing system. A detailed description of the image label contents, including the "round robin" series of sequential spacecraft commands, can be found in an article by Van Steenberg (1989).

129

15.3   The Core Data Items

The following is an alphabetized list of the FITS keywords for the CDIs. Each entry includes a definition and the sources used to verify the data. Where appropriate, a definition of the valid values and any further comments are included.

The FITS keywords for aperture-dependent CDIs are alphabetized by the second letter, ignoring the "x" that represents the aperture designation (L or S) in the actual keyword. Where the FITS keywords indicate Fine Error Sensor (FES) data, an "n" represents the FES number (1 or 2).

- **ABNBADSC**

  Bad Scan Flag

  VALID VALUES: YES, NO

  SOURCE: The number of bad scans occurring during a read was noted on the observing script.

  COMMENTS: This flag is set to YES to indicate that a bad camera static pointing was found at the beginning of a camera read. In this case, the read beam was repositioned to the original static pointing. The read was not restarted until a good scan was detected. This problem occurred almost exclusively during the first 2 years of operation for the LWP camera and is only flagged for that camera. For images acquired at GSFC, the number of bad scans is included in the COMMENT BY RA.

- **ABNHISTR**

  History Replay Flag

  VALID VALUES: YES, NO

  SOURCE: Images that required a history replay were noted on the observing script.

  COMMENTS: This flag is set to YES when the original image reconstruction was flawed and the image had to be recovered from the engineering history tape to obtain a good copy. Since the full image label is not available on these history tapes, the observatory spliced the full image label from the original reconstruction with the history replay version of the image. If this attempt was unsuccessful, the history tape version of the label was used which contains only the first few lines of the VICAR label. The users are warned that the VICAR label may be truncated.

- **ABNHTRWU**

  Heater Warm-up Flag

  VALID VALUES: YES, NO

  SOURCE: The use of the heater warm-up for the LWR camera was noted on the observing scripts.

COMMENTS: This flag is set to YES when a heater warm-up (usually 4 minutes) was performed during the prep sequence for the LWR camera. The heater warm-up procedure was used to reduce the occurrence of microphonics (see Chapter 3) which affected most LWR images. This flag is set only for LWR images. Note that while the occurrence of microphonics is significantly reduced with the use of the heater warm-up procedure, it is not eliminated.

- **ABNMICRO**

Microphonics Flag

VALID VALUES: YES, NO

SOURCE: NEWSIPS processing

COMMENTS: This flag is set to YES if microphonics are detected in the raw image. For images acquired at GSFC, the number and location of microphonics are noted on the observing script and in the COMMENT BY RA. Only LWR images are screened for microphonics, although SWP images occasionally have microphonics.

- **ABNMINFR**

Missing Minor Frame Flag

VALID VALUES: YES, NO

SOURCE: NEWSIPS processing

COMMENTS: This flag is set to YES if missing minor frames are detected in the raw image by an automated procedure in the NEWSIPS processing. For images acquired at GSFC, the number of missing minor frames is noted on the observing script and subsequently in COMMENT BY RA. This CDI supplements this comment. The number of missing minor frames determined by NEWSIPS may differ from the number recorded by the RA.

- **ABNNOSTD**

Non-standard Read Flag

VALID VALUES: YES, NO

SOURCE: This flag was set at the time the input CDIs for the image were manually verified, using the observing script and the TO and RA comments.

COMMENTS: This flag is set to YES for images taken in a non-standard manner. An example of a non-standard condition is an image read down with the G1 grid turned off. The reason this flag is set to YES is documented in the comments.

- **ABNOTHER**

Image Reconstruction Flag

VALID VALUES: YES, NO

SOURCE: Various observatory sources are used to set this flag including the observing script and problems that arise during image processing.

COMMENTS: This flag is set to YES for corrupted image reconstructions. It is unlikely that images with a corrupted reconstruction can be processed successfully by NEWSIPS.

- **ABNREAD**

Read Rate Flag

VALID VALUES: YES, NO

SOURCE: Non-standard read rates are noted on the observing script.

COMMENTS: This flag is set to YES when the image was read at a rate other than the standard 20 kb/s telemetry rate. The possible telemetry rates are: 40, 20, 10, 5, 2.5 and 1.25 kb/s. Since most calibration images were taken at 20 kb/s, only images read at that rate are well calibrated.

- **ABNUVC**

UVC Voltage Flag

VALID VALUES: YES, NO

SOURCE: Non-standard values were recorded on the observing script.

COMMENTS: This flag is set to YES when a non-standard Ultraviolet to Visible Converter (UVC) voltage was used during the exposure. The standard UVC setting for the LWP and SWP cameras is -5.0 kV, while the LWR camera has settings of either -4.5 or -5.0 kV.

- **APERTURE**

Aperture Mode

VALID VALUES: LARGE, SMALL, BOTH, NA

SOURCE: The aperture is found in the round robin portion of the image label. It is determined by locating a line preceded by 'TARGET' for the image and reading the third character in the last character string in the line. The observing script also contains this information. When the image processing software identifies undocumented spectral data in either aperture, the keyword is changed to BOTH.

COMMENTS: The aperture is one of the two entrance apertures in the focal plane of the telescope. When spectral data were collected through both apertures, either intentionally or serendipitously, APERTURE will be BOTH. This will give rise to 2 sets of aperture-dependent CDIs which may have different values. NA is used only for Flat-field images or Nulls.

Each spectrograph has a pair of entrance apertures consisting of a large (L) nominally 10×20 arcsecond oval, and a small (S) nominally 3 arcsecond large circle (see Chapter

2 for precise dimensions). The large oval-shaped aperture can be used for observing point-source objects, obtaining spatial information of extended sources, multiple exposures, and trailed exposures. The small aperture is unresolved and not photometrically accurate. Since the small aperture is never closed, large aperture exposures may generate a serendipitous image in the small aperture.

- **CAMERA**

Detector Designation

VALID VALUES: LWP, LWR, SWP, SWR, FES1, FES2

SOURCE: The camera identification is found on line 1 byte 50 of the *IUE* VICAR image label. The camera is designated by number in the label as follows:

1 - Long Wavelength Prime camera (LWP)

2 - Long Wavelength Redundant camera (LWR)

3 - Short Wavelength Prime camera (SWP)

4 - Short Wavelength Redundant camera (SWR)

8 - Fine Error Sensor 1 (FES1)

9 - Fine Error Sensor 2 (FES2)

The camera was also noted on the observing scripts.

COMMENTS: The default cameras initially used were the LWR and SWP cameras. In October 1983, the LWP camera replaced the LWR as the primary long wavelength camera. Only a few images were obtained with the SWR camera which has never operated to specification.

The camera number or name is noted many times in the VICAR label. At times (especially during the very early years of the *IUE* mission), the camera name and number for the image are not consistently noted in locations in the label. The camera designated in the first line of the VICAR label is taken to be the correct camera identification.

- **CC-MEDN**

Median Cross-correlation Coefficient

VALID VALUES: 0.0 to 1.0 (unitless)

SOURCE: NEWSIPS processing

COMMENTS: Median of the cross-correlation coefficients of all patches of the image for which cross correlation was successful (see Chapter 4).

133

- **CC-PERCN**

  Percentage of Successful Cross Correlations

  VALID VALUES: 0 to 100 %

  SOURCE: NEWSIPS processing

  COMMENTS: Percentage of the total number of sub-image arrays for which cross correlations were successful (see Chapter 4).

- **CC-STDEV**

  Standard Deviation of Cross-correlation Coefficients

  VALID VALUES: 0.0 to 1.0 (unitless)

  SOURCE: NEWSIPS processing

  COMMENTS: Standard deviation about the mean of the cross-correlation coefficients for all sub-image arrays for which cross correlation was successful (see Chapter 4).

- **CC-TEMPL**

  Cross-correlation Template Size

  VALID VALUES: 5×5 to 60×60 pixels

  SOURCE: NEWSIPS processing

  COMMENTS: While the template size may vary, the value of 23×23 pixels is most commonly used (see Chapter 4).

- **CC-WINDW**

  Cross-correlation Window Size

  VALID VALUES: 5×5 to 60×60 pixels

  SOURCE: NEWSIPS processing

  COMMENTS: While the window size is variable, the value of 29×29 pixels is the most commonly used (see Chapter 4).

- **xCNTRAPR**

  Predicted Center of Spectrum in SI File with Respect to Spatial Center

  VALID VALUES: 1 to 80 pixels

  SOURCE: NEWSIPS processing

  COMMENTS: NEWSIPS processing automatically takes into account predicted spectral format shifts based on time and THDA. Therefore, this CDI will normally be constant for each camera and aperture in low dispersion. The line number is normally 51 for the large aperture and 25 for the small aperture.

- **COMMENT BY GO**

  GO Comments about the Image

  SOURCE: The *IUE* GO for images taken at GSFC.

  COMMENTS: The GSFC *IUE* Project asked all GOs to provide pertinent comments for images acquired under their observing programs. Any responses from this survey are provided under this keyword and include such comments as: high background, poor S/N, target is brightest star in field, continuum has Mg II h/k lines of primary. If the GO responded but had no comments about an image, the phrase 'GO had no special comments' is placed in this keyword. Many GSFC images do not include a COMMENT BY GO.

- **COMMENT BY RA**

  RA Comments about the Image

  SOURCE: The GSFC observing scripts or the VILSPA observing log and the VICAR image label.

  COMMENTS: These comments include additional information about the image or the verification of the CDIs for the image that did not fit into the FITS CDI keywords. Explicit information about each exposure (*e.g.*, offset reference points for multiple exposures or exposure lengths for segmented observations) are included in these comments. Attached are examples of GSFC comments that are always in the same format. Not all the comments pertain to every image. Following the list of generalized examples are some specific examples. Note: "x" indicates data that vary and may not accurately indicate format as it might change slightly depending on the value.

```
EXP x APER x E=x,C=x,B=x
* Note: This comment incorporates the old database comments
field and was included at the request of users.

READ GAIN = HIGH

PARTIAL READ

EXPOSURE GAIN = MEDIUM FOR EXPOSURE x

EXPOSURE GAIN = MINIMUM FOR EXPOSURE x

BOTH DISPERSIONS

10 Kb/s READ

LWR xx-MINUTE HEATER WARMUP
```

xx MISSING MINOR FRAMES NOTED ON SCRIPT

xx BAD SCAN STARTS NOTED ON SCRIPT

EX = xxx, EY = xxx

TARGET + TFLOOD

TARGET + UVFLOOD

EXP x TRACKED ON GYROS

EXP x TRACKED ON FES

EXP x TRACKED ON GYROS AND FES

xx PREP USED

OFFSET x FROM: xxxxxxxxxxxxx
OFFSET x COORDINATES: hh mm ss.s sdd hh mm
OFFSET x MAGNITUDE: xx.xxx

****
Example of comments for a multiple exposure
****
INFORMATION ABOUT MULTIPLE EXPOSURES FOLLOWS
EXPOSURE x INFORMATION
DATEOBS x dd/mm/yy hh:mm:ss
EXPTIME x xxxxx.xxx SEC/(EFF); xxxxx.x SEC.(COM)
OFFSET REFERENCE POINT x IS UNKNOWN
OFFSET REFERENCE POINT x X= xxxxx,Y = xxxxx
FOCUS x =   xx.xx
THDASTRT x = x.xx
FPM x =   x.xx
FESCOUNT x =   FESMODE x = xx

R.P. USED FOR EXP x: xxxx, xxxx

****
Specific example of comments for a blind offset exposure
****

```
COMMENT BY RA:   EXP 1 APER L E=255,C=210,B=47
COMMENT BY RA:     0 MISSING MINOR FRAMES NOTED ON SCRIPT
COMMENT BY RA:   EXP 1 TRACKED ON FES
COMMENT BY RA:   S   PREP USED
COMMENT BY RA:   OFFSET 1  FROM: Star-3210480
COMMENT BY RA:   OFFSET 1  COORDINATES: 14 53 27.6 -32 26 06
COMMENT BY RA:   OFFSET 1  MAGNITUDE: 6.200
COMMENT BY RA:   OFFSET 2  FROM: Star-3111600
COMMENT BY RA:   OFFSET 2  COORDINATES: 14 50  7.3 -31 34 26
COMMENT BY RA:   OFFSET 2  MAGNITUDE: 8.800


************************************************************
Specific example of comments for a multiple exposure
************************************************************
COMMENT BY RA:   EXP 1 APER L C=181,B=40
COMMENT BY RA:   EXP 2 APER L C=181,B=40
COMMENT BY RA:   EXP 3 APER L C=181,B=40
COMMENT BY RA:   EXP 4 APER L C=181,B=40
COMMENT BY RA:     0 MISSING MINOR FRAMES NOTED ON SCRIPT
COMMENT BY RA:   EXP 1 TRACKED ON FES
COMMENT BY RA:   EXP 2 TRACKED ON FES
COMMENT BY RA:   EXP 3 TRACKED ON FES
COMMENT BY RA:   EXP 4 TRACKED ON FES
COMMENT BY RA:   S   PREP USED
COMMENT BY RA:   OFFSET 1  FROM: UNKNOWN
COMMENT BY RA:   OFFSET 1  COORDINATES: 01 09 11.3 +11 12 07
COMMENT BY RA:   OFFSET 1  MAGNITUDE: 8.800
COMMENT BY RA:   INFORMATION ABOUT MULTIPLE EXPOSURES FOLLOWS
COMMENT BY RA:   EXPOSURE 1 INFORMATION
COMMENT BY RA:   DATEOBS 1 18/11/79 03:09:32
COMMENT BY RA:   EXPTIME 1  1499.825 SEC.(EFF);  1500.0 SEC.(COM)
COMMENT BY RA:   OFFSET REFERENCE POINT 1 X =   -31, Y =  -208
COMMENT BY RA:   FOCUS 1 =   -0.64
COMMENT BY RA:   THDASTRT 1 =  6.80
COMMENT BY RA:   FPM 1 =    0.08
COMMENT BY RA:   FESCOUNT 1 =            FES-MODE 1 = B0
COMMENT BY RA:   EXPOSURE 2 INFORMATION
COMMENT BY RA:   DATEOBS 2 18/11/79 03:40:06
COMMENT BY RA:   EXPTIME 2  1499.825 SEC.(EFF);  1500.0 SEC.(COM)
COMMENT BY RA:   OFFSET REFERENCE POINT 2 X =   -18, Y =  -208
COMMENT BY RA:   FOCUS 2 =   -1.08
COMMENT BY RA:   THDASTRT 2 =  6.80
```

```
COMMENT BY RA:  FPM 2 =     0.50
COMMENT BY RA:  FESCOUNT 2 =           FES-MODE 2 = BO
COMMENT BY RA:  EXPOSURE 3 INFORMATION
COMMENT BY RA:  DATEOBS 3 18/11/79 04:10:36
COMMENT BY RA:  EXPTIME 3  1499.825 SEC.(EFF);  1500.0 SEC.(COM)
COMMENT BY RA:  OFFSET REFERENCE POINT 3 X =    -4, Y =  -208
COMMENT BY RA:  FOCUS 3 =   -1.10
COMMENT BY RA:  THDASTRT 3 =  7.20
COMMENT BY RA:  FPM 3 =     0.80
COMMENT BY RA:  FESCOUNT 3 =           FES-MODE 3 = BO
COMMENT BY RA:  EXPOSURE 4 INFORMATION
COMMENT BY RA:  DATEOBS 4 18/11/79 04:40:07
COMMENT BY RA:  EXPTIME 4  1499.825 SEC.(EFF);  1500.0 SEC.(COM)
COMMENT BY RA:  OFFSET REFERENCE POINT 4 X =    11, Y =  -208
COMMENT BY RA:  FOCUS 4 =   -1.20
COMMENT BY RA:  THDASTRT 4 =  7.20
COMMENT BY RA:  FESCOUNT 4 =           FES-MODE 4 = BO


*************************************************************
Specific example of comments for a segmented image
*************************************************************
COMMENT BY RA:  EXP 1 APER L E=5X,B=45
COMMENT BY RA:    0 MISSING MINOR FRAMES NOTED ON SCRIPT
COMMENT BY RA:    0 BAD SCAN STARTS NOTED ON SCRIPT
COMMENT BY RA:  EXP 1 TRACKED ON GYROS
COMMENT BY RA:  S    PREP USED
COMMENT BY RA:  EXPOSURE 1 SEGMENTED ( 5 EXPOSURES)
COMMENT BY RA:  SEGMENT  1 EXPOSED   899.768 SEC.(EFF);  900.0 SEC.(COM)
COMMENT BY RA:  SEGMENT  2 EXPOSED  1199.595 SEC.(EFF); 1200.0 SEC.(COM)
COMMENT BY RA:  SEGMENT  3 EXPOSED   899.768 SEC.(EFF);  900.0 SEC.(COM)
COMMENT BY RA:  SEGMENT  4 EXPOSED  1199.595 SEC.(EFF); 1200.0 SEC.(COM)
COMMENT BY RA:  SEGMENT  5 EXPOSED  1199.595 SEC.(EFF); 1200.0 SEC.(COM)
```

- **xDATABKG**

Estimated Background Level

VALID VALUES: 0 to 255 DN

SOURCE: NEWSIPS processing

COMMENTS: This CDI is based on an algorithm applied uniformly to all images and will often differ from the value indicated in the COMMENT BY RA. The value in the comments is based on measurements made at the the time of acquisition and is not uniform over the entire *IUE* mission.

- **xDATACNT**

  Estimated Continuum Level

  VALID VALUES: 0 to 255 DN

  SOURCE: NEWSIPS processing

  COMMENTS: This CDI is based on an algorithm applied uniformly to all images and will often differ from the value indicated in the COMMENT BY RA. The value in the comments is based on measurements made at the the time of acquisition and is not uniform over the entire *IUE* mission.

- **xDATEOBS**

  Date at the Start of Observation (UT)

  VALID VALUES: Dates for the life of the satellite starting at January 28, 1978.

  SOURCE: The date of read is extracted from bytes 1–5 in line 10 of the image label. Time stamps found in the round robin are used to correct the read date to the start date when needed. The start date of the observation is also found on the observing script. The start date for null images is set equal to the read date.

  COMMENTS: This is an aperture-dependent keyword. For multiple and segmented exposures, only the date of observation for the first exposure is placed in the FITS keyword. The dates of observation for the remaining exposures are entered as comments.

- **xDEC**

  Declination of the Observed Target (1950)

  VALID VALUES: −90 to +90 degrees

  SOURCE: For non-solar system objects, the declination stored in this field is extracted from the SIMBAD database by the Centre de Données Astronomiques de Strasbourg (CDS) for the *IUE* Project. All observations of the same target have identical homogeneous coordinates regardless of the coordinates supplied by the GO. Comet coordinates were provided by M. Festou of Observatoire de Besancon, France and documented in ULDA, Guide 2: Comets (ESA SP 1134, May 1990). Coordinates for other solar system objects and for sky background acquisitions are duplicated for this CDI from the original coordinates supplied by the GO. *No offsets have been applied to the homogeneous coordinates of the target. The offsets are documented in the* COMMENT BY RA *field.* The declination is zero-filled for Null, T-flood, and UV-flood images. If the pointed coordinates are available for WAVECAL images, they appear in this field; otherwise, this field is zero-filled.

  COMMENTS: The declination stored in this keyword is also known as the HOMOGENOUS DEC. The homogeneous declination is used by NEWSIPS processing whenever coordinates are required by a reduction algorithm.

139

- **DISPERSN**

  Spectrograph Dispersion Mode

  VALID VALUES: HIGH, LOW, BOTH, NA

  SOURCE: The observing scripts are the most accurate source for the dispersion and were used as the primary source during image verification. The dispersion is found in the binary portion (camera snapshots) of the VICAR label in lines 86–100. Characters 22–25 are read into character format and converted to byte format, then separated into bits. If the bits 4 or 6 are equal to 1, then DISPRS='L', else DISPRS='H'. One cannot tell easily from the label if both dispersions were used during acquisition of an image.

  COMMENTS: This CDI describes the dispersion mode of the spectrograph used in obtaining the image. The options are HIGH (echelle grating), LOW (single order), BOTH (for those images acquired with both dispersions superimposed) or NA (for Flat-field images). The CDI "DISPTYPE" records the dispersion parameter used in NEWSIPS processing.

- **DISPTYPE**

  Dispersion Designated for Processing

  VALID VALUES: HIGH, LOW

  SOURCE: This value is determined prior to processing by the image processing staff.

  COMMENTS: The value may be HIGH or LOW and may differ from the designated dispersion for images acquired with both dispersions, for images with no dispersion designated, and for certain types of engineering data (Nulls and Flat-field images). Images with DISPERSN='BOTH' or 'NA' will be processed twice, once with DISPTYPE='LOW' and once with DISPTYPE='HIGH'. Output files from both processings will be available in the archive.

- **EPOCH**

  Epoch of the Coordinates

  VALID VALUES: 1950

  SOURCE: The 1950 epoch is constant for the *IUE* mission.

- **xEXPMULT**

  Multiple Exposure Flag

  VALID VALUES: Y-OFFSETS, X-OFFSETS, ALONG-APER, OTHER, NO

  SOURCE: Exposure information is extracted from the round robin for each exposed spectrum of a multiple or a double aperture exposure. However, one cannot tell from

this information whether the image contains multiple spectra spatially offset or time-segmented spectra superimposed. Thus the notations made on the observing script are needed to differentiate these types of images.

COMMENTS: This flag indicates the acquisition of multiple spectra in the large aperture. Multiple exposures result in 2 or more individual spectra spatially displaced from one another. The flag is set to indicate that these spectra were displaced along the FES X-axis, the FES Y-axis, the major axis of the large aperture or another configuration. If the image does not contain multiple spectra, the flag is set to NO. Multiple spectra in the large aperture can be of the same object or of different objects. Multiple spectra may have been acquired by deliberately re-pointing the spacecraft for each separate spectrum or serendipitously, with a nearby object yielding an additional spectrum. The CDIs stored as FITS keywords are for the first exposure in the large aperture with the exception of exposure length which is the sum of all effective exposure lengths. A subset of data for subsequent large-aperture exposures is stored in the COMMENT BY RA keyword. This subset includes the start date and time of each exposure, the length of exposure (both commanded and effective), the offset reference point, focus, THDA at the start of the exposure, radiation counts, and the FES mode and counts.

- **EXPOGAIN**

SEC Exposure Gain Mode

VALID VALUES: MAXIMUM, MEDIUM, MINIMUM

SOURCE: The exposure gain can be extracted from the VICAR label by finding the line in the round robin preceded by 'EXPOBC' and reading character 26. The exposure gain is also noted on the observing script if it is not the normal value of MAXIMUM.

COMMENTS: The exposure gain depends on the accelerating voltage applied in the Secondary Electron Conduction (SEC) photocathode. The maximum gain is equal to -6.1 kV, medium gain -4 kV, and minimum gain -3.2 kV. The exposure gain can have different values for each exposure of a multiple exposure image or for dual aperture images. However, since this is an extremely rare (if existing) occurrence, the exposure gain is assumed to be the same for both. This rare situation will be noted in the COMMENT BY RA.

- **xEXPSEGM**

Segmented Exposure Flag

VALID VALUES: YES, NO

SOURCE: Exposure information can be extracted from the round robin for each exposure of a segmented image. However, one cannot tell explicitly from this information whether the image contains multiple spectra spatially offset or time segmented spectra superimposed. Thus the notations made on the observing script are needed to differentiate these types of images.

141

COMMENTS: This CDI flags superimposed spectra obtained by more than one commanded exposure. This situation may occur if no guide star is available for FES tracking during a long exposure and the target must be re-centered in the aperture or if the length of the exposure is greater than the maximum commandable exposure time (447 minutes). Segmented exposures result in a single spectrum. Where available, the number of segmented exposures and the commanded and effective exposure times for each exposure are stored in the FITS keyword COMMENT BY RA.

- **xEXPTIME**

Effective Exposure Time

VALID VALUES: 0.000 to 90000.000 seconds

SOURCE: The effective exposure time is derived from the commanded exposure time. The commanded exposure time is extracted from the round robin portion of the VICAR label by reading characters 8–13 from a line preceded by 'EXPOBC' into an integer variable compacted into the format mmmss (5 digits). When the TO has modified the initial commanded length of exposure, the modified commanded time is extracted from characters 16–21 of a line preceded by 'FIN'. The commanded exposure time is also noted on the observing script.

COMMENTS: The effective exposure time is used in the absolute calibration of spectral data. Both commanded and effective exposure times are retained in the Final Archive database for images acquired at GSFC. Only the effective exposure is retained for images acquired by VILSPA.

The effective exposure time is determined from the commanded exposure time by correcting for various known instrumental properties (*i.e.*, OBC quantitization and camera rise time). Details of the exposure time corrections for both point and trailed sources can be found in Chapter 10.

For multiple exposures, the effective exposure is calculated for each exposure and the results are added together for the FITS keyword (xEXPTIME). The effective exposure time for each exposure (where known) is placed in the FITS keyword COMMENT BY RA.

For segmented exposures, the effective exposure time is calculated for each segment of the exposure and the results are then added together. The commanded and effective exposure time for each segment is recorded in the FITS keyword COMMENT BY RA.

Trailed exposure times are not based on a commanded exposure time, but on the effective trail rate, the aperture size, and the number of passes through the aperture. The effective trail rate is derived from the commanded trail rate by applying an OBC quantitization correction. The determination of trailed exposure times is discussed in detail in Chapter 10.

- **xEXPTRMD**

  Trail Mode Flag

  VALID VALUES: X-TRAIL, Y-TRAIL, NO-TRAIL

  SOURCE: The trail mode is taken from the observing script.

  COMMENTS: The trail mode indicates if the target was trailed along either the FES X-axis, the FES Y-axis, or not trailed. If this flag is set, the keywords xTRAILRT and xTRAILNR indicating the trail rate and the number of passes will also be set.

- **xFESnBK**

  FES Background Counts

  VALID VALUES: 0 to 28672 FES counts

  SOURCE: The FES background counts are taken from the observing script.

  COMMENTS: This value records the intensity of scattered light from the FES anomaly and is only listed for data acquired since January 1991.

- **xFESnCN**

  FES Target Counts

  VALID VALUES: 0 to 28672 FES counts

  SOURCE: The FES counts may be extracted from the round robin of the VICAR label by reading the first integer field of a line preceded by 'FES CTS' or 'FESCT'.

- **xFESnMD**

  FES Tracking Mode for the Target

  VALID VALUES: F, S, O, U, FO, FU, SO, BO

  SOURCE: The FES mode is extracted from the round robin of the VICAR label and is stored in the second and third integer fields in the line preceded by 'FES CTS' or 'FESCT'. The mode is also noted on all observing scripts.

  COMMENTS: The track mode of the Fine Error Sensor (FES) with the target at the reference point. Fast (F) or Slow (S) track - Overlap (O) or Underlap (U), or Blind Offset (BO). If the track mode is missing, the corresponding CDI will be left blank.

- **xFLUXAVE**

  Average Extracted FN

  VALID VALUES: -1024 to $+1024$

  SOURCE: NEWSIPS processing

  COMMENTS: The average FN of the spectral data determined in the spectral extraction procedure (SWET). The average FN value is used to determine which fit will be used: an empirical or a default profile fit. See Chapter 9 for a detailed discussion.

143

- **xFOCUS**

  Camera Focus

  VALID VALUES: -25.0 to $+25.0$

  SOURCE: The focus step is calculated by extracting three temperatures from the spacecraft snapshots, converting them from raw telemetry units to engineering units, and inserting these numbers into a formula. The focus value is also recorded on the observing scripts by the TO.

  COMMENTS: The focus step is the value measured at the beginning of the exposure. This value is a linear function of three telescope temperatures. Typical values range from -10 to $+5$.

- **xFPM**

  Flux Particle Monitor Voltage

  VALID VALUES: 0.0 to 4.0 Volts

  SOURCE: This value was recorded on the observing script at the start of each exposure.

  COMMENTS: A measurement of solar radiation (both direct and from the Van Allen belts) at the beginning of the exposure. The background radiation fluxes were detected as an output voltage from a Geiger counter which had a threshold of 960 keV for electrons and 15 Mev for protons. The Flux Particle Monitor (FPM) malfunctioned in May 1991 and was turned off in October 1991. Therefore, only images taken prior to May 1991 have valid radiation values. The rate at which the background level accumulates on the most sensitive part of a detector is an exponential function of FPM, and is given by:
  $$DN/hour = A \times 10^{FPM}$$
  where A is 1.35 for the LWP, 0.73 for the SWP, and 1.00 for the LWR.

- **xGSTARnC**

  FES Guide Star Counts

  VALID VALUES: 0 to 28672 FES counts

  SOURCE: This value was recorded on the observing script.

  COMMENTS: The guide star counts are measured with either FES1 or FES2.

- **xGSTARnM**

  FES Tracking Mode for the Guide Star

  VALID VALUES: FO,FU,SO,F,S,NO

  SOURCE: This value is recorded on the observing script.

  COMMENTS: Similar to the FES tracking mode of the target.

- **xGSTARnX**

  FES Guide Star X-coordinate

  VALID VALUES: -2016 to $+2047$ FES Units

  SOURCE: This value is extracted from the round robin portion of the VICAR label and is the first integer value of a line preceded by 'GDE'. The value is also found on the observing script.

  COMMENTS: This entry can refer to either FES1 or FES2.

- **xGSTARnY**

  FES Guide Star Y-coordinate

  VALID VALUES: -2016 to $+2047$ FES Units

  SOURCE: This value is extracted from the round robin portion of the VICAR label and is the second integer value of a line preceded by 'GDE'. The value is also found on the observing script.

  COMMENTS: This entry can refer to either FES1 or FES2.

- **xHELCORR**

  Heliocentric Time Correction to the Midpoint of Observation

  VALID VALUES: < 1.0 days

  SOURCE: NEWSIPS processing

  COMMENTS: The heliocentric time correction is computed during processing for the midpoint of observation (xMJD-MID) such that $JD_{corr} = MJD\text{-}MID + HELCORR$. This may be important for some variable targets.

- **IMAGE NUMBER**

  Camera Image Sequence Number

  VALID VALUES: ≥ 500

  SOURCE: The image number is found on line 1 bytes 52–56 on the image label. This number is also found on the second line but is not always accurate, as it is hand entered by the TO. In addition, the image number is found on the observing script.

  COMMENTS: Camera-dependent sequential image number was assigned to an image at acquisition starting at 1000. Images that were inadvertently assigned duplicate image numbers have been reassigned numbers starting at 500 for each camera.

- **ITF**

  The Intensity Transfer Function Used in Image Processing

  VALID VALUES: SWP85R_, SWP92R_, LWP84R_, LWP92R_, LWR83R_

SOURCE: NEWSIPS processing

COMMENTS: Indication is given for the camera, last 2 digits of year of acquisition, last 2 digits of year of construction, and an alphabetic character representing the sequence of construction within the year (*e.g.*, SWP85R92A). The "R" character denotes "release".

- **xIUECLAS**

IUE Object Class

00 SUN	51 LONG PERIOD VARIABLE STARS
01 EARTH	52 IRREGULAR VARIABLES
02 MOON	53 REGULAR VARIABLES
03 PLANET	54 DWARF NOVAE
04 PLANETARY SATELLITE	55 CLASSICAL NOVAE
05 MINOR PLANET	56 SUPERNOVAE
06 COMET	57 SYMBIOTIC STARS
07 INTERPLANETARY MEDIUM	58 T TAURI
08 GIANT RED SPOT	59 X-RAY
09	60 SHELL STAR
10 W C	61 ETA CARINAE
11 WN	62 PULSAR
12 MAIN SEQUENCE O	63 NOVA-LIKE
13 SUPERGIANT O	64 OTHER
14 OE	65 MISIDENTIFIED TARGETS
15 OF	66 INTERACTING BINARIES
16 SD O	67
17 WD O	68
18	69 HERBIG-HARO OBJECTS
19 OTHER STRONG SOURCES	70 PLANETARY NEBULA + CENTRAL STAR
20 B0-B2 V-IV	71 PLANETARY NEBULA - CENTRAL STAR
21 B3-B5 V-IV	72 H II REGION
22 B6-B9.5 V-IV	73 REFLECTION NEBULA
23 B0-B2 III-I	74 DARK CLOUD (ABSORPTION SPECTRUM)
24 B3-B5 III-I	75 SUPERNOVA REMNANT
25 B6-B9.5 III-I	76 RING NEBULA (SHOCK IONIZED)
26 BE	77
27 BP	78
28 SDB	79
29 WDB	80 SPIRAL GALAXY
30 A0-A3 V-IV	81 ELLIPTICAL GALAXY
31 A4-A9 V-IV	82 IRREGULAR GALAXY
32 A0-A3 III-I	83 GLOBULAR CLUSTER

33 A4-A9 III-I	84 SEYFERT GALAXY
34 AE	85 QUASAR
35 AM	86 RADIO GALAXY
36 AP	87 BL LACERTAE OBJECT
37 WDA	88 EMISSION LINE GALAXY (NON-SEYFERT)
38 HORIZONTAL BRANCH STARS	89
39 COMPOSITE SPECTRAL TYPE	90 INTERGALACTIC MEDIUM
40 F0-F2	91
41 F3-F9	92
42 FP	93
43 LATE-TYPE DEGENERATES	94
44 G V-IV	95
45 G III-I	96
46 K V-IV	97
47 K III-I	98 WAVELENGTH CALIBRATION LAMP
48 M V-IV	99 NULLS AND FLAT FIELDS
49 M III-I	
50 R, N, OR S TYPES	

VALID VALUES: 0 to 99 (unitless)

SOURCE: The object class was designated by the GO as part of the proposal target list. This designation is found in bytes 54–56 of line 36 of the VICAR label. The GO also designated the object class on the observing scripts. If the designations differed, the object class on the scripts was used.

COMMENTS: *IUE* Project staff *did not* standardize the object classes. Object classes were changed from the GO designation only when the designation was obviously wrong (*e.g.*, sky around Jupiter designated as planetary nebula) or when a new classification was created (*e.g.*, Herbig-Haro objects). *Therefore, a single target observed multiple times may have several different object class identifications in the database.*

- **LAMP**

  Flood Lamp Flag

  VALID VALUES: TFLOOD, CALUV, NONE

  SOURCE: This information is extracted from the round robin portion of the VICAR label by locating a line preceded by the 'EXPOBC' command and reading the characters in bytes 29 through 31. This information is also noted on the observing script.

  COMMENTS: This keyword indicates if one of the on-board lamps was activated at any time after the camera prep and before the read. If no lamp was activated then this keyword is set to NONE. This keyword does not indicate the use of the Platinum-Neon

(Pt-Ne) Wavelength Calibration (WAVECAL) lamps, because they produce spectral data and are handled as science data. The lamp types are as follows:

TFLOOD: Tungsten Flood lamps normally used in the camera preparation sequence. However, they are also used in conjunction with the WAVECAL lamps to illuminate the reseau marks needed for the geometric correction and to raise the DN level of the fainter emission lines. In addition, they are occasionally exposed in conjunction with stellar images for test purposes to enhance the background.

CALUV: Ultraviolet (mercury discharge) Flood lamps that produce a monochromatic output at 2537Å. They are primarily utilized in generating the ITF images used for the photometric correction process.

- **xLAPSTAT**

  Aperture Status Flag

  VALID VALUES: C, O

  SOURCE: The status of the large aperture is recorded in the binary camera snapshots portion (lines 86–100) of the VICAR label. Characters 22–25 are read into character format and converted to byte format, then separated into bits. If the bits 7 and 8 are both equal to 0, then the large aperture was open, otherwise it was closed. This information was also recorded on the observing script.

  COMMENTS: This CDI describes whether the spectrograph large aperture was closed (C) or open (O) during the observation. Because opening and closing the large aperture may shift the reference point for centering objects in the aperture, the large aperture generally remains open. The small aperture is always open. The large aperture is typically only closed during wavelength calibration exposures and during high-dispersion observations of targets where light from a nearby source in the large aperture might contaminate the small-aperture spectrum.

- **MEANRAT**

  Ratio of Mean Flux in SI File to Mean Flux in LI File

  VALID VALUES: $-\infty$ to $+\infty$ %

  SOURCE: NEWSIPS processing

  COMMENTS: This CDI can give an indication of how well the flux was conserved in the resampling step. If the mean flux value in the LI image is near zero, however, the ratio is unreliable.

- **xMJD-MID**

  Mid-Point Date and Time of the Observation

  VALID VALUES: 43534.0 to end of *IUE* mission

SOURCE: NEWSIPS processing

COMMENTS: This value is stored as a modified Julian Date using the following formula:

$$Modified\ Julian\ Date = Julian\ Date - 2400000.5$$

- **xMJD-OBS**

Starting Date and Time of Observation

VALID VALUES: 43534.0 to end of *IUE* mission

SOURCE: NEWSIPS processing

COMMENTS: This value is stored as a modified Julian Date. In the case of multiple exposures in the large aperture, the modified Julian Date is only calculated for the first exposure.

- **xOBJECT**

HOMOGENEOUS Target Identifier

SOURCE: The Homogeneous Target Identifier was, in most cases, provided by CDS for the *IUE* Project. CDS used the original target designation from the GO for each image in the *IUE* archive to cross-match with the SIMBAD database, thus identifying all images of a particular target, regardless of the nomenclature used by the GO. CDS then assigned a homogeneous target ID according to the following priority list:

HD, BD, CD, CPD, V*, WD, GD, NGC, IC, PK, SK, AzV, LIN, LHA, DEM, MRK, PG, QSO, ABCG, NOVA, SN, LS, PHL, FEIG, ROSS, 3C, X, PKS.

When none of these identifiers existed for a target, the first identifier listed by SIMBAD was adopted. SK, AxV, LIN, LHA, and DEM were later transformed to MC. LS, PHL, FEIG, ROSS, 3C, X, PKS, and a few other catalogs were later transformed to AOO LS, etc. to facilitate searches for "any other object". The homogeneous target IDs for a few images were supplied or modified by VILSPA for accuracy during the final check.

COMMENTS: This item consists of three sections. The first four characters of the field are a catalog identifier, most of which are standard astronomical catalog abbreviations. The catalog designation ZZ stands for solar system objects and the designation 'IUE' is used for images acquired for *IUE* engineering and calibration purposes. The next 12 characters identify the object. The final 12 characters are the optional complementary ID, used to give additional or more specific identification of the target. Some examples of complimentary IDs include a nearby object for a sky background exposure or an area of a nebula or planet.

- **ORBANOMA**

Mean Anomaly of the Orbit

VALID VALUES: 0 to 359.999999 degrees

SOURCE: GSFC Flight Dynamics Predictions.

- **ORBASCEN**

  Right Ascension of Ascending Node of the Orbit

  VALID VALUES: 0 to 359.999999 degrees

  SOURCE: GSFC Flight Dynamics Predictions.

  COMMENTS: Typical values range from 98 – 208 degrees.

- **ORBECCEN**

  Orbit Eccentricity

  VALID VALUES: 0 to 1 (unitless)

  SOURCE: GSFC Flight Dynamics Predictions.

  COMMENTS: Typical values range from 0.13 – 0.24

- **ORBEPOCH**

  Date of the Orbital Elements (UT)

  VALID VALUES: February 22, 1978 to end of *IUE* mission

  SOURCE: GSFC Flight Dynamics Predictions.

  COMMENTS: The appropriate set of orbital elements for an image is determined using the date of exposure and the orbital elements epoch. Images are assigned the set of orbital elements that have the nearest preceding date. The only exception is for images taken after a Delta V, which are assigned the set of orbital elements with the nearest succeeding date.

- **ORBINCLI**

  Inclination of the Orbit

  VALID VALUES: −90 to +90 degrees

  SOURCE: GSFC Flight Dynamics Predictions.

  COMMENTS: Typical values range from 28 – 35 degrees.

- **ORBSAXIS**

  Semi-major Axis of the Orbit

  VALID VALUES: 0 to ∞ kilometers

  SOURCE: GSFC Flight Dynamics Predictions.

  COMMENTS: Typical values range from 42150 – 42180 kilometers.

- **PGM-ID**

  Observer Program ID

SOURCE: The program ID is stored on line 36 of the VICAR label in the first 5 characters. The program ID is also noted on the observing script.

COMMENTS: An alphanumeric code that identifies the observing program for which the observation was made. The program ID contains 5 characters. For NASA-approved programs of the first year, the first two letters identify the type of observing program and the last three are the initials of the principal investigator. After the first year of operation, the first two letters identify the type of observing program, the third letter represents the year, and the last two letters are the intials of the principal investigator. The program IDs for NASA discretionary programs begin with the letters OD. The last three characters are a sequential number and a letter. For ESA- and SERC-approved programs the program IDs are generally two letters followed by three numbers where the first letter designates the year. Program IDs are also assigned for images obtained for project-related programs such as calibration monitoring and camera testing.

- **POSANGLE**

Spacecraft Position Angle

VALID VALUES: 0.0 to 359.999999 degrees

SOURCE: For images acquired at GSFC, the position angle of the large aperture is calculated from the roll angle coordinates. The roll angle is entered during verification of the CDIs from the observing script. For images acquired at VILSPA, the position angle is computed from the coordinates and exposure start time.

COMMENTS: The position angle in the plane of the sky is defined such that 0 degrees points north and 90 degrees points east. The position angle is related to the spacecraft roll angle by:

$$Position\ Angle = Aperture\ Orientation\ Angle - Spacecraft\ Roll\ Angle$$

where the aperture orientation angles are defined with respect to the reference vector and increase counterclockwise from the reference vector. Note that the roll angle has been retained in the GSFC database for images read at GSFC.

- **xRA**

Right Ascension of the Observed Target

VALID VALUES: 0 to 359.999999 degrees

SOURCE: For non-solar system objects, the right ascension stored in this field is extracted from the SIMBAD database by the Centre de Données Astronomiques de Strasbourg (CDS) for the *IUE* Project. All observations of the same target have identical homogeneous coordinates regardless of the coordinates supplied by the GO. Comet coordinates were provided by M. Festou of Observatoire de Besancon, France and documented in ULDA, Guide 2: Comets (ESA SP 1134, May 1990). Coordinates for other solar system objects and for sky background acquisitions are duplicated for this CDI

151

from the original coordinates supplied by the GO. *No offsets have been applied to the homogeneous coordinates of the target. The offsets are documented in the* COMMENT BY RA *field.* The right ascension is zero-filled for Null, T-flood, and UV-flood images. If the pointed coordinates are available for WAVECAL images, they appear in this field; otherwise, this field is zero-filled.

COMMENTS: The right ascension stored in this keyword is also designated the HO-MOGENOUS RA. The homogeneous right ascension is used by NEWSIPS processing whenever coordinates are required by a reduction algorithm.

- **xRADVELO**

  Heliocentric Radial Velocity Correction for High Dispersion

  VALID VALUES: −34 to +34 kilometers per second

  SOURCE: NEWSIPS processing

  COMMENTS: Net radial velocity correction for high-dispersion data taking into account the motions of *IUE* and the Earth.

- **READGAIN**

  Read Gain Mode

  VALID VALUES: HIGH, LOW

  SOURCE: This value can be found in the event round robin portion of the VICAR image label and on the observing script.

  COMMENTS: This CDI is the gain of the camera head amplifier in the readout section of the SEC tube. Low gain is the standard mode and is the default where not noted explicitly on the observing script.

- **READMODE**

  Image Read Flag

  VALID VALUES: FULL, PARTIAL

  SOURCE: This value can be found in the round robin portion of the image label and on the observing script.

  COMMENTS: This keyword indicates if the image was read fully or partially. Partial reads are images for which only the part of the detector containing the spectrum was read. Full read is the standard read.

- **SHFTMAX**

  Maximum Shift Between Image and ITF.

  VALID VALUES: 0 to 10.0 pixels

  SOURCE: NEWSIPS processing

COMMENTS: Maximum of the magnitudes of the displacement vectors determined for the patches of the image used for cross correlation.

- **SHFTMEAN**

Mean Shift Between Image and ITF

VALID VALUES: 0 to 10.0 pixels

SOURCE: NEWSIPS processing

COMMENTS: Average of the magnitudes of the displacement vectors determined for the patches of the image used for cross correlation.

- **SERENDAP**

Serendipitous Image Flag

VALID VALUES: LARGE, SMALL

SOURCE: NEWSIPS processing

COMMENTS: This keyword is set equal to the aperture for which a serendipitous exposure is detected by the NEWSIPS software. This CDI only has a value when unexpected spectral data are detected in the NEWSIPS processing. If the presence of a serendipitous exposure, either in the other aperture or another camera, was indicated on the observing script, this CDI will be left blank.

- **STATION**

Observing Station Flag

VALID VALUES: GSFC, VILSPA

SOURCE: The observing station is found in character 49 of the first line of the VICAR label. This is an integer value where 1 equals GSFC and 2 equals VILSPA. The observing station is also documented on observing scripts and in Telescope Operation Control Center records.

COMMENTS: This flag indicates the observing station which read the image down from the satellite. For collaborative images, the station where the image was read is the designated observing station. The only time the observing station is not the one where the image was read is at times of equipment failure.

- **STDEVRAT**

Standard Deviation Ratio

VALID VALUES: $-\infty$ to $+\infty$ (unitless)

SOURCE: NEWSIPS processing

COMMENTS: The ratio of the standard deviation about the mean of the flux in the SI file to the standard deviation about the mean of the flux in the LI file. This

CDI can give an indication of how well the noise characteristics in the LI image were preserved in the resampling step. If the standard deviation about the mean of the flux in the LI image is near zero, the ratio is unreliable.

- **xTARGDEC**

  GO-designated Target Declination

  VALID VALUES: −90.0 to +90.0 degrees

  SOURCE: The GO defines the declination for the target as part of the target list submitted with the proposal. This declination is stored in line 37, bytes 8 through 14 of the VICAR label as degrees, minutes and seconds. The DEC is also recorded on the observing script. If the DEC from the VICAR label differs from that recorded on the observing script, the DEC from the script is used.

  COMMENTS: The GO-designated declination is used for preliminary positioning of the spacecraft.

- **xTARGET**

  GO-designated Target Name

  SOURCE: The object name is located in bytes 39-46 of the line 36 of the VICAR label. The object name is also located on the observing script.

  COMMENTS: The object name found in the VICAR label was supplied by the GO on the proposal target list. The GO may use a different target name on the observing script. GOs are encouraged to use the Henry Draper catalog designations for stars in this field, where appropriate.

- **xTARGRA**

  GO-designated Target Right Ascension

  VALID VALUES: 0 to 359.999999 degrees

  SOURCE: The GO defines the right ascension for the target as part of the target list submitted with the proposal. This right ascension is stored in line 37, bytes 1 through 7 of the VICAR label in hour, minute, second format. The RA is also recorded on the observing script. If the RA from the VICAR label differs from that recorded on the observing script, the RA from the script is used.

  COMMENTS: The GO-designated right ascension is used for preliminary positioning of the spacecraft.

- **xTHDAEND**

  Camera Head Amplifier Temperature at Exposure End

  VALID VALUES: −5.0 to +57.640 degrees Celsius

SOURCE: This value is found in the camera snapshot section of the binary section (lines 86–100) of the VICAR label and is not noted on the observing script. If the camera snapshot portion of the label is corrupted, the THDA is estimated using the THDA values from images taken before and after this image.

For images acquired before June 7, 1979 (day 158), THDA values cannot be obtained from the label. Thus THDAs for each camera at one hour intervals were digitized from the telemetry page snaps. Images were assigned the THDA value nearest in time to the end of the exposure for this time period.

COMMENTS: Temperatures generally range from 4.0 to 20.0 degrees Celsius. Average temperatures are typically about 9 degrees Celsius for the SWP and LWP cameras and 13 degrees Celsius for the LWR camera. This value cannot be verified against independent sources. The importance of THDA as a predictor of image quality was not established until the early 1980s.

- **THDAREAD**

  Camera Head Amplifier Temperature at Read Start

  VALID VALUES: −5.0 to +57.640 degrees Celsius

  SOURCE: This value is found in the camera snapshots section of the binary section (lines 86–100) of the VICAR label and is not noted on the observing script. If the camera snapshots portion of the label is corrupted, the THDA is estimated using the THDA values from images taken before and after this image.

  For images acquired before June 7, 1979 (day 158), THDA values for each camera at one hour intervals were digitized from the telemetry page snaps. Images were assigned the THDA value nearest in time to their read time.

  COMMENTS: Temperatures generally range from 4.0 to 20.0 degrees Celsius. Average temperatures are typically about 9 degrees Celsius for the SWP and LWP cameras and 13 degrees Celsius for the LWR camera. This value cannot be verified against independent sources. The importance of THDA as a predictor of image quality was not established until the early 1980s.

- **xTHDASTR**

  Camera Head Amplifier Temperature at Exposure Start

  VALID VALUES: −5.0 to +57.640 degrees Celsius

  SOURCE: This value is found in the camera snapshots section of the binary section (lines 86–100) of the VICAR label and is also noted on the observing script.

  For images acquired before June 7, 1979 (day 158), THDA values for each camera at one hour intervals were digitized from the telemetry page snaps. Images were assigned the THDA value nearest in time to the start of the exposure.

COMMENTS: Temperatures generally range from 4.0 to 20.0 degrees Celsius. Average temperatures are typically about 9 degrees Celsius for the SWP and LWP cameras and 13 degrees Celsius for the LWR camera. This value cannot be verified against independent sources. The importance of THDA as a predictor of image quality was not established until the early 1980s.

- **TILTCORR**

  Tilt Correction Flag

  VALID VALUES: YES, NO

  SOURCE: NEWSIPS module

  COMMENTS: The tilt correction is only applied to large-aperture, low-dispersion extended-source data, when appropriate, and multiple exposures taken along the major-axis of the aperture.

- **xTIMEOBS**

  Time (hour, minute and second) at Exposure Start (UT)

  VALID VALUES: 00:00:00 to 23:59:59

  SOURCE: The time of observation may be found in the image label by locating a line in the round robin preceded by 'EXPOBC', reading the characters 1–6 with format hhmmss and subtracting 6 seconds from it. However, when the exposure time has been modified, the time is extracted from the first 6 characters in the round robin line preceded by 'FIN'. This information is also found on the observing script.

  COMMENTS: For multiple or segmented exposures in the large aperture the start time of the first exposure will be stored in the keyword. Subsequent exposure values will be stored in the COMMENT BY RA.

- **xTRAILNR**

  Number of Passes in a Trailed Observation

  VALID VALUES: 1 to 9 (unitless)

  SOURCE: The number of passes (iterations) is extracted from the round robin portion of the VICAR label by locating a line preceded by 'ITER' and reading the one digit integer. This information is also recorded on the observing script.

  COMMENTS: The number of passes is needed to determine the trailed exposure time.

- **xTRAILRT**

  Effective Trail Rate

  VALID VALUES: 0.03 to 120.0 arcseconds per second

156

SOURCE: The effective trail rate is a calculated value using the commanded trail rate and allowing for OBC quantitization. The commanded trail rate can be extracted from the round robin portion of the VICAR label by locating a line preceded by 'TRAIL' and reading the real value number at the end of the line. The commanded trail rate is also noted on the script. See Chapter 10 for details on calculating an effective trail rate from the commanded trail rate.

COMMENTS: The effective trail rate is needed to determine the effective exposure time for trailed data.

- **UVC-VOLT**

    UVC Voltage Setting

    VALID VALUES: −5.0 to 0.0 kV

    SOURCE: The UVC voltage is found in the VICAR label by locating a line in the round robin preceded by 'FIN' and reading the integer value that follows the U field in that line. If a non-standard UVC voltage was commanded, this value would be noted on the script. The normal UVC voltage is −5.0 kV (see also ABNUVC).

    COMMENTS: After mid-1983 the LWR camera was routinely read at −4.5 kV to reduce the negative effect of the flare on the detector.

- **xXTRCNTR**

    Line Number in SI File at which the Peak Cross-dispersion Profile Flux was Found

    VALID VALUES: 1.0 to 80.0 pixels

    SOURCE: NEWSIPS processing

- **xXTRASYM**

    Assymetrical Extraction Profile

    VALID VALUES: YES, NO

    SOURCE: NEWSIPS processing

    COMMENTS: A flag indicating if the peak of the cross-dispersion flux was found to be more than 2 pixels (two lines in the SI file) away from the centroid of the profile.

- **xXTRMODE**

    Processing Extraction Mode

    VALID VALUES: POINT, EXTENDED

    SOURCE: NEWSIPS processing

    COMMENTS: The extraction mode in NEWSIPS processing is based entirely on the automated determination of spectral width and may differ from the original request by the acquiring GO on the observing script. As a result, the NEWSIPS spectral data may differ significantly from the original processing.

- **xXTRPROF**

  Weighted Slit Extraction Profile

  VALID VALUES: EMPIRICAL, DEFAULT POINT, UNIFORM

  SOURCE: NEWSIPS processing

  COMMENTS: If an empirical determination of the spectral cross-dispersion profile is not possible, a standard default profile is assumed. The standard default profile for point sources is a model based on standard-star images and for extended sources, a uniform boxcar weighting.

REFERENCES

Bevington, P. R. 1969, Data Reduction and Error Analysis for the Physical Sciences (New York, McGraw-Hill)

Bohlin, R. C. 1986, ApJ, 308, 1001

Bushouse, H. A. 1991a, IUE NASA Newsletter, No. 45, 46

Bushouse, H. A. 1991b, *Record of the IUE Three Agency Coordination Meeting*, November 1991, p. D-17

Cassatella, A. 1990, *Record of the IUE Three Agency Coordination Meeting*, May 1990, p. II-60

Cassatella, A., Barbero, J., and Benvenuti, P. 1985, A&A, 144, 335

Coleman, C., Golton, E., Gondhalekar, P., Hall, J., Oliver, M., Sanford, M., Snijders, T., and Stewart, B. 1977, *IUE Technical Note No. 31, Camera Users Guide*, October 1977, Appleton Laboratory, University College London

Crenshaw, D. M., Bruegman, O. W., and Norman, D. J. 1990, PASP, 102, 463

Crenshaw, D. M. and Park, E. A. 1989, *Record of the IUE Three Agency Coordination Meeting*, May 1989, p. II-14

De La Peña, M. D. 1989, IUE NASA Newsletter, No. 38, 41

De La Peña, M. D. 1992a, *Record of the IUE Three Agency Coordination Meeting*, June 1992, p. III-47

De La Peña, M. D. 1992b, IUE NASA Newsletter, No. 49, 63

De La Peña, M. D., Shaw, R. A., Linde, P., and Dravins, D. 1990, Proc. Int. Symp. 'Evolution in Astrophysics', ESA SP-310, 617

Garhart, M. P. 1991, IUE NASA Newsletter, No. 46, 65

Garhart, M. P. 1992a, IUE NASA Newsletter, No. 48, 80

Garhart, M. P. 1992b, IUE NASA Newsletter, No. 48, 88

Garhart, M. P. 1992c, IUE NASA Newsletter, No. 48, 98

Garhart, M. P. 1993, IUE NASA Newsletter, No. 51, 1

Goddard Space Flight Center, *System Design Report for the International Ultraviolet Explorer*, IUE-401-76-099, August 1976

González-Riestra, R. 1991, *Record of the IUE Three Agency Coordination Meeting*, June 1991, p. VI-82

González-Riestra, R., Cassatella, A., and de la Fuente, A. 1992, *Record of the IUE Three Agency Coordination Meeting*, November 1992, p. D-78

Harris, A. W. 1985, IUE NASA Newsletter, No. 28, 22

Harris, A. W. and Cassatella, A. 1985, IUE ESA Newsletter, No. 22, 9

Holm, A. V. and Panek, R. J. 1982, IUE NASA Newsletter, No. 18, 56

Horne, K. 1986, PASP, 98, 609

Imhoff, C. L. 1984a, private communication

Imhoff, C. L. 1984b, *Record of the IUE Three-Agency Coordination Meeting*, April 1984, p. B7-1

Imhoff, C. L. 1986, *Record of the IUE Three-Agency Coordination Meeting*, June 1986, p. 2a-1

Imhoff, C. L. 1991, *Record of the IUE Three-Agency Coordination Meeting*, June 1991, p. VII-8

Kinney, A. L., Bohlin, R. C., and Neill, J. D. 1991, PASP, 103, 694

Nichols-Bohlin, J. 1988, IUE NASA Newsletter, No. 34, 57

Nichols-Bohlin, J. 1990, Proc. Int. Symp. 'Evolution in Astrophysics', ESA SP-310, 207

Northover, K. J. 1980, in IUE Data Reduction, edited by W. W. Weiss *et al.* (Austrian Solar and Space Agency, Vienna), pp.61-73

Numerical Algorithms Group Limited 1990, Numerical Algorithms Group Fortran Library, Mark 14, Oxford, United Kingdom

Panek, R. J. and Schiffer, F. H. 1981, *Minutes of the Meeting of the International Ultraviolet Explorer Users' Committee*, September 1981, Apendix H

Panek, R. J. 1982, IUE NASA Newsletter, No. 18, 68

Ponz, J. D. 1980a, IUE ESA Newsletter, No. 8, 12

Ponz, J. D. 1980b, in IUE Data Reduction, edited by W. W. Weiss *et al.* (Austrian Solar and Space Agency, Vienna), pp.75-83

Reader, J., Acquista, N., Sansonetti, C., and Sansonetti, J. E. 1990, ApJS, 72, 831

Shaw, R. A. 1989, IUE NASA Newsletter, No. 38, 34

Shaw, R. A. 1990, Proc. Int. Symp. 'Evolution in Astrophysics', ESA SP-310, 621

Smith, M. A. 1990, Proc. Int. Symp. 'Evolution in Astrophysics', ESA SP-310, 627

Teays, T. J. and Garhart M. P. 1990, IUE NASA Newsletter, No. 41, 94

Thompson, R. W. 1988, IUE NASA Newsletter, No. 35, 108

Turnrose, B. E. and Harvel, C. A., *International Ultraviolet Explorer Image Processing Information Manual, Version 1.0*, Computer Sciences Corporation, CSC/TM-79/6301, January 1980

Turnrose, B. E., Harvel, C. A., and Stone, D. F., *International Ultraviolet Explorer Image Processing Information Manual, Version 1.1*, Computer Sciences Corporation, CSC/TM-81/6268, November 1981

Turnrose, B. E. and Thompson, R. W., *International Ultraviolet Explorer Image Processing Information Manual, Version 2.0*, Computer Sciences Corporation, CSC/TM-84/6058, December 1984

Van Steenberg, M. E. 1989, IUE NASA Newsletter, No. 40, 37

Ward, A. K. 1977, *IUE Technical Note No. 30, Camera Operations Manual*, October 1977, Appleton Laboratory, University College London